UNIVERSITY OF BIRMINGHAM

Research on a New Hybrid Wind Turbine System

Thesis submitted for the degree of Doctor in Philosophy

in

School of Electronic, Electrical and Computer Engineering

by

Hao Sun

Supervisor: Prof. Jihong Wang

Dr Stuart Hillmansen

June 2014

Acknowledgements

First and foremost, I would like to show my sincere appreciation to my supervisor, Prof. Jihong Wang, for her invaluable support inspiration and patience. And I am really grateful for all her precious time dedicated to me, anytime. Her knowledge and guidance have allowed me to produce a thesis that I can be proud of. Thanks for giving me the opportunity to study in this growing and interesting field of energy storages. I owe her lots of gratitude for having me shown this way of research.

Dr. Stuart Hillmansen also deserves my appreciation for providing me with the idea for this research and for helping me through the initial stages.

Many thanks go to Dr. Xing Luo, for sharing his invaluable knowledge and experience in the field of pneumatic system and laboratory experiments. I am really grateful for his time spent to discuss about the problems I needed to face and how to solve them. I would also like to thank Shen Guo, for his constant support and cooperation during my stay.

I would like to thanks Dr. Leonid Shpanin, Liu Hao, Yue Wang, for the continued support and pleasure working together in the project. The other colleagues also deserve thanks for their kind assistant and discussions during my study.

I gratefully thank Prof. Zengcai Wang from Shandong University for his important advice and assistant in the field of mechanical design.

I gratefully thank Birmingham Science City Energy Efficiency and Demand Reduction project for the financial support to the project.

Furthermore, I would like to express my special acknowledgements to Dr. Jing Chen, for his deep concern over the period of my studying.

Most importantly, none of this would have been possible without the love and patience of my family. I am greatly indebted to my parents, who have been a constant source of love, concern, support and strength all these years.

Abstract

Nowadays, the world is facing the challenge to meet the continuous increase of energy demand and reduce the harmful impact to our environment. In particular, wind energy appears as preferable solution to take a considerable portion of the power generation market, especially in the UK. Multifarious wind turbine concepts have been developed; single-machine capacity can vary from 1kW to 7MW. However, the key challenge faced by all kinds of wind power generations is intermittency. It is highly desired to alleviate such impacts through alternative technologies.

One proposed solution is to introduce an element of storage or an alternative supply for use when the ambient flux is insufficient for a guaranteed supply to the demand. Such devices do not increase power output; in fact, energy conversion always results in lost power because of low efficiency. The primary cause is that energy storage can make wind power available when it is most demanded. Currently, most energy storage options are expensive and still under research and development, such as hydroelectric pumped storage, compressed air energy storage (CAES), supercapacitors, flywheels, super conducting magnetic energy storage (SMES). Among all the options, compressed air energy storage has attracted more and more attention during past few decades. As CAES is sustainable and will not produce any chemical waste, compared with other types of energy storage schemes. In a CAES system, the excess power is used to compress air which can be stored in a vessel or a cavern. The energy stored in compressed air will be used to generate electricity when required.

In this project, the typical stand-alone wind power generation system is introduced based on the literature review and a complete mathematical model for a 3-blade horizontal wind turbine is built as well. Comparative review and investigations on different energy storage technologies have been reviewed, which reveals advantages of CAES system in this research project. Thus, a new hybrid small scale wind turbine system structure is proposed, which integrates a typical wind turbine with CAES system. The mathematical models of each subsystem are studied separately; and then composed for the overall system. Thereinto, the air motors, which are considered as "compressed air- electricity transformers", are the core components of the designed hybrid system. Both vane and scroll type air motors have been studied through the previous research project. A new model of 2.41-wrap scroll air motor has been built and validated. The novel direct electro-mechanical hybrid transmission with CAES is introduced, which is inspired by the study of Hybrid Electric Vehicle (HEV) structures. Multi-mode control strategy is investigated to ensure the system work smoothly and efficiently. It combines fuzzy-logical pitch control, PID pressure control and CAES engagement control depending on the multi operation phases. The complete process mathematical model is derived and implemented in MATLAB/SIMULINK environment. The encouraging simulation results demonstrated that the whole hybrid system can generate steady power output under the variable wind speed profile.

Based on the model work, a prototype for implementing the proposed mechanism is built and tested as proof of the concept. The design and drawings of the construction are totally presented in the thesis. And the hybrid test finally proves the concept of the new hybrid wind

turbine feasible. At last, the experimental system result analysis is described in this thesis. Simulation and experimental study shows that the proposed hybrid wind turbine system is technically feasible with energy efficiency around 50%.

Contents

List of figures

List of tables

Nomenclature

A_a	Effective port width of control valve in vane type air motor
A_i A_o	Effective area of inlet and outlet valves in scroll air motor
B	Damping coefficient
B_v	Radius of vane-type air motor body (m)
C_0	Gas flow constant
C_d	Gas discharge coefficient
C_{dc}	DC link capacitance (F)
C_p	Wind turbine power coefficient
c_p	Specific heat of air at constant pressure
E	Available energy of compressed air (J)
E_{air_in}	Energy from the input compressed air (J)
$E_{compressor}$	Energy consumed by compressor in CAES (J)
E_{load}	Work done by air motor to drive the load (J)
E_{ng}	Total fuel energy consumed in CAES (J)
e	Eccentricity of vane type air motor
F_G	Viscous friction of generator rotor
f_{wg}	Wind gust frequency (Hz)
i_a, i_b, i_c	Phase currents of AC generator (A)
i_d, i_q	d and q axis currents of AC generator (A)

i_{drec}	Rectifier DC-side current (A)
i_{dinv}	Inverter DC-side current (A)
L_d, L_q	d and q axis inductance s of AC generator (H)
L_g	Equivalent inductance of utility grid (H)
L_v	Vane active length in the axial direction (m)
M_f	Air motor friction coefficient
M_g	Molar mass of gas (g/mol)
m_g	Mass of gas (kg)
J	Moment of inertia (kg×m^2)
K_P	Proportional gain
K_I	Integral gain
K_D	Differential gain
P	Power (W)
P_{air_in}	Power of the input compressed air (W)
P_{cm}	Power of the compressor motor (W)
p	Pressure (Pascal)
p_G	Generator pole number
q_m	Air mass flow rate through wind turbine (kg/s)
R_a	Ideal gas constant of air
R_g	Equivalent Resistance of utility grid (Ω)
R_S	Resistance of generator stator windings (Ω)
r	Radius (m)

r_h	Radius of the scroll air motor housing body (m)
r_s	Radius of the moving scroll orbit (m)
r_v	Rotor radius of vane type air motor (m)
τ	Torque (N×m)
T	Temperature (K)
U_P	Proportional controller
U_I	Integral controller
U_D	Differential controller
U_a, U_b, U_c	Phase voltages of AC generator (V)
U_d, U_q	d and q axis voltagess of AC generator (V)
U_i	Inverter voltage (V)
U_g	Utility grid side voltage (V)
v_w	Wind speed (m/s)
v_{wg}	Wind gust (m/s)
$\tilde{v}_w$	Average wind speed (m/s)
V	Volume (m^3)
V_{total}	Total control volume of the scroll air motor (m^3)
w	Mass flow rate (kg/s)
X	Valve displacement (m)
x_a	Vane working radius measured from the rotor centre (m)
z_s	Depth of the scroll air motor
α_s	Orbit angle of moving scroll

β_C	Compression ratio of compressor
ε	Flux amplitude induced by the permanent magnets of the rotor (wb)
ς	Speed ratio of gearbox
ς_b	Speed ratio of the belt transmission
δ_s	Thickness of the moving and fixed scroll (m)
ρ_a	Air density (kg/m^3)
ρ_s	Radius of a point on the scroll spiral (m)
κ	Heat ratio of air
η	Efficiency of hybrid transmission
θ	Angle (rad)
θ_p	Blade pitch angle (degree)
θ_v	Vane type air motor rotating angle (rad)
λ	Wind turbine tip speed ratio
κ_s	Ratio between the line segment and tangent angle segment of a scroll spiral
τ	Torque (N×m)
φ_s	Tangent angle of a point on the scroll spiral
ω	Rotating velocity (rad/s)
ω_{ref}	The reference generator velocity (rad/s)
ω_s	Scroll air motor rotating velocity (rad/s)

Subscripts

act	Active plate of the belt transmission
am	Air motor
atm	Atmosphere condition
belt	Belt transmission
c	Scroll air motor central chamber
C	Compressor
cb	Clutch B
cm	Compressor motor
dc	DC link
e	Exhaust port
emf	Electromagnetic field in AC generator
G	Generator
g	Utility grid
H	Wind turbine high speed shaft
L	Wind turbine low speed shaft
pas	Passive plate of the belt transmission
RMS	Root mean square value
s	Supply port
si	Scroll air motor side chamber
T	Wind turbine rotor
t	Air tank
v	Vane-type air motor
*v*_0	Balance position in vane-type air motor

v_a	Chamber A in vane-type air motor
v_b	Chamber B in vane-type air motor

Acronyms

AC	Alternating current
AFC	Alkaline fuel cell
CAES	Compressed air energy storage
dq0	Direct–quadrature–zero
DC	Direct current
ES	Energy storage
HAWT	Horizontal axis wind turbine
HEV	Hybrid electric vehicle
HIL	Hardware- in-the-loop
MCFC	Molten carbonate fuel cell
PEMFC	Polymer electrolyte membrane fuel cell
PID	Proportional-integral-derivative
PMSG	Permanent magnet synchronous generator
DFIG	Double fed induction generator
SMES	Superconducting magnetic energy storage
SOFC	Solid oxide fuel cell
SVPWM	Space vector pulse width modulation
VAWT	Vertical axis wind turbine

Chapter 1

Introduction

1.1 Background of the research project

With growing concerns about environmental pollution and possible energy shortage, great efforts have been taken by the governments worldwide to implement renewable energy programs, based mainly on wind power, solar energy, small hydro-electric power, etc. Recently, wind-energy development has experienced a significant level of interest. With improving techniques, reducing costs and low environmental impact, wind energy seems certain to play a major part in the world's energy future. In the year 2011, the worldwide wind capacity reached 237016 Megawatt, after 196 630 Megawatt in 2010 and 159 050 MW in 2009. All wind turbines installed by the end of 2011 worldwide can provide 500 Terawatt hours per annum, accounting for around 3 % of the global electricity consumption (World Wind Energy Association, 2012).

Above all, one key challenge for wind power is that electricity generation depends on when and how wind blows consistently rather than when consumers most need power, resulted from its intermittency. The variability of wind power can lead to changes in power output from hour to hour, which arises from changes in wind speed. Figure 1 shows that the power output from a diversified wind power system is usually changing hourly from 5% to 20%, either higher or lower (Environmental change

institute of Oxford University, 2005). Besides, energy regulatory policies all around the world have been characterized by introducing competition in the power industry and market, both at the wholesale and at the retail levels. The variable market brought uncertain variations onto power transmission and distribution networks, which have been studied at length (Akhmatov, 2002) (Hansen and Michalke, 2007).

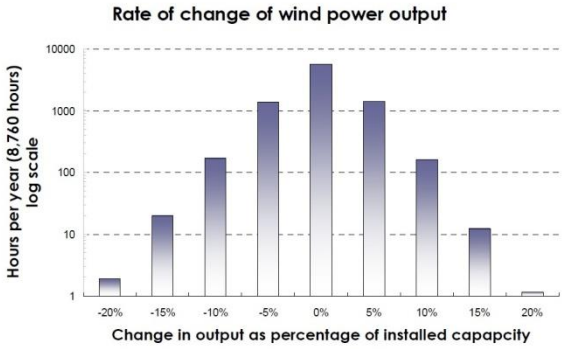

Figure 1.1 Hourly change of wind power output (Oxford University, 2005)

It becomes the great challenge to ensure the reliable energy supply to satisfy the energy demand variations in the time scales of seconds, minutes, hours, days and seasons. Wide range of efforts has been recently put into flexible power network to match the energy supply to the load demand in the contents of "Smart "Grid". The 'Smart' energy grids, dynamic grids with improved metering and increased demand control, are expected to provide one of possible solutions through efficient load management by shifting the demand to the period of renewable generation in operation (Taylor and Halnes, 2010). Apart from the effort, it is well recognised that energy storage is in the strong position and a promising mean to address the challenge.

Hybrid of a variable renewable power generation with energy storage could provide

firm, dispatch-able power and alleviate the stability threats arisen for integrating renewable energy into power grids. From current's available technology, it is still hard to directly store a massive quantity of electricity (Ibrahim, Ilinca and Perron, 2008). An energy storage system normally needs to convert the surplus renewable energy into other form of storable energy and then the stored energy will be used for power generation when the intermittent power cannot satisfy the load demand. Such devices do not increase power output; in fact, energy conversion always results in lost power because of relatively low conversion efficiency. The primary cause is that energy storage can make wind power available when it is most demanded. Currently, most energy storage options are expensive or still under research and development, such as hydroelectric pumped storage, compressed air energy storage (CAES), supercapacitors, flywheels, supercon ducting magnetic energy storage (SMES) (U.S. Department of Energy, 2006). Any technological breakthrough in one of these storage options could enhance the ability of wind energy to supply large quantities of electricity on demand, but whether such breakthroughs are imminent is unpredictable.

Compressed air energy storage (CAES) is a well-known controllable and mature technology, which has been in use as a peak shaving option since 1970s. As it derives from gas turbine technology, CAES technology is readily available and reliable. Two grid scale storage plants have been constructed in the world so far (Salgi and Lund, 2008). The first CAES plant, a 290 MW facility (Crotogino, Mohmeyer and Scharf, 2001), was started in Huntorf, Germany in 1978. A 110 MW plant commenced operation in McIntosh, Alabama in 1991 (Mack, 1993). A proposal has been under

development to convert an idle limestone mine in Norton, Ohio into the storage reservoir for a 2700MW CAES facility (McDowall and James, 2007). The Iowa Association of Municipal Utilities is developing a CAES project in Dallas Center, Iowa that will be directly coupled to a wind farm (Daneshi, Srivastava, Daneshi, 2010). For smaller scale applications, the Energetix Group company has developed a CAES based back up power supply for standard and custom units from 1kW to 3MW (Energetix, 2012). CAES can work in large and small scales; also, it is second cheapest large scale energy storage technology for grid scale application while hydro pump storage is the most economic viable technology nowadays. However, compared with the relatively armature utility-scale CAES technology, the small scale CAES system is still a novel research topic. It is anticipated that the small scale CAES system will have wide applications in off-grid and remote areas.

In the recent decades, the research on hybrid electric vehicles (HEV) is highlighted in both industrial and academic fields. Due to the similarity of hybrid of different energy sources, the research of HEV transmission could inspire the development of this kind of novel CAES system.

The hybrid wind turbine generator has two power sources, one is wind power and the other is pneumatic power. Wind turbine and air motor could drive the generator individually or simultaneously. Therefore, hybrid power train plays a key role for hybrid system concepts.

Hybrid train systems involve two or more than two power sources for power generation. For instance, CAES itself can store or compensate power in the form of

pneumatic power. It is commonly coupled with either traditional coal-fired power plant or renewable power system. While in hybrid electric vehicle (HEV), the primary power source is supplied by an internal combustion engine, and the secondary power is usually an electrical machine. In recent years, hybrid train system is becoming increasingly popular with the development of HEV due to the concerns about the energy availability and environmental impacts. Thus, the point of view from the HEV would be helpful for the hybrid wind turbine project.

There has been several types of hybrid electric vehicle techniques have be applied by the vehicle companies, including GM's two mode hybrid system, Honda's single axle parallel integrated motor assist system and Toyota's series-parallel hybrid system (Gurkaynak et al., 2009). In addition there are many novel hybrid mechanisms under research & development by the academics. Generally, according to the automobile industry, the power train can be classified into two main categories based on their configurations.

1). Series hybrid drive train is a hybridisation of energy sources, as described in Figure 5.1. In the series hybrid, engine and battery are the main energy sources, hybrid electrically. The non-mechanical structure gives the flexibility to the engine to operate within it power/fuel efficient area, independent from torque and speed of the wheels. However, the overall efficiency decreases due to two energy conversions (Gurkaynak et al., 2009).

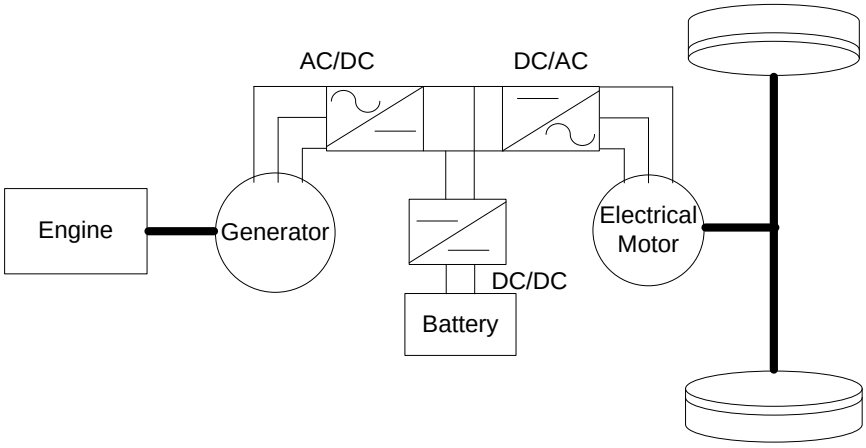

Figure 1.2 Series hybrid drive train in HEV (Van den Bossche et al., 2002)

2). Parallel hybrid drive train on the other hand, is a hybridization of drive system. The battery energy is first converted into kinetic energy, and then coupled to the engine mechanically with speed or torque coupler. Compared with series hybrid, parallel hybrid drive train has only one energy conversion phase, which assures higher efficiency and small scale. However, the engine operating is limited due to the direct connection with wheel.

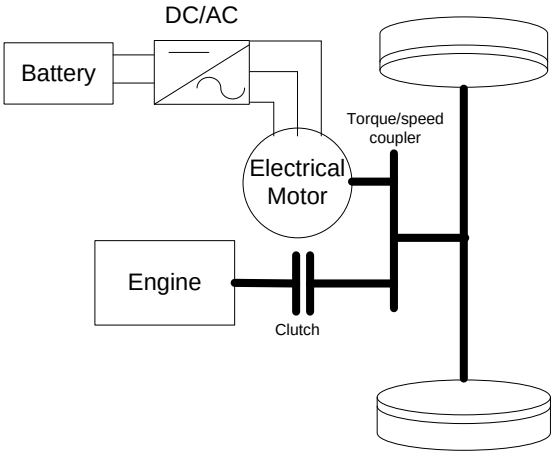

Figure 1.3 Parallel hybrid drive train in HEV (Du et al., 2011) (Yang et al., 2011)

During the PhD study, one cooperative project related to the hybrid wind turbine

system was conducted by Birmingham Science City Energy Efficiency and Demand Reduction project. The funding for setting up laboratory is from the Advantage West Midlands and the European Regional Development Fund and the prototype test rig was constructed through this funding as well. This PhD project work has focused on achieving the goal of modelling, simulation and experimental work. Additionally, during the research period, I have worked together with colleagues at Power and Control Systems Research Laboratory in modelling and validation of pneumatic actuators.

1.2 Objective of the PhD project

This PhD project is related to the innovation of a new hybrid wind turbine system. The main objective is to conduct a feasibility study on integrating a CAES system with a typical wind turbine. For appropriate use of excess wind power, a key component is the CAES system. The following tasks were performed to achieve the objectives:

1) Study the wind turbine, CAES, hybrid transmission systems based on the literature review and previous research work.
2) Design the prototype system with the hybrid of CAES and typical wind turbine system.
3) Develop a complete mathematic model for the proposed system and implement the model in the Matlab/Simulink environment and to conduct simulation study for the whole system dynamic behaviour.

4) Realise the system in a simplified version in the research laboratory to validate the basic concept of the proposed system.
5) Build a proper control strategy for managing the overall system operation in both simulation and experiment.
6) Study the energy conversion flow and power efficiency of the hybrid system through the simulation and experimental results.

1.3 Thesis outline

The thesis is divided in eight chapters as briefly described below:

Chapter 1. The background and objectives of the research project are presented.

Chapter 2. The fundamental principles of wind power generation systems are studied. The complete mathematical model of each subsystem is derived. The simulation studies show the dynamic responses of a typical wind turbine under the random wind speed input.

Chapter 3. The overview of the development of energy storage technologies is presented. Especially, the development of compressed air energy storage (CAES) is emphasised. Also there is an introduction of both utility and small scale CAES systems in the chapter.

Chapter 4. The fundamental principles of pneumatic actuator systems are described. The mechanical geometry structure and working principle of rotary motion vane-type air motors and scroll air motors are respectively introduced. And then the mathematical models can be derived. A piece of energy efficiency analysis has been

conducted between these two types of air motors based on the simulation results. Additionally, simplified models for compressors and air tank are studied as a preparation to implement the CAES system model.

Chapter 5. This chapter introduce the design and modelling on hybrid wind turbine system. It begins from the study of the Hybrid Electric Vehicle (HEV) powertrain design and current CAES structure. A novel direct mechanical integration for small scale hybrid wind turbine system is presented. The mathematical model of this hybrid system is built with the composing of each subsystem, the dynamic responses of the proposed system are analysed.

Chapter 6. Multi-mode control strategy is developed for supporting the overall system operation. Wind turbine pitch control, air motor supply pressure control and CAES engagement control are described. The performances of the non-controlled and controlled hybrid system have been compared based on the simulation results.

Chapter 7. The proposed system is constructed in the laboratory, the design and mechanical drawings are all shown in this chapter and Appendix. The model validation and power efficiency analysis are conducted based on the real experiment results.

Chapter 8. Major project achievements are concluded and recommended future work is presented as well.

1.4 Author's publications

Part of the materials of this thesis has been published, referring to the following list:

[1]. Sun, H., Luo, X. & Wang, J., 2013. Simulation study of energy efficiency for a hybrid wind turbine system. *Industrial Technology (ICIT), 2013 IEEE International Conference on*, pp.781–786.

[2]. Sun, H., Wang, J., Guo S. and Luo X., 2011. Study on a Wind Turbine in Hybrid Connection with an Energy Storage System. In *Electrical Engineering and Applied Computing*. Springer Netherlands, pp. 39–52.

[3]. Sun, H., Luo, X. & Wang, J., 2011. Management and control strategy study for a new hybrid wind turbine system. In *IEEE Conference on Decision and Control and European Control Conference*. IEEE, pp. 3671–3676.

[4]. Sun, H., Luo, X. & Wang, J. Feasibility study of a hybrid wind turbine system integration with compressed air energy storage. Accepted by the Applied Energy.

[5]. Luo, X., Wang, J., Sun, H., Derby, J. W. and Mangan, S. J., 2012. Feasibility study on recovering exhaust energy from a vehicle engine system by a scroll expander. *Advanced Intelligent Mechatronics (AIM), 2012 IEEE/ASME International Conference on*, pp.689–694.

[6]. Luo, X., Wang, J., Sun, H. and Xu H., 2012. Study of a New Strategy for Pneumatic Actuator System Energy Efficiency Improvement via the Scroll Expander Technology. *Mechatronics, IEEE/ASME Transactions on*, PP(99), pp.1–11.

[7]. Luo, X., Sun, H. & Wang, J., 2011. An energy efficient pneumatic-electrical system and control strategy development. *American Control Conference (ACC), 2011*, pp.4743–4748.

Chapter 2

Mathematical modelling and control strategy of wind turbine systems

This chapter reports the work in deriving a complete mathematical model of a horizontal axial 3-blade wind turbine system in preparation for the overall hybrid system model for simulation and feasibility study. The chapter starts from the introduction and fundamental principle of traditional wind power generation. In this section, the structure of a wind turbine is described in terms of various subsystems, of how they are functioned: turbine blades aerodynamic, drive train, electric generator and power electronic models. To determine the amplitude and the frequency of the output voltage, the associated Space Vector Pulse Width Modulation (SVPWM) control strategy is also introduced. Thus the mathematical model for the wind turbine dynamic process is completely derived, and the simulation performance results are presented in this chapter.

2.1 Introduction of wind power generation system

Since the earliest time, human started harnessing the energy of wind, with the first wind mill recorded as early as the 6th century AD. The technology has diversified over the years for different tasks, including pumping water, grinding grain, powering sawmills and most recently generating electricity, which is the fastest growing energy market

worldwide now (British Wind Energy Association, 2005). The origin of wind is from the uneven heating of the earth's surface, which drives a global atmospheric convection system. There is an estimated 72 to 170 TW of wind power on the earth that can potentially be explored for commercial purpose (Ananthaswamy and Le Page, 2012). The modern wind industry began in the early 1980s when the first utility-scale wind turbines were installed in California and Denmark. The development of wind power today was driven by high energy prices, energy insecurity, and concerns about environmental degradation. Early wind turbines were rather primitive from today's technical view, and suffered from poor reliability and high costs. Like most new technologies, early wind turbines had to go through a process of "learning by doing," where shortcomings were discovered, components were redesigned, and new machines were installed in a continuing cycle. Today's wind industry is notably different from that in the early 1980s. Wind turbines now are typically 100 times more powerful than early versions and employ sophisticated materials, electronics, and aerodynamics. Costs have declined, which makes wind power more competitive. Large companies and investment banks now drive most wind power activities by collaborating scientists, inventors, and entrepreneurs (Logan and Kaplan, 2008).

Without doubt, wind power has become one of pillars of the energy systems in many countries and is recognised as a reliable and affordable source of electricity. Altogether, 96 countries and regions have been identified worldwide to use wind energy for electricity generation. The wind sector in 2011 had a turnover of 50 billion Euro/65 billion USD. All wind turbines installed by the end of 2011 worldwide can

provide 500 Terawatt hours per annum, around 3% of the global electricity consumption. The worldwide wind power generation capacity reached 237,016 Megawatt, out of which 40,053 Megawatt were added to the system in 2011, more than ever before. World Wind Energy Association sees a global capacity of 500,000 Megawatt as possible by the year 2015 and more than 1,000,000 Megawatt by the year 2020 (World Wind Energy Association, 2012).

Following the shift of the energy sector from a centralised energy grid to the distributed network, small wind systems and its hybrid applications are playing an increasingly important role. As of the end of 2009, a cumulative total of 521,102 small wind turbines were installed, over 60,000 of which were newly installed that year with a sales revenue over 215 million USD. Until the end of 2010, the world total cumulative installed small wind power generation systems reached 656,084 units, demonstrating a 26% growth from 2009 and generating approximately a total of over 382 gigawatt-hour (GWh) in annual energy production worldwide.

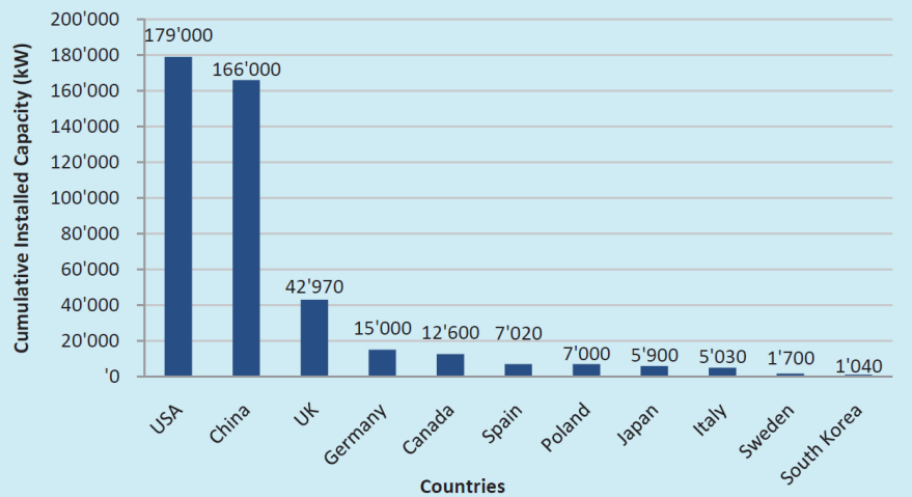

Figure 2.1 Total Cumulative installed capacity of small wind turbines at the end of 2011 (World Wind Energy Association, 2012)

Figure 2.1 shows that the total installed capacity of small wind turbines around the world has reached 443MW at the end of 2011 (Zhang, 2012).

To the potential of wind power market in the UK, it is expected to continue the growth for the foreseeable future. At the beginning of September 2012, the installed capacity of wind power in the United Kingdom was 6,858 megawatts (MW), with 357 operational wind farms and 3,873 wind turbines in the UK. The UK is ranked as the world's eighth largest producer of wind power. New 723 MW wind power capacity was brought online during the year of 2011. 2012 is also recognised to be a significant year for the offshore wind industry with potentially 5 farms becoming operational with over 1,300 MW of generating capability (RenewableUK, 2012). Renewable UK estimated in 2010 that more than 2,000 MW of capacity would be deployed per year until 2017 (RenewableUK, 2012). By 2020, the UK is expected to have more than 28,000 MW of wind power capacity (Juliette, 2012). The UK government offer supportive schemes to the development of the wind power generation; through the Renewables Obligation, British electricity suppliers are now required by law to provide a proportion of their sales from renewable sources such as wind power or pay a penalty fee. The supplier then receives a Renewables Obligation Certificate (ROC) for each MWh of electricity they have purchased. Moreover, as public and commercial awareness of the benefits of micro-generation expands, an increasing number of sites will become commercially attractive for small wind systems across the UK. Small wind systems under 50 kW in the UK which previously received 2 ROCs, are now eligible for support under the Feed In Tariff, which is an incentive

scheme introduced by the government to encourage people to generate their own low carbon electricity. The idea is that the homeowners receive a payment from the government for every unit of electricity they generate. The UK's Feed-in-Tariff incentives, combined with corresponding and growing levels of consumer interest and increasing levels of inward investment make the UK's small wind market more attractive than ever before from a report in 2010 (Department of Energy and Climate Change, 2010).

2.2 Fundamental principles of wind turbine system

From the perspective of energy conversion, a typical wind turbine consists of two parts: rotor blade, which can convert wind energy to rotational mechanical energy; and generator system, that transforms mechanical energy to electrical energy. Generally, a typical wind turbine system includes rotor blade, gear box, generator, yaw system, control system, support tower and other major components.

Industrial wind turbines are divided into two general classes depending on how they spin: vertical axis and horizontal axis. The only vertical axis wind turbine (VAWT) type in commercial production at any volume is the Darrieus machine, named after the French engineer Georges Darrieus who patented the design in 1931 (Danish wind industry association, 2003). The basic theoretical advantages of a vertical axis machine are:

(1) The generator, gearbox etc. may be placed on the ground, with no need of a tower for the turbine

(2) There is no need to a yaw mechanism to turn the rotor against the wind.

The main disadvantages are:

(1) Wind speeds are very low close to ground level, as there is not a tower to lift the rotor to the high level;

(2) The overall efficiency of the vertical axis machines is lower than that of horizontal ones;

(3) The machine is not self-starting (e.g. a Darrieus machine needs a "push" before it starts), which is inconvenient for grid connected turbines;

On the contrary to VAWT, the horizontal axis wind turbines (HAWT) have come to dominate today's markets, majority of grid-connected commercial wind turbines today are built with a propeller-type rotor on a horizontal axis.

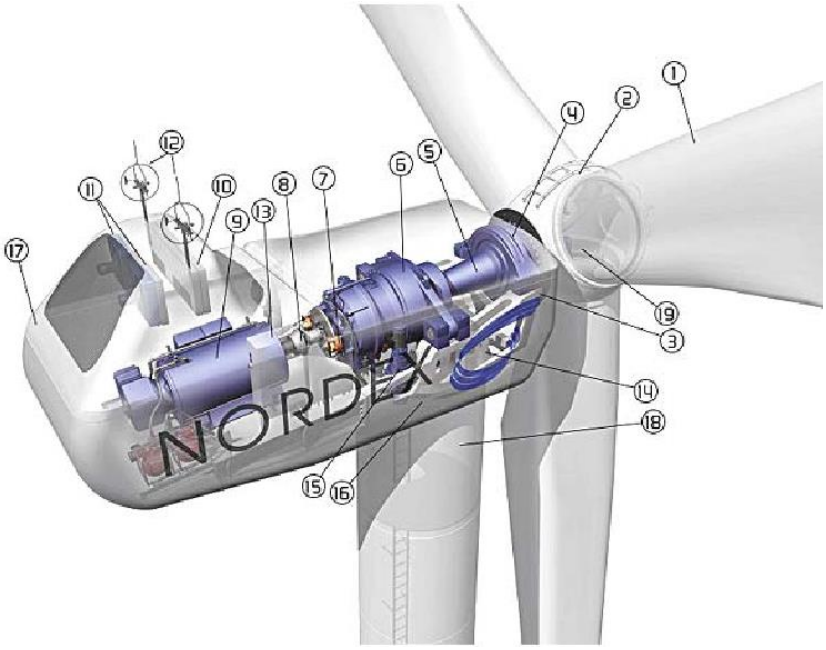

Figure 2.2 Configuration of Nordex N54 wind turbine (Jin. 2007)

1) rotor blade; 2) wheel hub; 3) hub framework; 4) coupling between wheel and main shaft; 5) main shaft; 6) gearbox; 7) brake; 8) coupling between generator and main shaft; 9) generator; 10) cooler; 11) cooling fan; 12) wind sensors; 13) control system; 14) hydraulic drive; 15) yaw drive; 16) yaw ring; 17) hub; 18) tower; 19) hydrulic pitch system

Figure 2.2 shows the configuration a typical horizontal axis wind turbine- Nordex N54 type. The wind blows the rotor blade with an appropriate angle, driving the blades to produce rotating torque, thus convert the wind energy into mechanical energy. The blade speed is set up by gearbox to a value suitable for the generator. Then kinetic energy is transformed to electrical energy for grid connection.

2.3 The mathematical model of a wind turbine system

The mathematical model for wind turbine systems has been reported in many different publications. The description in this chapter is mainly based on the previously published literature. In this project, a typical wind turbine system with permanent magnetic synchronous generator (PMSG) is modelled, which will be integrated with compressed air energy storage system to make up a hybrid turbine system.

The dynamic model of a horizontal wind turbine system is derived for various types of analysis related to system dynamics, e.g. stability, control system analysis and optimization, etc. The model will describe the dynamics of the system from the turbine rotor where the kinetic wind energy is converted to mechanical energy, to the grid connection point where the electric power is fed into the grid. The whole

structure of the wind turbine model is demonstrated in Figure 2.3. It consists of rotor blade aerodynamic model, drive train model and electric system model.

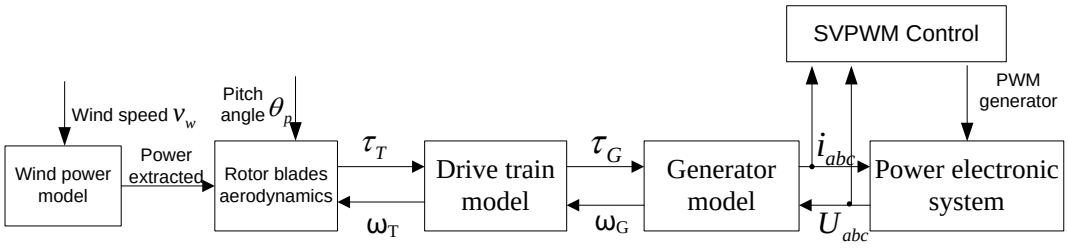

Figure 2.3 Overall structure of a horizontal wind turbine model

The blades aerodynamic model considers an equivalent wind speed v_w, the wind turbine blades speed ω_T and the blade pitch angle θ_p as inputs. Its output is the turbine driving torque τ_T

The drive train model is linked to the generator model as described above, and to the blades aerodynamic model. The input to the drive train model is the turbine driving torque τ_T .and generator speed ω_G. The outputs are the wind turbine blades speed ω_T and the generator driven torque τ_G.

The generator model is connected with the power electronic system through the voltages U_{abc} and currents i_{abc}. On the backwards, it provides the generator speed ω_G to the drive train block and uses the generator driven torque T_G as input. The electric model also represents the measured voltages and currents for the SVPWM double loop control.

In the simulation work, a power electronic system model, including converter, inverter and DC link, compatible with commercial power system analysis tools would be in imminent need, like Simulink/Simpower (Lei *et al*., 2006).

2.3.1 Wind power and blade aerodynamic modelling

a). wind speed model

The wind speed usually varies considerably, and has a stochastic character. Therefore, in general, the wind speed could be modelled as a stochastic process. But for the analysis of wind turbine system operation in an electrical power system, the wind variation can be modelled as a sum of harmonics in the range 0.1-10 Hz. Wind gusts are usually also include in the wind model (Slootweg et al., 2003):

$$v_w(t) = \tilde{v}_w(1 + \sum_k A_k \sin(\omega_k t)) + v_{wg}(t) \tag{2.1}$$

where $\tilde{v}_w$ is the mean value of wind speed; A_k is the amplitude of *k*th harmonic, ω_k is frequency of the *k*th harmonic, $v_{wg}(t)$ is the wind gust, which can be modelled by the following function (Lubosny, 2003):

$$v_{wg}(t) = \frac{2v_{wg\max}}{1 + e^{-4(\sin(f_{wg}t)-1)}} \tag{2.2}$$

where $v_{wg\max}$ is gust amplitude, f_{wg} is gust frequency. The amplitude and frequency refers to the quantifiable variation of the wind gust.

b). Model of the turbine blades

A wind turbine is a device for extracting kinetic energy from the wind. The force of the wind creates aerodynamic lift and drag forces on the rotor blades, which in turn produce the torque on the wind turbine rotor. The aerodynamic behaviours of wind turbines can be analysed through the energy extraction process, as described in Figure 2.4.

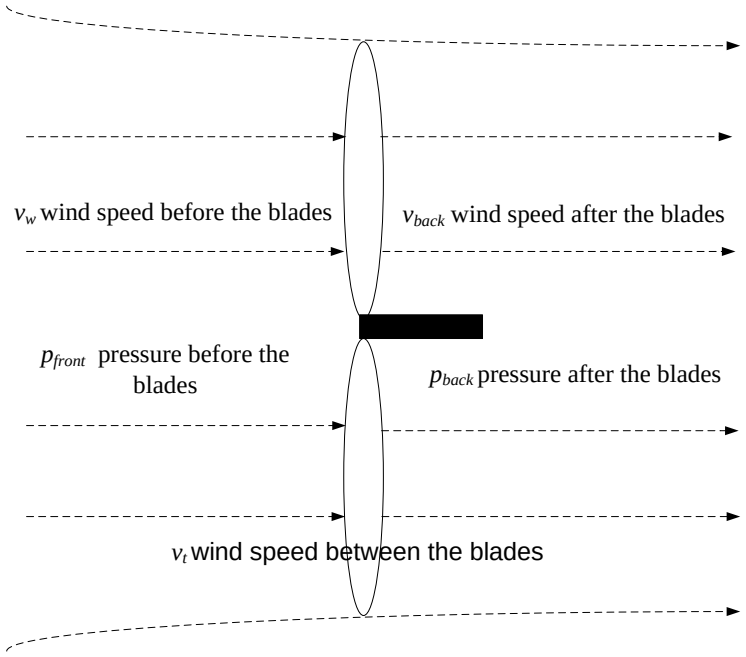

Figure 2.4 Energy extracting of wind turbines

Give the kinetic energy of the air P_a passing through $1\,m^3$ volume,

$$E_a = \frac{1}{2}\rho_a v_w^{\ 3} \tag{2.3}$$

where, ρ_a is the air density.

According to Bernoulli Equation,

$$\frac{1}{2}\rho_a(v_w^2 - v_{back}^2) = p_{front} - p_{back} \tag{2.4}$$

where, p_{front} is the pressure before the blades, while p_{back} is the pressure after the blades. And v_w and v_{back} mean the wind speeds before and after the blades, respectively.

The force affected on the blades,

$$F = \pi r_T^{\ 2}(P_{front} - P_{back}) = \frac{1}{2}\rho_a \pi r_T^{\ 2}(v_w^2 - v_{back}^2) \tag{2.5}$$

where, r_T is the blade radius.

Define q_m as the air mass flow rate through wind turbine:

$$q_m = \rho_a \pi r_T^{\,2} v_t \tag{2.6}$$

According to the above equation and principle of momentum, the average wind speed between the blades is:

$$v_t = \frac{1}{2}(v_w + v_{back}) \tag{2.7}$$

The power extracted from the wind P^* equals the differences of the kinetic power before and after the blades, substitute q_m and v_t

$$P^* = \frac{1}{2} q_m v_w^2 - \frac{1}{2} q_m v'^2 = \frac{1}{2} \rho_a \pi r_T^{\,2} v_t (v_w^2 - v'^2) = \frac{1}{4} \rho_a \pi r_T^{\,2} (v_w + v')(v_w^2 - v'^2) \tag{2.8}$$

Similarly, the total incoming wind power before the blades P_{in}^* is obtained:

$$P_{in}^* = \frac{1}{2} \rho_a \pi r_T^{\,2} v_w^3 \tag{2.9}$$

Power coefficient C_P namely turbine efficiency, reveals the capability of turbine for obtaining energy from wind. It is described as:

$$C_P = \frac{P^*}{P_{in}^*} \tag{2.10}$$

Defining $a = \dfrac{v'}{v_w}$

$$C_P = \frac{P^*}{P_{in}^*} = \frac{\frac{1}{4} \rho_a \pi r_T^{\,2} (v_w + v')(v_w^2 - v'^2)}{\frac{1}{2} \rho_a \pi r_T^{\,2} v_w^3} = \frac{(1+a)(1-a^2)}{2} = f(v_w, v') \tag{2.11}$$

As v_1 is a known value, calculate the derivation of v_2, it can be easily proven that the maximum of power coefficient C_P is obtained when $v' = \frac{1}{3} v_w, a = \frac{1}{3}$

$$C_{P\max} = 0.593$$

Then the maximum power can be extracted $E_{\max}^*$ is:

$$P_{\max}^* = 0.593 E_{in}^* = 0.593 \times \frac{1}{2} \rho_a \pi r_T^{\,2} v_w^3 \tag{2.12}$$

(Liu and Zhang etc, 2006)

As C_p requires knowledge of the aerodynamics and the computations are rather complicated, numerical approximations have been developed, where the power coefficient is defined as a function of tip speed ratio $\lambda = \omega_T \cdot r_T / v_w$ and the blade angle, ω_T denotes the turbine speed. (Heier and Waddington, 2006). Here the following function will be used, which is accepted in the Matlab/Simulink toolboxes:

$$C_p(\lambda, \theta_p) = 0.22\left(\frac{116}{\lambda_i} - 0.4\theta_p - 5\right)e^{\frac{-12.5}{\lambda_i}} \tag{2.13}$$

with

$$\frac{1}{\lambda_i} = \frac{1}{\lambda + 0.08\theta_p} - \frac{0.035}{\theta_p{}^3 + 1} \tag{2.14}$$

(Mathworks, 2012)

where θ_p represents the pitch angle. The above equations lead to the $C_p(\lambda, \theta_p)$ versus λ characteristics for various values of θ_p as depicted in Figure 2.5.

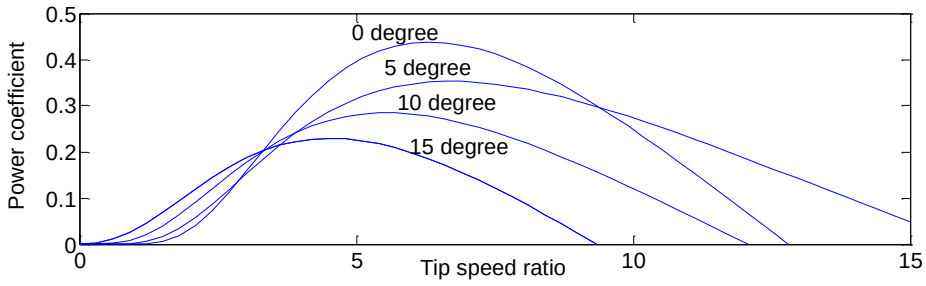

Figure 2.5 Power coefficients as a function of tip speed ratio and pitch angle

Using the actual values of the wind and rotor speed, which determine λ, and the pitch angle, the mechanical power extracted from the wind can be calculated using equations (2.9) to (1.10) (Slootweg, Polinder and Kling, 2001).

$$P_T = \frac{1}{2}\rho_a \pi r_T^{\,2} v_w^3 C_p \tag{2.15}$$

2.3.2 Drive train modelling

The drive train of a wind turbine system in general consists of a blade pitching mechanism with a spinner, a hub with blades, a rotor shaft, and a gearbox with brake and generator. In practical, the efficiencies related to tooth friction losses only for single tooth meshes can reach 98-99% (Burns, 2009). However, the gearbox is not necessary in some systems with permanent magnet synchronous generator (PMSG), as the PMSG built with multi pole pairs can achieve low speed and high torque operation. Since a gearbox causes higher weight, costs and demands maintenance (Westlake, Bumby and Spooner, 1996), a gearless construction represents an efficient and robust solution, which was believed to be beneficial especially for offshore applications.

The mechanical model is derived with emphasis to include only the parts of the dynamic structure of the wind turbine, which are important to the interaction with the grid, i.e. which influences significantly on the fluctuations of the power (Sørensen *et al.*, 2001). The acceptable (and common) way to model the wind turbine drive train system is to treat it as a number of discrete masses linked together by springs defined by damping and stiffness coefficients. The minimal realisation of the drive train model utilised as an element of the wind turbine system model is based on the assumption of two lumped masses: the turbine blade (with hub) mass and the high speed shaft (with gearbox) mass (Lubosny, 2003). One simplification has been made that the drive train is a stiff shaft system, as the mechanical model illustrated in Figure

2.6.

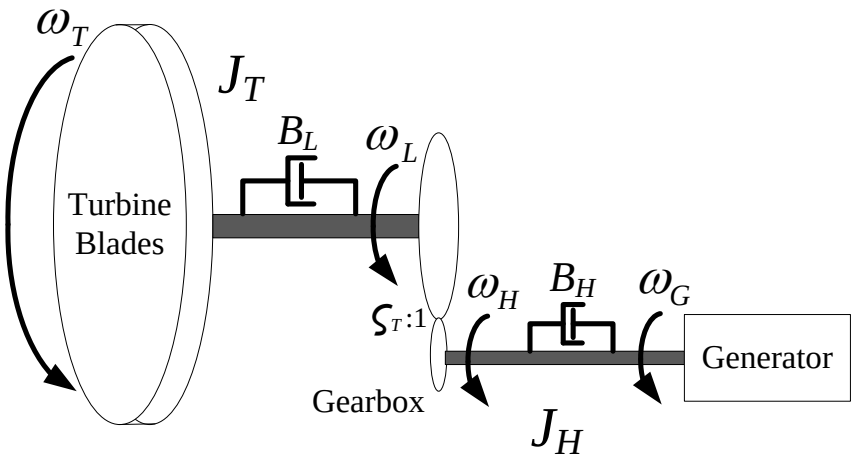

Figure 2.6 Mechanical model of the wind turbine drive train system

Thus the torsion stiffness is large enough; the turbine blade and high speed shaft have the same rotation freedom (Jin, 2007). The low-speed shaft is driven by the turbine blades, which extracts aerodynamic power. The high-speed shaft is linked to the generator, driving the electromagnetic field (EMF) load (Muljadi and Butterfield, 2001). According to the rotational motion equations, the model of the drive train system can be described by Equations (2.16-2.19):

$$J_T \frac{d}{dt}\omega_T = \tau_T - \tau_L - B_L\omega_T \tag{2.16}$$

$$J_H \frac{d}{dt}\omega_H = \tau_H - \tau_G - B_H\omega_H \tag{2.17}$$

$$\omega_G = \omega_H = \frac{\omega_L}{\varsigma_T} = \frac{\omega_T}{\varsigma_T} \tag{2.18}$$

$$\tau_H = \eta_T \varsigma_T \tau_L \tag{2.19}$$

where J is the inertia, τ stand for the torque, B is the damping coefficient, and subscripts of T, L, H, G represent the turbine blade, low speed shaft, high speed

shaft, generator respectively. η_T and ς_{T} are the efficiencies and speed ratio of gearbox.

For the simplicity of modelling, One-mass lumped model is also considered, which accounts for all the rotating components of the wind turbine drive train. The differential equation of motion can be expressed as:

$$(\varsigma_{\mathrm{T}}{}^2 J_T + J_G)\frac{d\omega_G}{dt} = \eta_T \varsigma_{\mathrm{T}} \tau_L - \tau_G - B_{eq}\omega_G \tag{2.20}$$

where B_{eq} is the equivalent damping coefficient on the generator side.

2.3.3 Introduction and modelling of the wind turbine generators

a). Variable speed wind turbine generator selection

Three-phase alternators (AC generators) are used almost exclusively for electrical power generation. When a three-phase generator feeds directly into a grid, that operates at a fix frequency (e.g. 50 Hz in Europe, 60 Hz in the USA) the angular velocity of the generator is fixed- or almost fixed. In this situation the capability of wind power generation will not be utilised fully for variable wind speed. Resulted from the highly developed converter technology of today, it is now possible to operate with variable generator speeds; during gusty winds it also substantially decreases the mechanical stresses in the blades and the shaft between the turbine and generator (Gasch and Twele, 2007). The main advantage of wind turbine variable speed operation is that the wind energy capture can be optimised associated with Maximum Power Point Tracking (MPPT) control. One study has pointed out that the optimum of variable speed operation could provide 20% more power generated than fixed speed

(Idan, Idan and Shaviv, 1998). Even there is more optimistic claim that this gain is up to 38% (Zinger and Muljadi, 1997).

Currently, there are two different types of variable speed operating concepts, according to the different combination of generator and converter. They are described below:

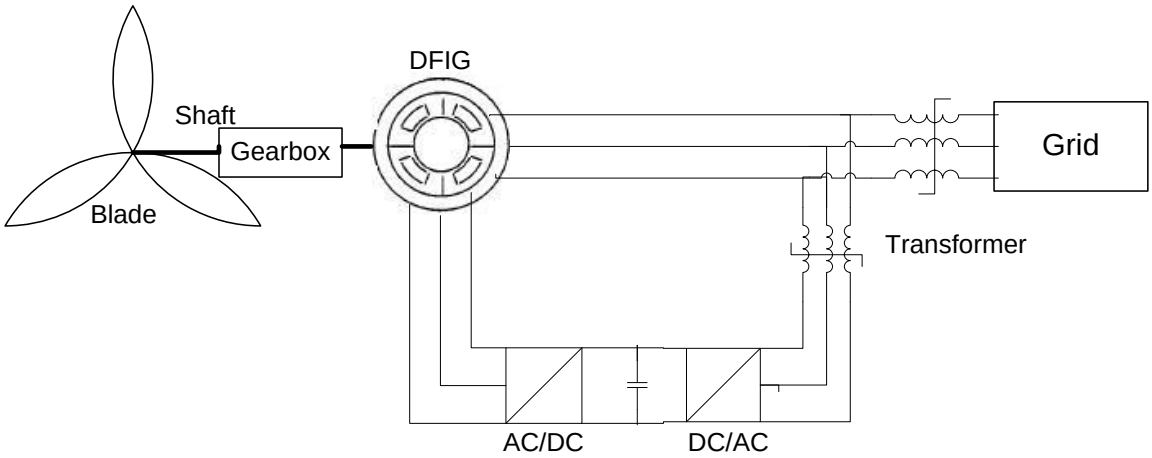

Figure 2.7 DFIG wind turbine

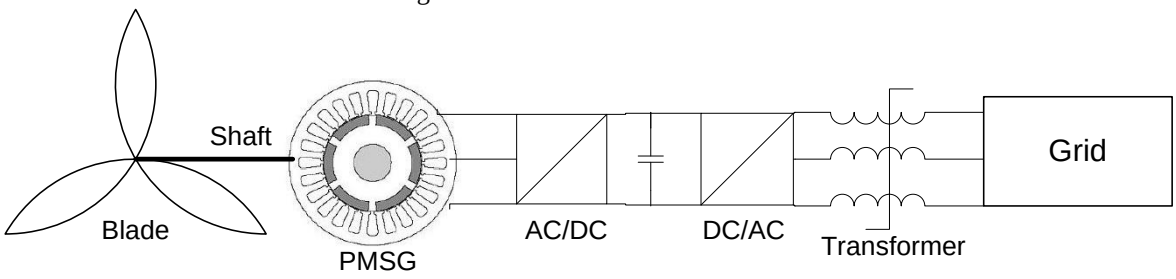

Figure 2.8 Direct Driven PMSG wind turbine

In Figure 2.7, the decoupling of the grid frequency and the mechanical rotor frequency is implemented by using a doubly fed induction generator (DFIG) with a back-to-back voltage source converter feeding the rotor. While in Figure 2.8, it is implemented by fully decoupling the direct driven permanent magnetic synchronous generator (PMSG) from the grid using a back-to-back voltage source converter or a

combination of a diode rectifier coupled to the generator stator winding and a voltage source inverter coupled to the grid (Heier and Waddington, 2006; Slootweg *et al*., 2003). The converter and inverter, installed between the power system element and the machine terminal, can regulate and improve the quality of electricity to meet the demand of grid or load.

A double-fed induction machine is a standard, wound rotor induction machine with its stator windings directly connected to the grid and its rotor windings connected to the grid through a frequency converter, where both windings transfer significant power between shaft and electrical system. In this configuration, the induction generator can have a speed range as wide as that of a synchronous generator with a full power converter. However, the converter in the rotor circuit has to cover only about 20% of the rated power. Therefore, it is less expensive and also has smaller losses. The more sophisticated control in the rotor circuit can also decide whether the induction machine should consume or supply reactive power in order to meet the present needs of the grid (Gasch and Twele, 2012).

While in PMSG, its armature current is interacted with a field produced by permanent magnets (PM), which have been widely used to replace the excitation winding in synchronous machines. The use of PMs instead of electromagnets is motivated to have simpler rotor construction, i.e. no field coils have to be electrified. Furthermore, the efficiency is improved, as rotor coil losses are practically eliminated (Deglaire *et al*., 2007). The efficiency of a PMSG wind turbine was thus assessed to be higher than other variable-speed wind turbine concepts (Grauers, 1996). However, the

disadvantages of the permanent magnet excitation are high costs for permanent magnet materials and a fixed excitation, which cannot be changed according to the operational point. Nevertheless, a full scale IGBT back-to-back voltage source converter is essential, by which the generator is connected to the power grid. Due to the intensified grid codes, wind turbines with full scale power converter might be favoured in future compared to wind turbine concepts using doubly-fed induction generators (Pena *et al.*, 1996; Muller *et al.*, 2002). As the power converter decouples the generator system from the grid, fault ride through and grid support is easier to accomplish (Li *et al.*, 2008).

The structure diversity between DFIG and PMSG results in different characteristics, which are summarised in Table 2.1:

Table 2.1 Comparison between DFIG and PMSG

Item	DFIG		PMSG	
Structure	demerits	Same stator as synchronous generator, squirrel cage rotor, brush and slip ring	merits	No excitation winding and amortisseur winding on the rotor compared with common synchronous generator, brushless
Excitation		Receive excitation current fed from the grid, do not need excitation device and regulator		No excitation
Size and weight		Large and heavy		Simply rotor and no gearbox, smaller and lighter
Noise		More noisy because of the gearbox		Less noisy
Maintenance		Same maintenance of stator, Little maintenance of rotor		Seldom maintenance
Power Factor	merits	Determined by frequency fed by converter, easily regulated	demerits	Difficult to change because of no excitation regulator
Grid Connection		Mandatory grid, do not need Synchronizer		Need Synchronous switching device

Item	DFIG		PMSG	
Stability		Not be able to lost synchronism, need appropriate load limit when operation		May lost synchronism when load changes dramatically
impulse current		Mandatory grid, impulse current is great, need current limit sometimes		Impulse current is little because of the Synchronous device

(Fitzgerald, Kingsley and D.Umans, 1992; Chapman, 2005)

As a result of these disparities, DFIG wind turbines dominate the MW-class market, mainly served for large grid; while PMSG takes the highest proportion in the KW-class market, especially for household applications. Also the market surveys on the product variety of some famous wind turbine brands verify this conclusion. For this small power scale project, PMSG has the key advantages, such as simple scale, little maintenance and noise, which makes it a better choice in not only civil market but also lab for experiment.

b). Permanent magnet synchronous generator (PMSG)

For analysing the transient response of the alternator system, Park's transformation is employed in the modelling work. In electrical engineering, Park's transformation is a common methodology to simplify the analysis of three-phase circuits. It is a transformation of coordinates from the three-phase stationary coordinate system ($X_{abc} = \begin{bmatrix} X_a \\ X_b \\ X_c \end{bmatrix}$) to the $dq0$ rotating coordinate system ($X_{dq} = \begin{bmatrix} X_d \\ X_q \\ 0 \end{bmatrix}$). For the generator model in this project, the zero axis component in the $dq0$ vector representation is zero as the neutral connection is not applied, that is, $i_0 = \frac{1}{3}(i_a + i_b + i_c) = 0$. The

transformation matrix (T_{park}) is defined as (Kimbark, 1995; Pillay and Krishnan, 1988, 1989):

$$T_{park} = \frac{2}{3}\begin{bmatrix} \cos p_G\theta_G & \cos(p_G\theta_G t - \frac{2}{3}\pi) & \cos(p_G\theta_G t + \frac{2}{3}\pi) \\ -\sin p_G\theta_G & -\sin(p_G\theta_G t - \frac{2}{3}\pi) & -\sin(p_G\theta_G t + \frac{2}{3}\pi) \end{bmatrix} \quad (2.21)$$

where θ_G is the angular position of the AC generator; p_G is the number of the pole pairs in the stator. The vector X_{dq} can be obtained through the multiplication of the vector X_{abc} by the transformation matrix T_{park},

$$X_{dq} = T_{park} X_{abc} \quad (2.22)$$

From Equations (2.21) and (2.22), the following voltage equations can be derived:

$$U_q = \frac{1}{3}[\sin(p_G\theta_G) * (2U_{ab} + U_{bc}) + \sqrt{3}U_{bc}\cos(p_G\theta_G)] \quad (2.23)$$

$$U_d = \frac{1}{3}[\cos(p_G\theta_G) * (-2U_{ab} - U_{bc}) - \sqrt{3}U_{bc}\sin(p_G\theta_G)] \quad (2.24)$$

where U_d, U_q are the voltages of d-axis and q-axis respectively. U_{ab} and U_{bc} denote the line voltages of the AC generator.

Considering the dq-axis voltage and current in the synchronous frames are all constant values in steady state, it is convenient to use them directly for steady state analysis (Lang *et al.*, 2011). The equivalent stator circuit of the dq-axis model e is described in Figure 2.6 (Rahman, 1996; Park *et al.*, 2007; Hemeida *et al.*, 2011).

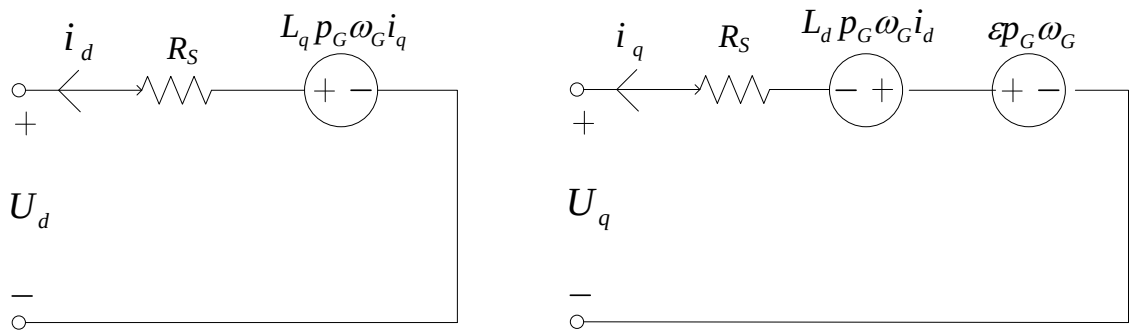

(a) d-axis circuit (b) q-axis circuit

Figure 2.9 PMSG equivalent circuits on dq coordinate system

The following equations can be derived from Figure 2.9 (Mathworks, 2012):

$$\frac{d}{dt} i_d = \frac{1}{L_d} U_d - \frac{R_s}{L_d} i_d + \frac{L_q}{L_d} p_G \omega_G i_q \tag{2.25}$$

$$\frac{d}{dt} i_q = \frac{1}{L_q} U_q - \frac{R_s}{L_q} i_q - \frac{L_d}{L_q} p_G \omega_G i_d - \frac{\varepsilon p_G \omega_G}{L_q} \tag{2.26}$$

where, ω_G is the generator rotating velocity; L is the inductance; R_S is the resistance of stator windings; ε is the amplitude of the flux induced by the permanent magnets of the rotor in the stator phases; v means voltage; i is current with subscripts of a, b, c, d, q representing the axis of a, b, c, d, q for different electrical phases.

And the electromagnetic torque τ_{emf} of the PMSG can be obtained by the following equation (Mathworks, 2012):

$$\tau_{emf} = 1.5 p_G [\varepsilon i_q + (L_d - L_q) i_d i_q] \tag{2.27}$$

Considering the generator is driven by the high speed shaft, the mechanical rotation part of the PMSG can be calculated from the Newton's Law to the rotation motion:

$$\frac{d}{dt} \omega_G = \frac{1}{J_G} (\tau_G - \tau_{emf} - F_G \omega_G) \tag{2.28}$$

$$\frac{d\theta_G}{dt} = \omega_G \tag{2.29}$$

where F_G means the viscous friction of generator rotor; τ_G denotes the generator driving torque; J_G is the combined inertia of generator rotor and load.

2.3.4 Introduction of power electronic systems

Power electronics are devices used to perform specific energy conversion functions, as in AC to DC, DC to AC, one voltage to another or one frequency to another. Power electronics have many applications in wind energy systems. They are being used more often as the technology develops and as costs drop (Manwell, McGowan and Rogers, 2009).

In this proposed model, the PMSG was connected to a host AC power grid by a full scale power converter system which comprised an uncontrolled diode rectifier, an internal DC-Link modeled as a capacitor and a SVPWM voltage-source inverter. This architecture offers a high degree of controllability over system variables (Strachan and Jovcic, 2007).

A transformer is located between the inverter and the Point of Common Connection (PCC) in order to raise the voltage by avoiding losses in the transport of the current. The layout of the electrical part is depicted in Fig. 2.10 (Rolan *et al*, 2009).

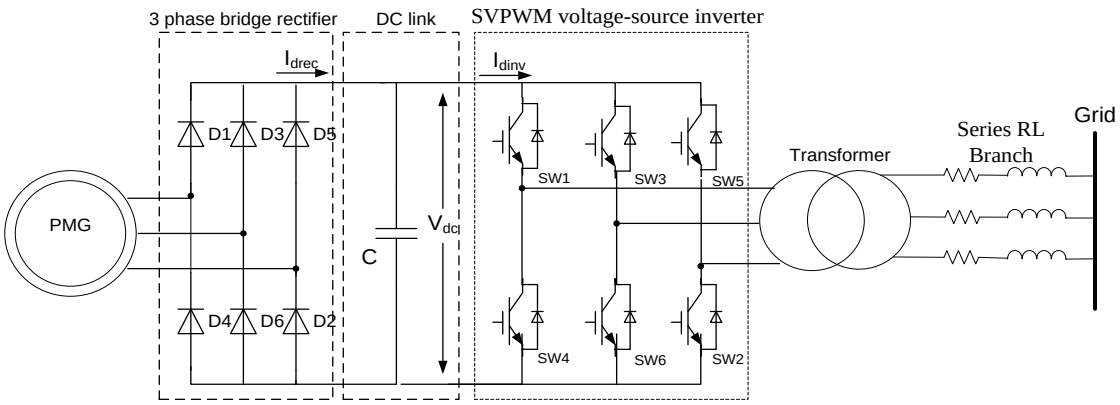

Figure 2.10 Power electronic systems for grid connection

In general, the rectifier and inverter can have various structures and can be built based on various types of types of switches, e.g. diodes, GTO (gate turn-off thyristor), IGBT (isolated-gate bipolar transistor), etc. The simplest type of rectifier utilises a 3-phase diode bridge circuit to convert the AC to DC. An example of such a rectifier is shown in Figure 2.10. The output voltage waveform consists of six active pulses, each $\pi/3$ wide. Each pulse shows the response of a circuit mode in the steady state. The state of diodes and the transfer of currents are shown in the following table (Agrawal, 2001):

Table 2.2 The state of diode and current transfer

Pulse number (mode)	Conducting diode	Current transition
1	D6	D5 to D1
2	D1	D6 to D2
3	D2	D1 to D3
4	D3	D2 to D4
5	D4	D3 to D5
6	D5	D4 to d6

For this rectifier, the input is 3-phase AC power; the output is DC. The average DC

voltage U_{dc}, resulting from rectifying a 3-phase voltage of U_{RMS} is:

$$U_{dc} = \frac{3\sqrt{2}}{\pi} U_{RMS} \tag{2.30}$$

In the case a capacitor used as the DC link, the model is defined as:

$$C_{dc} \frac{dU_{dc}}{dt} = i_{drec} - i_{dinv} \tag{2.31}$$

where, C_{dc} is the DC link capacitance, i_{drec} is the rectifier DC-side current, i_{dinv} is the inverter DC-side current (Lubosny, 2003).

2.3.5 Space Vector Pulse Width Modulation (SVPWM) system modelling

To output the grid-accepted voltage waveform, SVPWM technique is employed for the control of the power inverter.

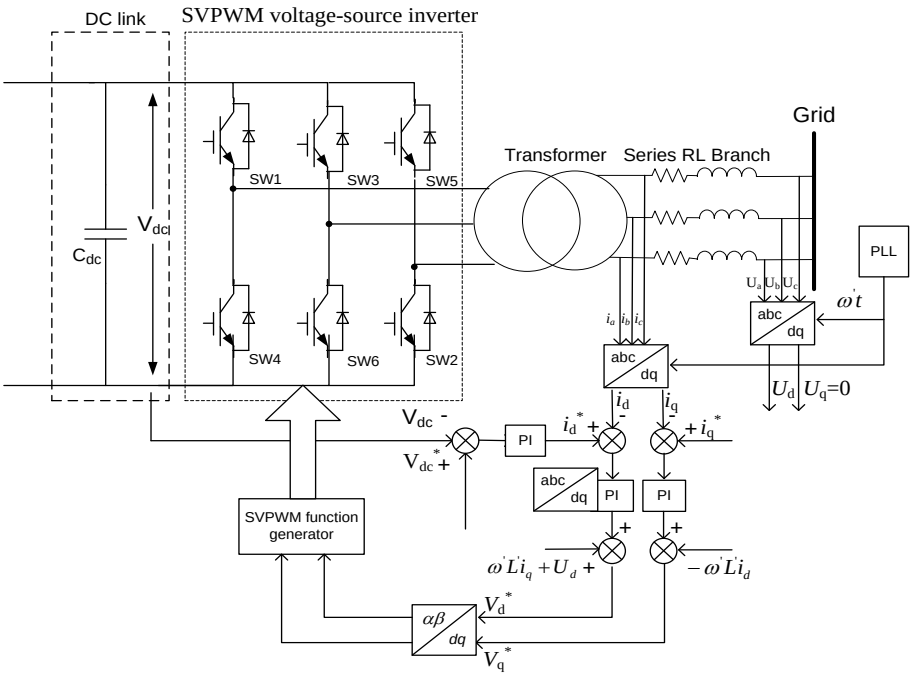

Figure 2.11 Diagram of SVPWM control inverter scheme (Luo *et al*., 2008)

Figure 2.11 shows the diagram of SVPWM control inverter scheme. Double control

loops are employed, outer control loop is voltage loop and inner one is current loop. Outer loop delivers the difference between target and instantaneous DC link voltage to a PI controller to adjust the d axis current for active power control. This makes sure that the power coming from the converter is directly injected into the grid. Similarly, the inner loop controls the reactive power through the PI controller regulated q axis current. The second channel provides a voltage reference to the SVPWM function generation which is added rotational electromagnetic field compensation terms (Thongam *et al*., 2009). Since such study requires a complete modeling of the power electronic system in an electromagnetic transient software environment, Simpower is chosen. With the rich and ready-to-use module library, this software is specifically designed to simulate very closely the behavior of typical systems in actual operation (Rahman and Varma, 2011).

2.4 The simulation study on the wind turbine system

Based on the sub-models introduced above, a complete wind turbine system could be built in Matlab/Simulink. Figure 2.12 shows the block diagram of the system model for Simulation. It includes the wind turbine blades, drive train, PMSG and SVPWM modules.

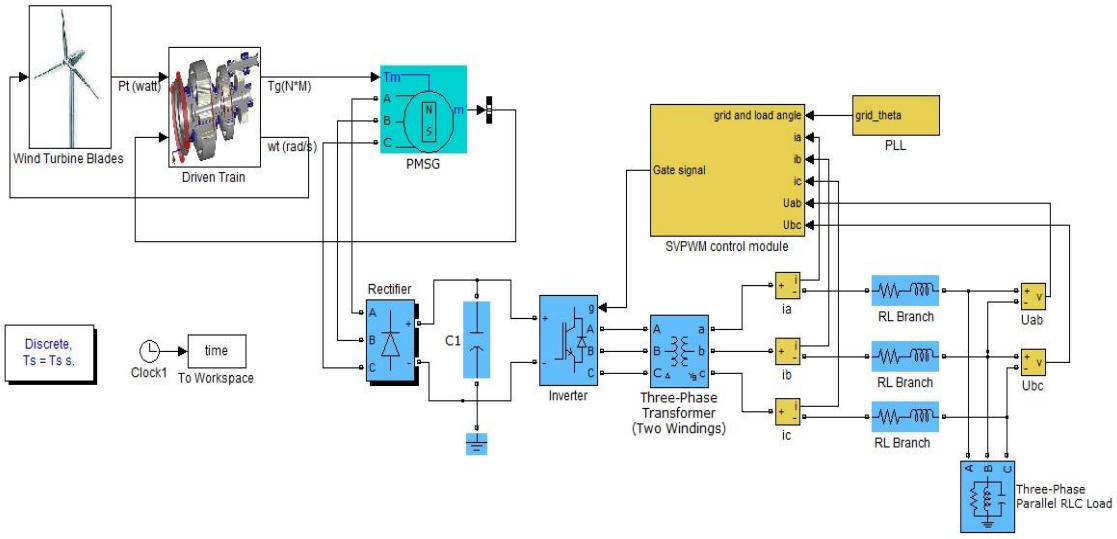

Figure 2.12 Simulink block diagram of the wind turbine system

From the modelling point of view, the following simplifying hypotheses are considered:

- The variable pitch control scheme is not activated during model test. The turbine blade pitch angle is always constant 0 degree.
- The density of air flow is a constant.
- The wind turbine yaw system is not considered. The turbine will always head into the wind.
- The connected electric load is a constant load with 2 kW active power.
- The 3 phases in Y connection are perfectly balanced.

The parameters for the wind turbine system simulation are shown in Table 2.4.

Table 2.3 The parameters of the wind turbine simulation

Symbol	Description	Value
J_G	Generator inertia	0.000227 kg× m^2
$L_d L_q$	Generator Stator inductance	0.002075 H
p_G	Generator poles	2

ε	Generator EMF flux	1.08 Wb
F_G	Generator friction factor	0.004 N × m × s
R_S	Generator stator resistance	1.3 ohm
ς_T	Turbine gearbox ratio	1/6
r_T	Turbine blade radius	1.7 m
θ_p	Blade pitch angle	0 degree
B_{eq}	Drive train system damping ratio	0.005
J_G	Turbine inertia	5 kg × m^2
ρ_a	Air density	1.25 kg/m^3
η_T	Drive train system efficiency	0.97
C_{dc}	DC link capacitance	3 × 10^3 F
T_{tran}	Transformer power rating	3000 W
R_g	Equivalent resistance of utility grid	6 Ohm
L_g	Equivalent inductance of utility grid	5 × 10^{-4} H
	SVPWM switching frequency	2000 Hz
	Utility frequency requirement	50 Hz
	Utility voltage requirement	230 V (RMS) 325 V

The PMSG parameters used in the simulation are validated through comparing the step input open-loop dynamic system responses which are obtained from both experiments and simulation (for details, referring to Chapter 6).

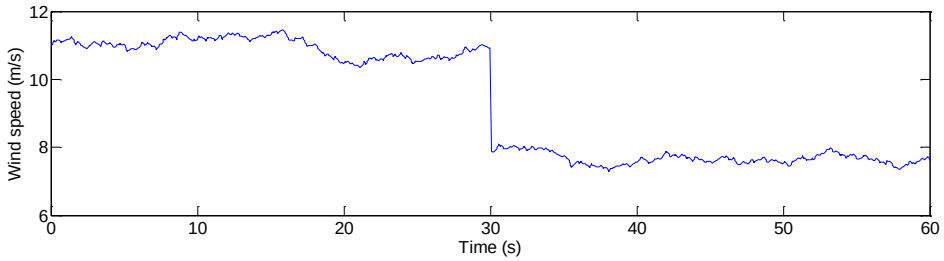

Figure 2.13 Simulated wind speed profile

Figure 2.10 shows the input wind speed. In the simulation study, the given wind speed steps down within a 60 seconds' time series observation window, that is, the mean speed drops from 11 m/s to 8 m/s at the time of 30 seconds. The wind speed profile is simulated based on Equation 2.1 and 2.2, to describe the wind speed change in a certain period.

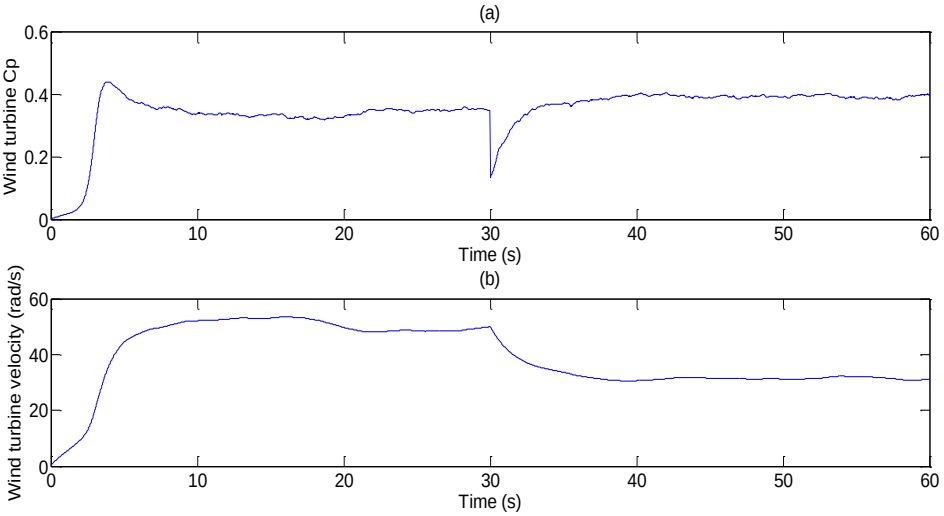

Figure 2.14 Wind turbine operation statuses

Figure 2.11 demonstrates the wind turbine running performance; (a) is the C_p curve and (b) is the turbine velocity. The higher power coefficient indicates higher energy conversion efficiency. In this simulation case, C_p drops dramatically at the 30 second, due to the sudden changing wind speed. Apart from this, the C_p value are quite steady with few changes, because the tip speed ratio does not vary too much.

Similarly, the turbine speed is also smooth even under the wind speed fluctuations resulted from the system's high inertia mass.

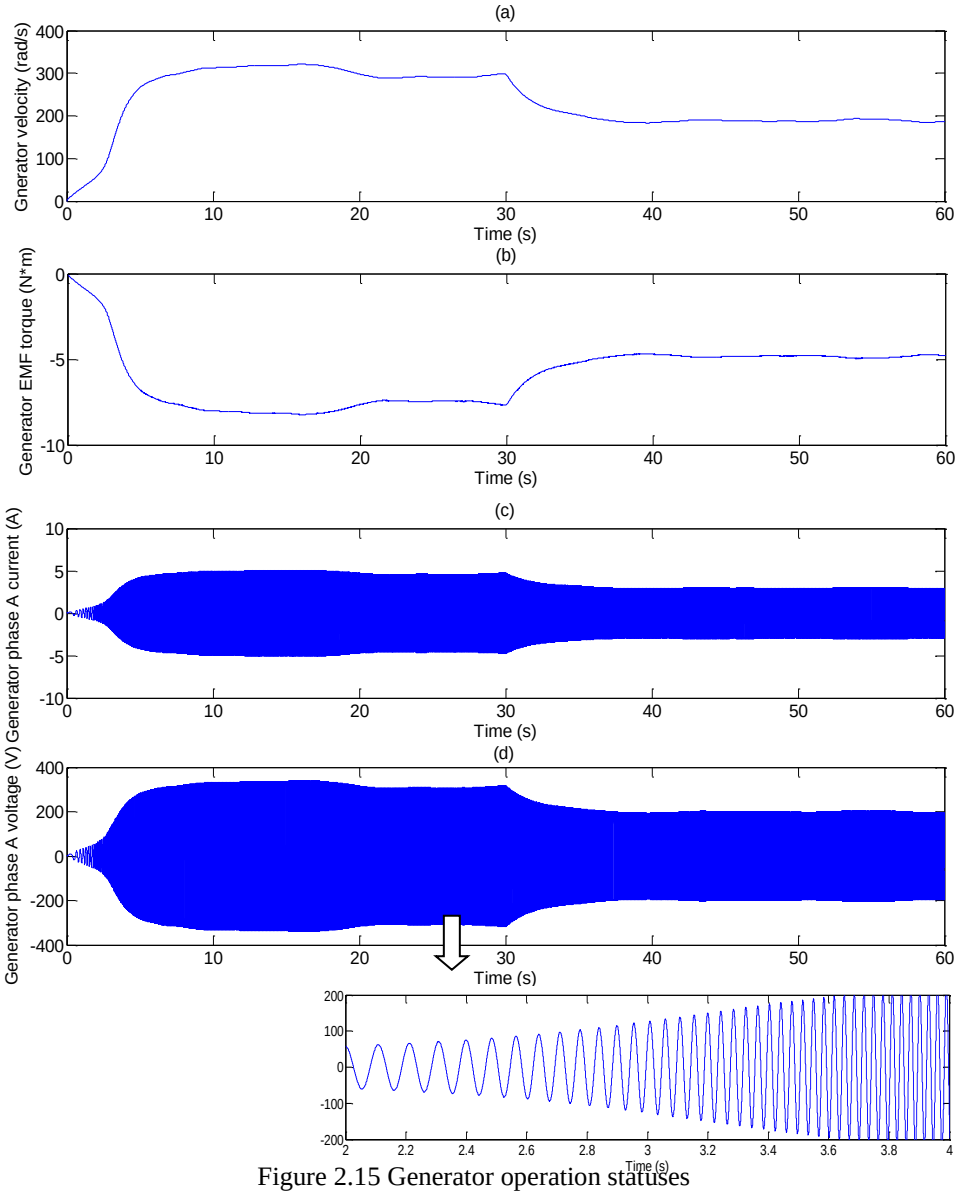

Figure 2.15 Generator operation statuses

The simulation results of generator dynamics are given in Figure 2.12; (a) is the generator rotating velocity, (b) is the electromagnetic field torque, (c) is the stator current of phase A, (d) is the stator voltage of phase A. It can be easily seen that the velocity of generator is proportional to that of the turbine rotor; the ratio is dependent

on the gearbox. The electromagnetic field torque works as load, driving by the high speed shaft. According to (c) and (d), the phase B and C have the same waveform that is offset by 120 degree, as it is a balanced three-phase system. It is noticed that the frequency and amplitude are changing due to the wind speed variation.

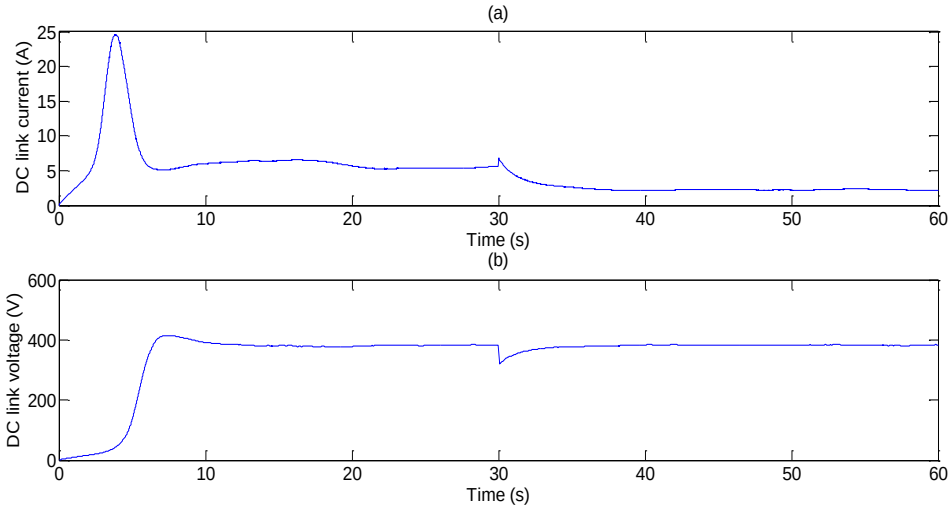

Figure 2.16 DC link current and voltage

Figure 2.13 (a) and (b) show the DC link current and voltage, respectively. The voltage is well maintained at a certain value, obtained by the SVPWM active power control. However, the sharp cutoff of DC voltage is still not recovered originated from the rapid decline of wind power.

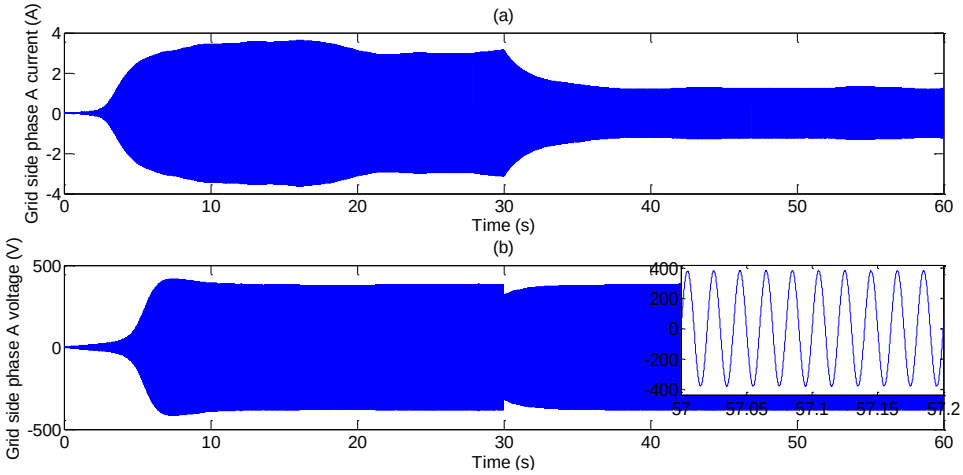

Figure 2.17 Grid side Phase A current and voltage

In Figure 2.14, it shows the current and voltage of Phase A on utility grid side. It can be seen that the voltage from SVPWM controlled inverter is perfect sine waveform with 50 Hz frequency and 311V amplitude, which can fit the utility electricity network.

2.5 Summary

This chapter focuses on the study of modeling of the wind turbine system. It is obtained that the wind power is in proportion to the cubic of the wind speed. The generator power output could fluctuate apparently because of the natural wind variability. It is highly desired to apply alternative technology to alleviate this impact. Based on the simulation work, the technical performance and dynamic responses of wind turbine are investigated. This system model is essential to understand the characteristic of the wind power generation and in the following chapters, it will be employed in the modeling of the complete hybrid system.

Chapter 3

Review of Compressed Air Energy Storage (CAES)

This chapter contributes to the review of compressed air energy storage (CAES) systems/technology. It begins with an overview of different energy storage technologies, including batteries, fuel cells, flywheels, pumped hydroelectric energy storage, superconducting magnetic energy storage and supercapacitors. While various aspects of CAES system are emphasised in detail. To serve the study of the hybrid wind turbine system, three different types of small scale energy storage technologies are placed in a group for comparison.

3.1 Overview on energy storage technologies

For the past decade, it is envisaged the rapid growth of power generation using decarbonised energy sources and dramatic increase of penetration in renewable energy to the power network. Although the renewable energy, such as wind, seems to be abundant and technologies on generation systems are constantly progressed, the major distinguished feature compared with traditional fossil fuel power generation is their intermittency. With the increased penetration of intermittent renewable energy power generation to grid, a great challenge present in maintaining load balance as the power generation need to match the load demand variations in the time scales of

seconds, minutes, hours, days and seasons. A wide range of efforts has recently been put into flexible power network for load balancing in the contexts of "Smart Grid". With improved metering and control methods, the consumers and industrial appliances would communicate with the utility using digital means, and could be switched on and off by the utility to run at off-peak hours. Then it is expected to provide one of possible solutions through efficient load management by shifting the demand to the period of renewable generation in operation (Taylor and Halnes, 2010). Apart from "Smart Grid", it is well recognised that energy storage is in the strong position and a promising mean to address the challenge.

Hybrid connection of a variable renewable power generator with energy storage could provide firm, dispatch-able power and alleviate the stability threats to power grid arisen from integration of renewable energy. From the current available technology, it is still hard to directly store massive quantity of electricity (Ibrahim, Ilinca and Perron, 2008). An energy storage system normally needs to convert the surplus electrical energy generated from a variety of sources, which usually has to be wasted in conventional power system, into other form of storable energy. Then the stored energy can be used to compensate the power generation when the period of peak demand is encountered. So the power transmission and distribution facilities are able to operate at their full capacities during peak times without worrying about the load/demand fluctuation. Then, it is not necessary to extend power network capacity to meet the peak demand; this will help increase the facility usage and decrease the need for new or upgraded facilities. Besides, storing energy for short time periods can also work as

uninterrupted power supply (UPS) and back-up power usage whenever the main power supply fails. Additionally, energy storage could also assist power systems to smooth operating fluctuations.

The storage technologies that answer to specific technical and economic criteria, which considerably vary depending on their applications and needs, can be grouped into different types. The following subsections will provide brief descriptions to various types of electrical energy storage methods, some of which are already in use, while some are still under research and development.

3.1.1 Battery

Battery converts and stores electrical energy in the form of chemical energy, through the reactions generated in electrochemical components of the battery. It is common to build a battery with a set of multiple cells, connected in series or in parallel or both, in order to achieve the desired voltage and capacity. And each cell is made up with three segments: electrolyte, a positive electrode (anode) and a negative electrode (cathode). During discharge, electrochemical reactions occur at the two electrodes generating a flow of electrons through an external circuit. The reactions are reversible, allowing the battery to be recharged by applying an external voltage across the electrodes (Chen *et al*., 2009).

The main advantage of this technology is that it is readily available. Many types of batteries are now mature technologies. In fact, research activities involving Lead-Acid batteries have been conducted for over 140 years (Díaz-González *et al*., 2012). Battery is ideally suitable for electrical energy storage applications, as it can be easily

engaged with grid through power electronic utilities. It has rapid responses to load changes and is compatible with different power sources, thus ensuring the power system stability. Batteries usually have relatively small standby losses so have higher energy efficiency (60–95%) (Kondoh *et al*., 2000) (Kluiters *et al*., 1999). However, large-scale utility battery storage systems are rare developed so far, simply because it is difficult to achieve the economic viable large storage due to the battery's weaknesses in low energy density, small power capacity, high maintenance cost, limited cycle life and decreasing health state. Moreover, most batteries contain toxic materials (Chen *et al*., 2009), which may cause environmental harm if they are not recycled properly.

3.1.2 Fuel cells—hydrogen energy storage

Fuel cells, operating with hydrogen or hydrogen-rich fuels, convert stored chemical energy into electrical energy. Different from batteries that only store charged energy, fuel cells can produce electricity continuously as long as fuel and air are supplied (Edwards *et al*., 2008). The most common and preferred resource for fuel cells is hydrogen. There are two attractive features of hydrogen. First, Hydrogen-powered fuel cells emit only water and have effectually no pollutant emissions, even nitrogen oxides, because they can react with oxygen at relatively low temperatures. Second but the most important, the energy density of hydrogen is much higher compared with any other common fuels. The higher and lower heating values of common fuels are listed in Table 3.1.

Table 3.1 Heating values of common fuels (U.S. Department of Energy, 2001)

Fuel	Higher Heating Value (at 25 ºC and 1 atm)	Lower Heating Value (at 25 ºC and 1 atm)
Hydrogen	141.86 kJ/g	119.93 kJ/g
Methane	55.53 kJ/g	50.02 kJ/g
Propane	50.36 kJ/g	45.6 kJ/g
Gasoline	47.5 kJ/g	44.5 kJ/g
Diesel	44.8 kJ/g	42.5 kJ/g
Methanol	19.96 kJ/g	18.05 kJ/g

Both the higher and lower heating values indicate the quantity of energy for a certain weight of fuel. Hydrogen has the highest energy-to-weight ratio of any fuel since hydrogen is the lightest element and has no heavy carbon atoms. Hydrogen has an average energy density of 130.89 kJ/g, while the next highest of available energy source option is gasoline, with an energy density of 46 kJ/g (U.S. Department of Energy, 2001).

Several types of fuel cells suitable for different energy applications with varying power scales have been developed, sharing the foundamental design of two electrodes (anode and cathode) separated by a solid or liquid electrolyte or membrane, as described in Figure 3.1. Hydrogen (or a hydrogen-containing fuel) and air are fed into the anode and cathode of the fuel cell, and the electrochemical reactions assisted by catalysts take place at the electrodes. The electrolyte enables transport of ions between the electrodes while the excess electrons flow through an external circuit to provide electrical power (Edwards *et al*., 2008).

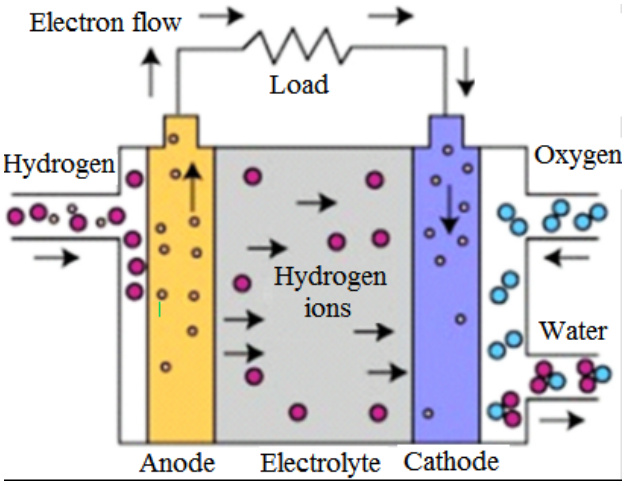

Figure 3.1 Composition of a fuel cell (Ibrahim, Ilinca and Perron, 2008)

Various types of fuel cells are classified depending on the nature of their electrolyte, including the polymer electrolyte membrane fuel cell (PEMFC), alkaline fuel cell (AFC), molten carbonate fuel cell (MCFC) and solid oxide fuel cell (SOFC). These different types of fuel cells vary in their electrolyte composition, operating temperature, and a range of applications (Neumiller, 2006). However, combining an electrolyser and a fuel cell for electrical energy storage is a low-efficient solution (at best 70% for the electrolyser and 50% for the fuel cell, and 35% for the combination. As well, the investment costs are prohibitive and life expectancy is very limited, especially for power network applications (Ibrahim, Ilinca and Perron, 2008). A possible method to increase roundtrip efficiency would be a move towards steam electrolysis which has much greater efficiency, but this is not currently a commercially available technology (Strbac *et al*., 2012).

3.1.3 Flywheel

A flywheel stores energy in a rotating mass. Depending on the inertia and speed of the

rotating mass, a given amount of kinetic energy is stored as rotary energy. Usually, flywheels are composed of metal with large mass in order to increase the rotary inertia and subsequently store kinetic energy. In fact, the energy stored by the flywheel is dependent on the square of the rotating speed and its inertia. The flywheel is placed inside a vacuum containment to eliminate friction-loss from the air and suspended by bearings for a stabile operation. Kinetic energy is transferred in and out of the flywheel with an electrical machine that can function either as a motor or generator depending on the load angle (phase angle). When acting as motor, electric energy supplied to the stator winding is converted to torque and applied to the rotor, causing it to spin faster and gain kinetic energy (Bolund *et al*., 2007). The entire energy stored by a flywheel system is a function of the rotor size and velocity, and the power out rating is dependent on the electrical machine. In generator mode kinetic energy stored in the rotor applies a torque, which is converted to electric energy (Chen *et al*., 2009). Figure 3.2 demonstrates the basic structure of a flywheel energy storage system.

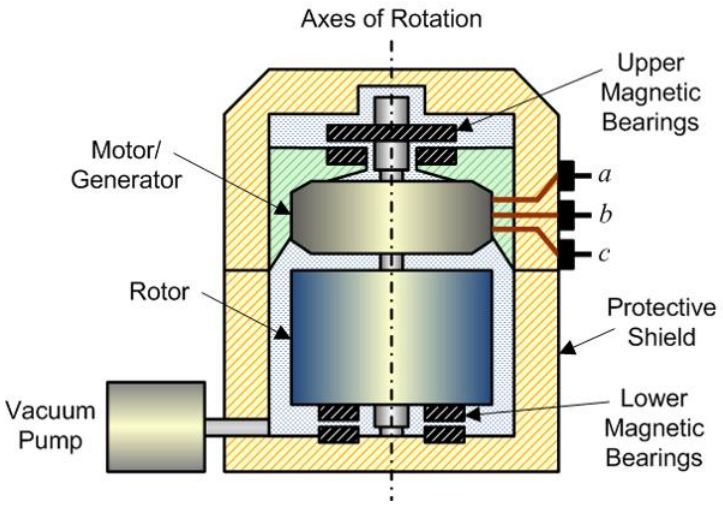

Figure 3.2 Basic structure of a flywheel energy storage system (Molina, 2010)

To store energy in an electrical power system, high-capacity flywheels, with either high velocity or large mass, are needed. However, the large mass system could cause high friction losses, thus to reduce the overall efficiency. Friction losses of a 200-tons flywheel are estimated at about 200 kW. Using this hypothesis and instantaneous efficiency of 85%, the overall efficiency would drop to 78% after 5 h, and 45% after one day. Long-term storage with this type of apparatus is therefore not foreseeable. The flywheels are preferred to be applied on short duration/high power applications (e.g. 100 s of kW/ 10 s of seconds). The current application of flywheels of all designs is to provide high output voltage assistance to components or machines during a power surge or a shutdown (Neumiller, 2006).

Kinetic energy storage could also be used for the distribution of electricity in urban areas through large capacity buffer batteries, comparable to water reservoirs, aiming to maximize the efficiency of the production units. For example, large installations made up of forty 25 kW–25kWh systems are capable of storing 1MW that can be released within 1 h.

3.1.4 Pumped hydroelectric energy storage

Pumped hydroelectric energy storage (PHES) is usually built for large scale power system. Its operating principle is based on managing the gravitational potential energy of water, by pumping it from a lower reservoir to an upper reservoir during periods of low power demand. When the power demand is high, water flows from the upper reservoir to the lower reservoir, activating the turbines to generate electricity. The energy stored is proportional to the water volume in the upper reservoir and the height

of the waterfall (Díaz-González *et al*., 2012).

The stored energy capacity depends on two parameters: the height of the waterfall and the volume of water. Currently, PHES is one of the most effective and preferable strategies of large scale energy storage, representing around 99% of the global grid scale energy storage capacity (Strbac *et al*., 2012). From the point of view of a power network, PHES has a conversion efficiency of about 65–80%, depending on equipment characteristics ((Ibrahim, Ilinca and Perron, 2008). However, for the overall efficiency during long time operation, leakoff and sealing properties may become an issue. These problems apart, PHES has several key advantages. In general, the life time of its installations is around 30–50 years, with power capital costs of 500–1500 €/kW and 10–20 €/kW h (Kaldellis *et al*., 2007). Additionally, it is remarkable that the power generation response is significantly fast. Even if the system is completely standby, full power operating is able to recover within one minute (Neumiller, 2006). Such fast response time enables the PHES as important components to control electrical network frequency and in provision of reserve generation. The major disadvantage of this technology is that this type of storage is the lack of suitable geologic formations with limited potential for new sites. Two large reservoirs are required with a sufficiency of vertical distance to obtain enough potential energy difference. This type of scenario is so uncommon and usually exists in mountain settings where connection to a grid is not possible and construction is quite tough (Neumiller, 2006).

3.1.5 Superconducting magnetic energy storage

The Superconducting Magnetic Energy Storage (SMES) system is a relatively recent technology, which is designed to store and discharge large amounts of power instantaneously. A SMES system stores energy in a magnetic field created by a DC current flow through a large superconducting inductor at its superconducting critical temperature.

Energy storage is made possible through the superconducting material of the coil. This material type enhances storage capacity because the electric currents encounter the minimal resistance at a cryogenic temperature state. However, the characteristic to maintain minimal resistance without the temperature restraint is still currently under research and development. The idea of a SMES system was first proposed by Ferrier in 1969, but the first system was not reallised until 1986, a 5 MJ system. While, the energy stored is calculated as the product of the self- inductance of the coil and the square of the current flowing through it (Ribeiro *et al*., 2001).

Undoubtedly, a defining feature of SMES systems is their environmentally friendly characteristic because superconductivity does not yield a chemical reaction and no toxins are created (Cheung *et al*, 2002/2003). Besides, these systems are able to inject or absorb large amounts of energy in a very short time. Some experimental studies show that the power-charge of a 1 MW/1 kW h SMES can be increased in 200 kW in only 20 ms (Sannomiya *et al*., 2001). The energy capacity of these systems ranges from 100 kW to 10 MW, and it is possible to charge their rated power only for a few minutes before being discharged (Ribeiro *et al*., 2001). This technology offers high

cycle life and rapid response, but currently has a relatively low energy density and high cost, and requires external energy to constantly cool the magnet (Strbac *et al*., 2012).

3.1.6 Supercapacitors

Supercapacitors are also known as ultracapacitors or doublelayer capacitors. A normal capacitor has an energy density of 0.5 Wh/kg, while these novel supercapacitors can store four times the amount of electrical energy (Neumiller, 2006). Supercapacitors are a practical alternative for the traditional battery. Unlike batteries that store energy chemically, capacitors stores energy within an electric field. To create an electric field, the conductive parallel plates hold opposite charges that are separated by a dielectric insulator. Compared with batteries, supercapacitors are totally environmental friendly with a much longer life time, more than 5×10^4–10^5 cycles larger power density, Other important feature of supercapacitors are their high power density with virtually no maintenance and energy efficiency of about 75–80% (Helwig *et al*., 2009). However, its specific energy and energy density are low, 2–5 Wh/kg and 10,000 Wh/m^3, due to the difficulties in accessing to the porous surface of the electrode by ions (Du Pasquier *et al*., 2003) (Cericola *et al*., 2010).

3.2 Introduction on compressed air energy storage

CAES is a method that the energy is stored in the form of compressed air internal energy during the low energy demand (off-peak) periods and then is released during the high demand (peak time) period. CAES can be grouped into two categories,

according to its applications: 1) large scale application to serve power grid load balance; 2) small scale applications (such as uninterrupted power supply and grid frequency control element). CAES is a well-known controllable and mature technology with fast responses and good partial-load operation characteristics. As it derives from gas turbine technology, CAES technology is readily available and reliable. CAES has already been used in grid management applications, such as load shifting and regulation control (Succar and Williams, 2008).

Although compressed air energy systems for civic uses started operation in European cities since the 1870s and even by 1986 the Paris system had been used for the main source of house-delivered energy and other utility facilities, the concept of using compressed air as energy storage for power network was proposed until the mid of the 20th century (James, 2012). A compressed air storage system with an underground air-storage cavern was patented by S. Laval in 1949 (Ter-Gazarian, 1994). The world's first utility-scale CAES system had been installed and commissioned with Brown Boveri as the main plant supplier at Huntorf, Germany, in 1978 (Davidson, 1980). The salt dome was used as the storage cavern, with 290WM, to provide load following and to meet peak demand while maintaining constant capacity factor in the nuclear power industry (Samir, 2011) (Succar and Williams, 2008). In 1991, the 110 MW grid-scale CAES plant with a storage capacity of 2,700 MWh (full power output up to 26 hours) commenced operation at McIntosh, Alabama, US (University of California, 2012). This plant is used to store off-peak power, generate peak power and provide spinning reserves (James, 2012). In addition, to the small-to-medium scale

CAES facilities, in 2009, the Energetix Group Ltd. has developed a CAES based back up power supply for standard and custom units from 3kW to 3MW, which are available for standby and Uninterrupted Power Supply applications (Energetix Group Ltd., 2012).

There are also several large scale CAES proposals being planned or under progress. For example, a unit has been under construction to convert an idle limestone mine in Norton, Ohio. With 9.6 million cubic meters of storage, which can operate within the pressure range from 55 bar to 110 bar, the Norton Energy Storage project intends to be built in several phases, from about 270 MW to a total capacity of up to 2,700 MW (Linden, 2007). Currently the Norton CAES Project keeps moving forward (Chen *et al*., 2009).

The Iowa Association of Municipal Utilities is developing a new energy park in Dallas Center, Iowa that integrates a 75-150 megawatt wind farm with Compressed Air Energy Storage technology (Daneshi *et al*., 2010). This proposed 270 Megawatt (MW) CAES project is expected to be in service in 2015 (ISEP, 2011).

Ridge Energy Storage & Grid Services L.P. had announced to build a 4 × 135 MW system in Matagorda County, Texas, based on the McIntosh Dresser-Rand design (Samir, 2011). The proposed system aims to utilise a previously developed brine cavern. The domal salt formations have been used at the existing Huntorf and McIntosh sites, which has been proven to work well under CAES operations (Succar and Williams, 2008). In 2007, Luminant and Shell-Wind Energy announced that they would explore using compressed air energy storage for their proposed world's largest

wind farm in Texas (Energy Efficiency & Renewable Energy, 2007). However, there is no recent news to these two CAES related projects.

3.2.1 Operation principles of CAES system

a). Large scale CAES systems

Large scale CAES system technology development has experienced three generations: the first, second and the third generation. The first generation system, which is often referred to as 'conventional', is the only CAES system that is in commercial use, in Huntorf and McIntosh.

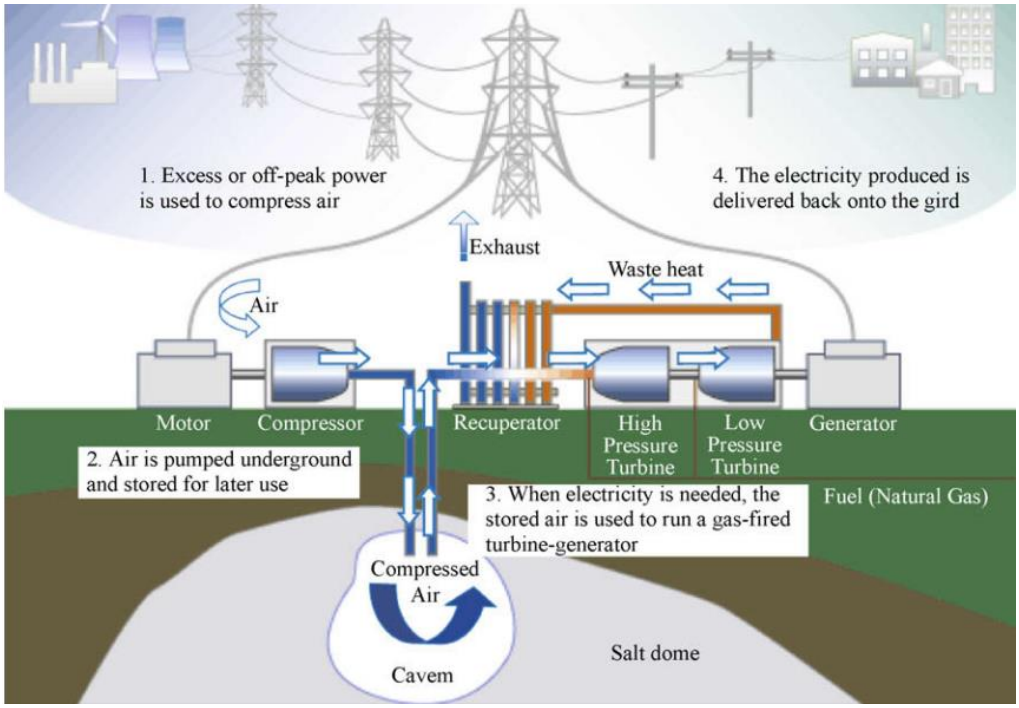

Figure 3.3 Schematic diagram of a large scale CAES system (McDowall, 2004)

A generic CAES plant design, as shown in Figure 3.3, is based on typical first generation technology. The core equipment of this CAES power plant consists of five parts: (1) a motor/generator unit combined with clutch mechanisms to provide

alternate engagement ability to the compressor and turbine trains; (2) a multi-stage air compressor unit operating with intercoolers and after-coolers to achieve the economy of air compression and to reduce the moisture content of compressed air; (3) a turbine train, which typically includes two turbines, one high pressure (HP) and one low pressure (LP) gas turbine respectively; (4) A container for storing a large volume of compressed air. Usually, reservoirs are capable to store up to 50 hours of power and operate between 950 – 1,250 psig (Ridge Energy Storage & Grid Services L.P, 2005). (5) Control and auxiliary units such as fuel storage and heat recuperator units (Chen *et al*., 2009).

The original CAES technology derives from the gas turbine technology. In a typical gas turbine cycle, the air compressor is directly driven by a gas turbine. Consequently, whenever gas is combusted in the turbine, the energy output is used for compression. CAES removes the combustion and turbine operation from the compression phase. The extracted air is directly compressed using off-peak power and then injected into a subsurface reservoir. In the existing CAES systems, the air has to be cooled down to ambient temperature during compression phase for storage. Typically, a solution-mined salt cavity, a mined hard rock cavity, or an aquifer is used for underground storage. Above ground storage in tanks is also an option, but this alternative is quite costly (Neumiller, 2006). As the air has already been compressed, a CAES turbine can generate three times the amount of electricity as a simple cycle turbine that requires connection to the air compressor (Ridge Energy Storage & Grid Services L.P, 2005). When peak time power is demanded, the compressed air is draw

by a production well. Virtually, the air need be heated to avoid freezing the components and obtain a proper operating condition during air expansion in the turbine. Currently, this is achieved through a recuperator and the burning of a fuel such as natural gas. The air with high temperature is then expanded in the turbine train; the HP turbine reduces risk by moderating operation conditions and airflow upon entrance into the LP turbine. Thus the generator is driven to produce electricity.

The second generation CAES is very similar to the first generation. However there is technical advancement in design since the first generation systems were constructed. There are many different designs, or 'hybrids', which are all based on modifications to existing gas turbines. For example, Dr. Michael Nakhamkin have patented two second generation CAES system design, respectively integrated with 'extracted from expanders' air injection and inlet chilling technologies (Nakhamkin, 2010), as described below:

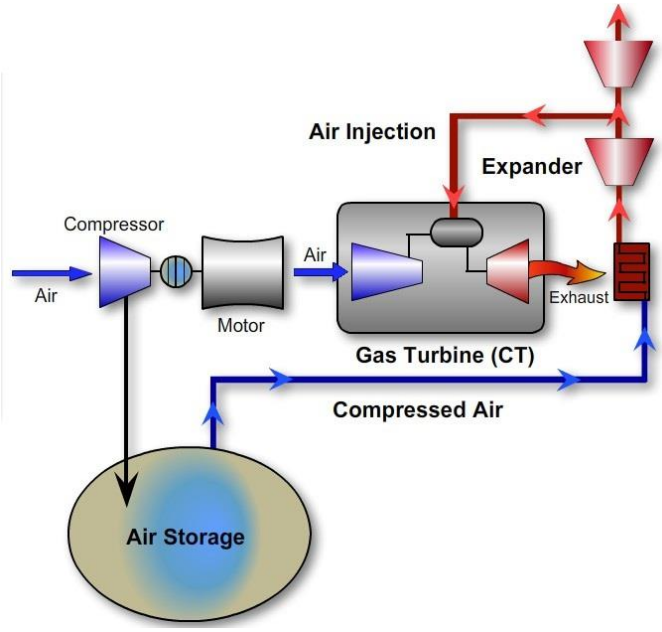

Figure 3.4 Schematic of the second generation CAES with air injection

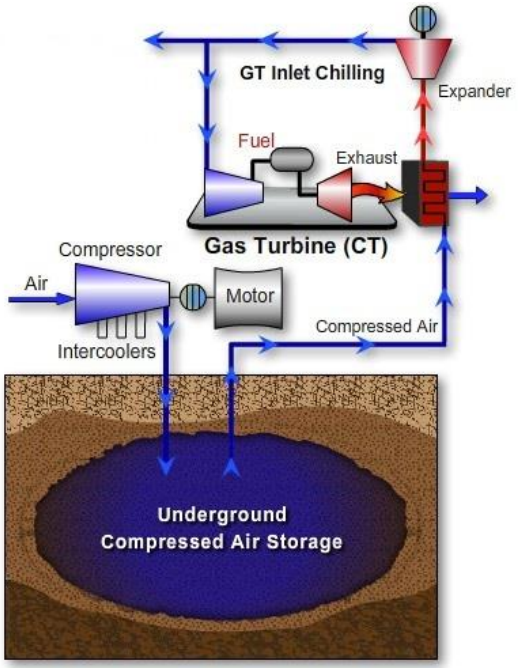

Figure 3.5 Schematic of the second generation CAES with inlet chilling

The advantages of the second generation CAES consist of optimizing the system unit to march the smart grid and renewable energy requirements, such as eliminating switchover time limitations by decoupling the compression and turbo expander train, leveraging existing power plant infrastructure, etc.

It can be seen that fuel is combusted during generation for capacity, efficiency and operational considerations during the first and second generation system's operating. It also means that the traditional CAES plants are not completely pollution free (Greenblatt *et al*., 2006).

Theoretically, it is feasible to store the heat generated by compression separately from the air itself (Bullough *et al*., 2004). The compressed air enters the turbine train during the discharging phase without being heated by natural gas combustion, which entirely eliminates the need with fuel in a CAES facility. This would remarkably decrease CO2 emissions. Thus is the proposed third generation system. Third

generation, also known as adiabatic, CAES systems involve no combustion cycle during the discharging phase. Thermal energy storage is integrated to cool the compressors and heat of the stored air for power production. During the charging phase, 'cold oil' is used to intercool the compressed air, and produce 'hot oil' for use during power production. This 'hot oil' is then used to heat the stored compressed air from the storage reservoir before compressed air enters the air turbine for power generation (Nakhamkin, 2010). It can be considered as a hybrid of CAES and thermal energy storage. These systems are still in a research and development stage, primarily due to technology issues related to heat storage. The most featured benefit of this system is zero carbon emissions as there is no fuel consumption required in the turbine section (Taylor and Halnes, 2010). Figure 3.6 shows an example of this type of system.

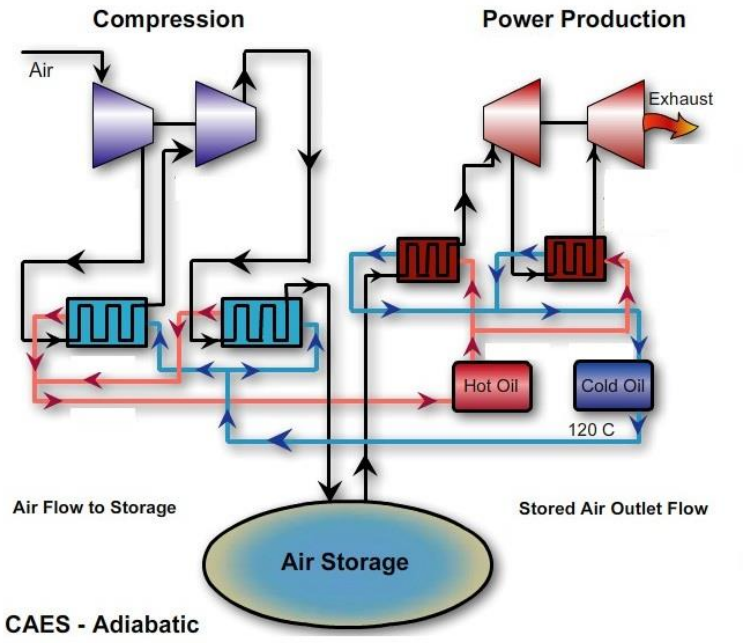

Figure 3.6 Third generation CAES diagram

b.) Small scale CAES systems

There has long been recognition that the CAES is only suitable for large scale power systems for a variety of reasons, mainly with two fields. First of all, integration of the electricity generation systems and compressed air systems is a kind of electrical connection. For example, during a full charge and discharge cycle, the compressor is driven by the excess electricity and compensated energy is finally converted into electricity and then injected into power grid. In this way, large-capacity power electronic systems are unavoidable for electricity transmission, which are neither cost effective nor power effective for small scale systems. Secondly, the fuel combustion systems in the first and second generation system and even the thermal energy storage in the third generation CAES are also unrealistic in small scale power network. Without that, the discharging phase could not run at the optimised state, which may greatly impact the overall efficiency.

However, with the technology development of pneumatic actuators, the CAES system structure can be miniaturised under the promises of efficiency. Such kind of small scale CAES concept has successfully built by the UK Company Energetix Group, Pnu-Power – compressed air UPS systems. The working principle of Pnu-Power systems is of using compressed air stored in tanks to power an energy efficient scroll air motor (scroll expander) then to drive an electricity generator to produce AC or DC electrical power for back-up power usage. Compared to the existing Huntorf and McIntosh CAES plants, the Pnu-Power system does not have a combustion process during the discharge phase. Energetix Group claimed that there

have a number of benefits from Pnu-Power systems, such as low initial and maintenance cost compared to conventional UPS/standby batteries, lower energy usage in standby model and outstanding power reliability than flywheels and batteries, relatively high efficiency mainly due to adopting the energy efficient scroll expender, consistently giving high efficiency performance, and etc (Wang *et al*., 2011) (Energetix Group Ltd., 2012).

Figure 3.7 Schematic diagram of Pnu Power device (Energetix Group Ltd., 2012)

After the first commercial Pnu-Power UPS launched in 2009, it has been proven that this type of systems can be considered as an alternative to the traditional small scale energy storage systems such as batteries and mechanical flywheels for industrial applications. Energetix Group now can design and manufacture small-scale standardised compressed air back-up power systems, also known as compressed air batteries, with capacity range of 3, 5, 10, 20, 100 and 200 kW (Energetix Group Ltd., 2012). Energetix Group can also produce relatively large-scale containerised 1 to 3 MW Compressed Air Diesel Rotary UPS Systems. Such systems have been successfully applied as data centre UPS solutions. On August 13th 2012, the

Cooperative Bank's Pyramid building in Stockport U.K. has become the first major data centre in the world to use a compressed air electricity generating system produced by Energetix Group to supply back-up power (Airuser, 2012). In recent years, Pnu-Power UPS has been widely adopted by companies including UK National Grid and USA, Telecom Italia (Italy), Eskom (South Africa), ATK (USA) and Harris (USA) (Energetix Group Ltd., 2012).

Based on the scroll air expender technology, a novel hybrid wind turbine system is proposed which engages compressed air energy storage directly with the power generation mechanism. As shown in Figure 3.8, the energy stored in compressed air is released through a mechanical transmission system. This direct electromechanical integration offers simplicity in design and higher efficiency. Also, the direct compensation of torque variation of the wind turbine will alleviate the stress imposed onto the wind turbine mechanical parts. This concept is promising for using small scale CAES in power generation from wind from both the simulation and experimental studies conducted in this project.

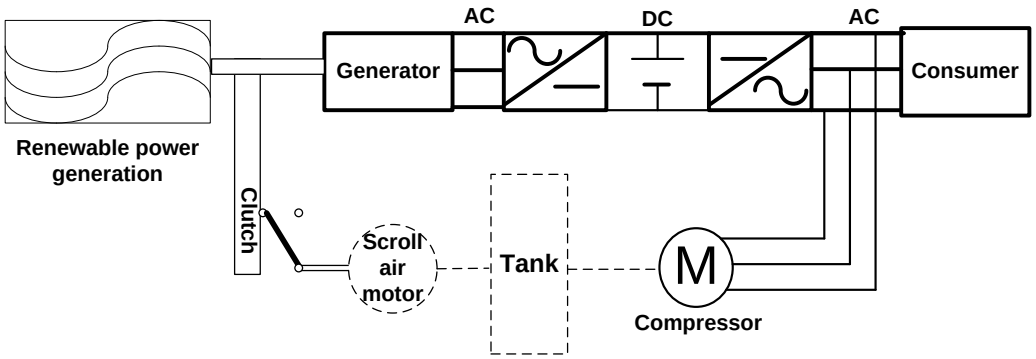

Figure 3.8 Small scale CAES system scheme

3.2.2 Energy transfer analysis

CAES system is electromechanical energy storage and conversion system in which the stored energy is obtained by increasing the enthalpy of air mass, caused in turn by a higher pressure (Martínez, 2010). During the charging phase, the electrical power is consumed by compressor driving motor, mechanical power is delivered to the compressed air, thus most of kinetic power is converted and stored in the compressed air. Then the compressed air is sealed in underground cavern or cylinders or tanks as a stable storage. During discharging phases, an air motor/expander is capable of restoring the energy carried by the compressed air to mechanical kinetic energy to drive a generator rotating. For such an energy conversion and transmission process, energy losses are inevitable, such as heat losses during compression and mechanical losses due to friction, vibration and etc. For the small scale CAES system, the energy transmission and conversion is schematically shown in Figure 3.9.

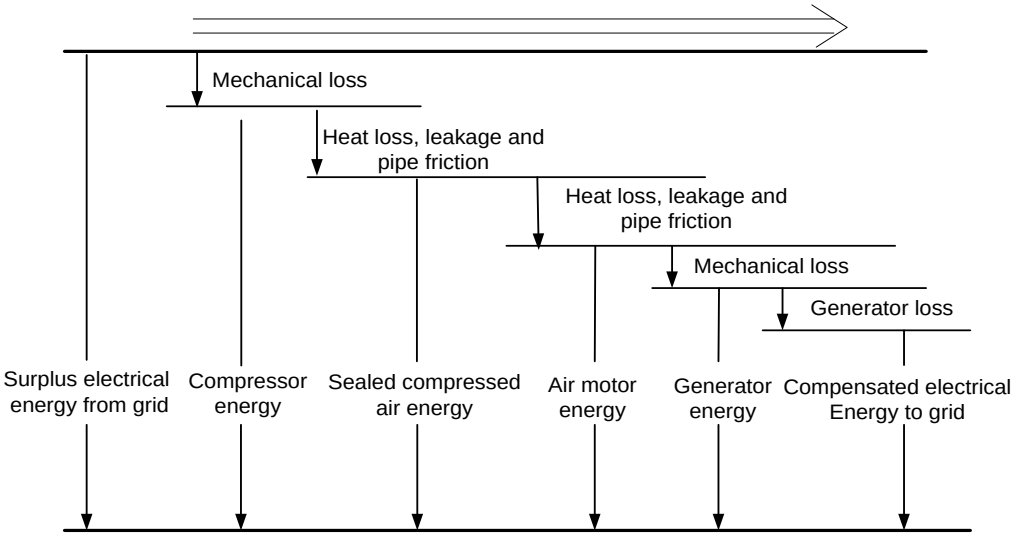

Figure 3.9 Processes of energy transfer and conversion in small scale CAES

In the first and second generation CAES systems, the combustion cycle in the discharging phase can be considered as an external energy input, also with a certain amount of energy losses. In this way, the CAES may compensate more energy depending on energy contributed by input fuel. Their energy flow diagram can be described by Fig 3.10:

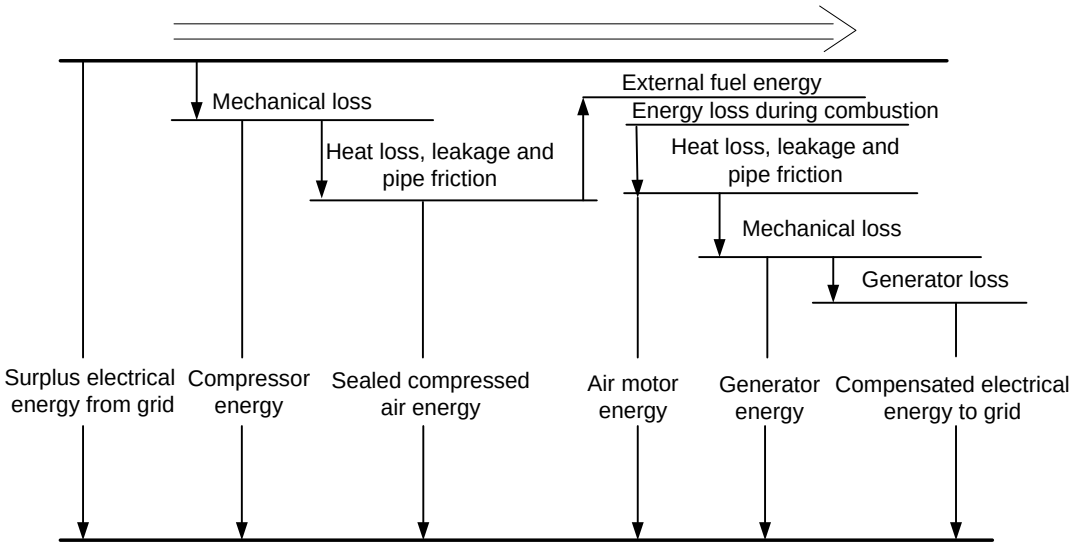

Figure 3.10 Processes of energy transfer and conversion in CAES with combustion cycle

While in the third generation CAES systems, the heat losses during the charging phase is partially stored as thermal energy, which is reused to heat the compressed air in the discharging stage. The thermal energy recycle will improve the roundtrip system efficiency. A comparative energy flow diagram is also demonstrated in Figure 3.11:

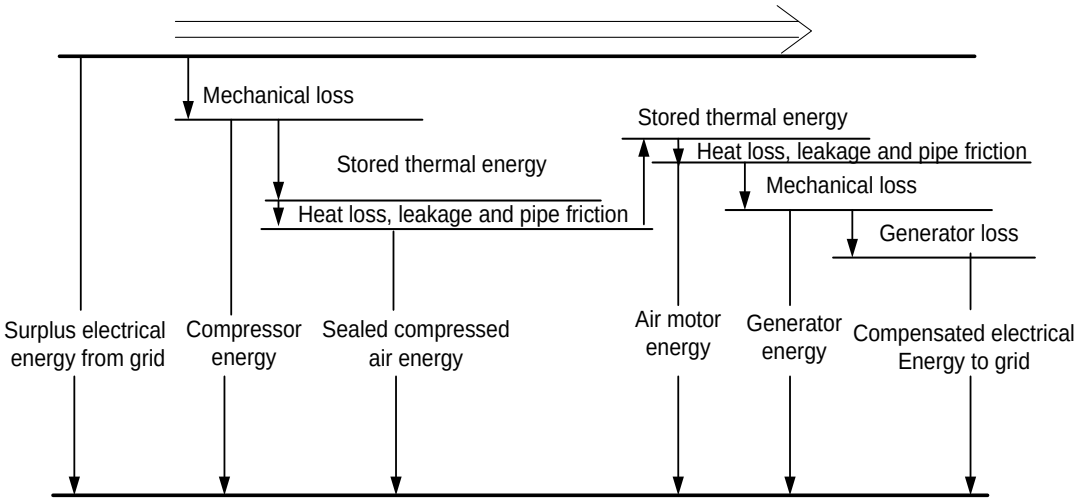

Figure 3.11 Processes of energy transfer and conversion in CAES with thermal energy storage

3.2.3 Energy management analysis

Generally, the total compressed air energy sealed in cavern/cylinder represents the energy capacity of a CAES system. In this respect, the available energy of compressed air can be defined as the amount of energy that can be delivered by compressed air under the atmosphere pressure. This available energy is a relative quantity, along with the factual basis that the CAES system is operated under the atmospheric condition. This available energy can be obtained using the equation (3.1) (Cai and Kagawa, 2001):

$$E = pV[\ln \frac{p}{p_{atm}} + \frac{\kappa}{\kappa+1}(\frac{T-T_{atm}}{T_{atm}} - \ln \frac{T}{T_{atm}})] \quad (3.1)$$

where, E is available energy of compressed air, p is pressure of the stored compressed air, V is volume, κ (specific heat ratio of air) equals 1.4, T is temperature in Kelvin unit, subscript atm means atmosphere condition.

From this equation, the energy stored in 1 m^3 volume compressed air can be calculated in diverse pressure and temperature conditions, as shown in Figure 3.12.

For the convenience of reading, the temperature axis is in ^{o}C unit.

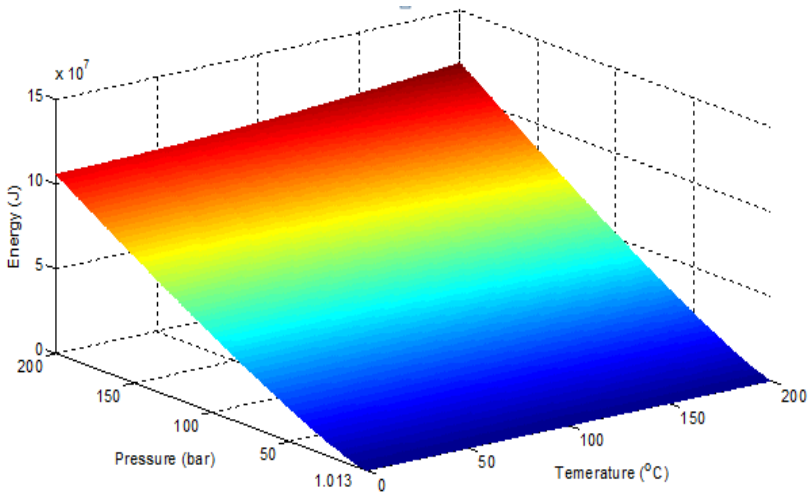

Figure 3.12 The compressed air energy in 1 m^3 volume

For instance, with the conditions: pressure 50 bar, temperature 20°C and volume 1 m^3, the available energy of compressed air is 5960 KJ (1.6555 kWh), which makes the compressed air can be managed within the same unit. Applying this equation, the input energy of CAES plant can be quantitatively analysed.

Also, the energy density can be converted in the mass unit according to the ideal gas law.

$$pV = \frac{m_g}{M_g} R_a T \tag{3.2}$$

where, m_g is the mass of gas and M_g is the molar mass of gas, then $\frac{m_g}{M_g}$ equals the moles number that is a constant. R_a equals 8.314, which is the ideal gas constant.

It is worth noting that the energy density of compressed air per mass unit is only proportional to its absolute temperature, not related to the volume and pressure. For the example mentioned above, the mass of compressed air is 59.46 kg. So, its energy

density is 100.26 KJ/kg.

3.2.4 Energy efficiency analysis

The energy performance of a conventional fossil fuel power plant is easily described by a single efficiency: the ratio of electrical energy generated over the thermal energy from the fuel. Similarly, some storage systems such as electrochemical or pumped hydroelectric storage are typically characterized by a roundtrip electrical storage efficiency η_{RT} defined as:

$$\eta_{RT} = (electrical\ \ energy\ output) \Big/ (electrical\ \ \ energy\ \ input) \tag{3.3}$$

However, the situation is more complicated for the efficiency calculation of CAES system. Mainly because the electricity input varies depend on different situations:

a) The first and second generation CAES

On one hand, electricity is used to drive the compressors and on the other hand natural gas or oil is burned to heat the air prior to expansion. This situation makes it difficult to describe CAES performance via a single index in a way that is universally useful due to the presence of two very different energy inputs (Succar and Williams, 2008).

Here, the input electrical energy calculation should be defined as:

$$electricity\ \ input = E_{compressor} + \eta_{ng} \times E_{ng} \tag{3.4}$$

where, $E_{compressor}$ is the energy consumed by compressor; the second term is the amount of electricity that supplied by a stand-alone power plant at efficiency η_{ng} that is used to fire a CAES unit, E_{ng} is the total fuel energy consumed (Succar and Williams, 2008).

This methodology has the advantage of providing an electricity-for-electricity

roundtrip storage efficiency that isolates the energy losses in the conversion of electricity to compressed air and back to electricity. CAES is typically in the range 66-82% (Succar and Williams, 2008). Referred to Electric Power research institute's report, the McIntosh, Alabama CAES plant consumes 2.5 MJ of electricity and 1.2 MJ lower heating value (LHV) of gas for each megajoule of energy output (Pollak, 1994). While the parameters for the natural gas plant applied in McIntosh is 6.8 MJ, at 53% thermal efficiency (Wiki-Compressed air energy storage, 2012). Thus, depending on the index chosen for its measure, the roundtrip efficiency for McIntosh CAES power plant:

$$\eta = \frac{1\times10^6}{2.5\times10^6 + 1.2\times10^6 \times 53\%} = 31.9\%$$

b) The third generation large scale CAES and small scale CAES

Since there is no external energy input in such kind of systems, the electricity input is purely the surplus electrical power from grid. Equation 3.3 can be employed directly for efficiency calculation; the ratio is directly related to the energy storage efficiency. The theoretical efficiency could approaches 100% with perfect heat transfer during its operating. However, neither of these ideal thermodynamic cycles is virtually achievable due to the unavoidable heat losses. Actually, the roundtrip efficiency of adiabatic CAES is expected to be 70% (Wiki-Compressed air energy storage, 2012). It varies depending on different scales and designs.

In summary, CAES system can be employed in a wide power and energy range of electrical networks and the typical power rating is approximately within 3 kW to 430 MW (Chen *et al*., 2009) (ConvenEnergy Storage & Power LLC, 2012) (Energetix

Group Ltd., 2012). And the energy rating varies from 580 to 2860MWh (Ridge Energy Storage & Grid Services L.P., 2012). The specific energy density is approximate 100 KJ/kg depending on it storing temperature. The life time is from 20 to 40 years and the cycling capability is from 104 to 3×104 (Chen *et al*., 2009) (Denholm *et al*., 2004) (Díaz-González *et al*., 2012). CAES system is capable of energy management, bridging power and power quality applications due to its wind range of suitable storage duration which can be from a few hours to several months even over one year with quite tiny self-discharge per day.

3.3 Small scale energy storage options for hybrid wind turbine project

In this project, the feasibility of energy storage for 2 kW household small scale wind turbine is analysed. Battery, flywheel and CAES are chosen in prior, as these three are most common mature energy storage technologies for small scale applications without environmentally harmful emission.

Considering the project length and lab conditions, the following factors are considered in prior as rational: technical maturity, capacity and power rating, service time and cycle time, energy efficiency, energy density, capital cost, maintenance. The chosen technology should be mature with high performance. The performance parameters of the storage systems are compared in detail based on the "performance index" which is defined by technical performance more relevant to the hybrid wind turbine operations.

3.3.1 Technical maturity

The battery, especially the lead-acid battery, has been applied for over 100 years. In the small scale energy storage field, it is the most mature technology. While, even though flywheel and CAES are well developed in the recent decades with some commercially available products; they are still not widespread accepted by the public as battery technology. Their reliability and stability need more R&D by the electricity institute and industry.

3.3.2 Capacity and power rating

The capacity of battery is directly related to the active material in the battery. As the electromotive force of a single battery cell provides only about two volts voltage due to its electrochemical characteristics and enormous amount of cells therefore are required to be connected in series/parallel to obtain a higher energy capacity. And the electric load will determine the battery's output power rating. For the compressed air system, the capacity correlates to the volume of the air storage tank, the power rating is determined by the pneumatic drives. The capacity of flywheel system depends on the inertia and speed of the rotor, and its power rating is dependent on the connected electrical machine. It's important to note that the stored energy could be fully discharged if the storage duration is longer than 1 day, so the proper storage period for flywheel is limited within tens of minutes (Chen *et al*., 2009). However, battery and CAES with appropriate size are capable of the 2 kW wind turbine system for up to 20 hours' operation. In conclusion, the all the three options can satisfy the power rating requirement, however the battery and CAES have the advantages in storage duration.

3.3.3 Cycle life

The main drawback faced by battery is relatively short lifetime that mainly expressed on the limited charge/discharge cycle life. For example, lead-acid batteries' cycle life is roughly in the range of 500-1500 cycles. This issue can be more serious when it is applied to wind power generation due to the high variation in wind speed and low predictability to the wind power variation patterns, that is, the battery will be more frequently charged and discharged. For CAES, the pneumatic drives, including compressor, air motor, tank, pipes and valves, are relatively robust; the major components have up to 50-year lifetime. Similarly, flywheel is also built with conventional mechanical engineering, and it can serve for tens of years due to the robust mechanical components.

3.3.4 Energy efficiency

It is well recognised that the energy loss commonly accompany energy conversion process, as the energy cannot be 100 per cent converted to different forms. Thus, the battery and flywheel may obtain much high efficiency with simple energy conversion processes. Generally, the cycle efficiency during one charge and discharge of lead-acid battery and flywheel is 80% (Chen *et al*., 2009). In contrast, CAES has rather lower energy efficiency. Much energy is lost during the process of thermal energy conversion (Sun *et al*., 2011).

3.3.5 Energy density

Energy density indicates the rated output power per unit volume or unit mass. This value directly determines the size and weight of the energy storage devices, somehow influences the system cost, feasibility and mobility. The energy-volume density and

energy-mass density of flywheel, CAES and several common types of batteries are expressed in the Table 3.2.

Table 3.2 Energy density of the selected energy storage systems (Chen *et al*., 2009)

Energy storage systems	Energy-volume density (Wh/L)	Energy-mass density (Wh/kg)
Flywheel	10-30	20-80
CAES	30-60	3-6
Lead acid battery	30-50	50-80
Nickel cadmium battery	50-70	60-150
Sodium sulphur battery	150-240	150-250
sodium nickel chloride battery	100-120	150-180
Lithium ion battery	75-200	200-500

Clearly, batteries retain a clear edge in energy density, either per volume or mass. As a result, batteries have significant advantages in size and weight. That is the reason why they are widely in portable device applications. In contrast, flywheel and CAES are more cumbersome as their energy densities are quite low.

3.3.6 Capital cost

Capital cost is one of the most important parameters for the industry and economic area. It is defined as the total ownership cost, including the operation and management cost and the impact of components service life. Table 3.3 shows the cost per unit energy of flywheel, CAES and several common types of batteries.

Table 3.3 Capital cost of the selected energy storage systems (Chen *et al*., 2009)

Energy storage systems	Capital cost ($/kWh)
Flywheel	1000-5000
CAES	2-50
Lead acid battery	200-400

Nickel cadmium battery	800-1500
Sodium sulphur battery	300-500
sodium nickel chloride battery	100-200
Lithium ion battery	600-2500

From this table, it is obviously seen that CAES is the most cost-effective solution by a wide margin among the selected small scale options. Mainly because its storage media-compressed air is practically free. The capital cost of CAES is roughly 1% of that of batteries. Although flywheel is similarly based on mechanical engineering, it costs hundreds time higher than CAES does due to its extremely low storage energy density.

3.3.7 Maintenance

In consideration of the lab work in the research field, the maintenance becomes an important factor. As most batteries are built with series connection for high supply voltage, the whole battery may fail to store or offer energy in the manner desired, if one cell within the battery system goes wrong. Discouragingly, it is very hard currently to diagnose which cell in the system fails and it is expensive and not cost-effective to replace the whole pack of batteries. Besides, most lead-acid batteries designed for the deep discharge are not sealed, and the regular maintenance is therefore required due to the gas emission caused by the water electrolysis while overcharged. Comparing with these characteristics of batteries, CAES and flywheel are mechanically solid and robust; only need regular leakage test and oil maintenance.

3.4 Summary

Various energy storage technologies are reviewed for a better understanding of their characteristics. Different technologies have different performances and are applied in different circumstances. To facilitate the hybrid wind turbine system, three different types of small scale energy storage technologies are chosen as candidates. To sum up, battery, flywheel and CAES have their own advantages in different aspects. However, CAES is relatively well balanced with some key features such as good cost-effectiveness, robustness and expectance. Through the comparisons, CAES is testified the best choice with its most competitive advantages. So in this project, CAES principle is selected as the energy storage solution. Based on this, research and development on pneumatic actuators, hybrid transmission and control strategy are conducted for an optimised performance and efficiency.

Chapter 4

Introduction and modelling of pneumatic systems

Before attempting to build the hybrid system and conducting the energy efficiency analysis, it is important to understand the dynamics of pneumatic actuators. Because that they are the core components to build CAES system. This chapter contributes to study of pneumatic systems in terms of the working principles and mathematical description. It begins with the overall building structure of a pneumatic system via an illustration of a complete pneumatic actuator system from air compression to actuation. Then the fundamental operation principles and mathematical model of the major components, including air motors, air tank and compressor are studied. The work presented in the chapter prepares the first step towards the development of the whole hybrid system model for simulation studies.

4.1 Introduction to pneumatic systems

A typical pneumatic actuator system, as shown in Figure 4.1, is composed of an air motor, air tank and a compressor with the associated devices and components including air dryers/filters, lubricators, regulators, meters, valves and pipeline network. The major components are described in below.

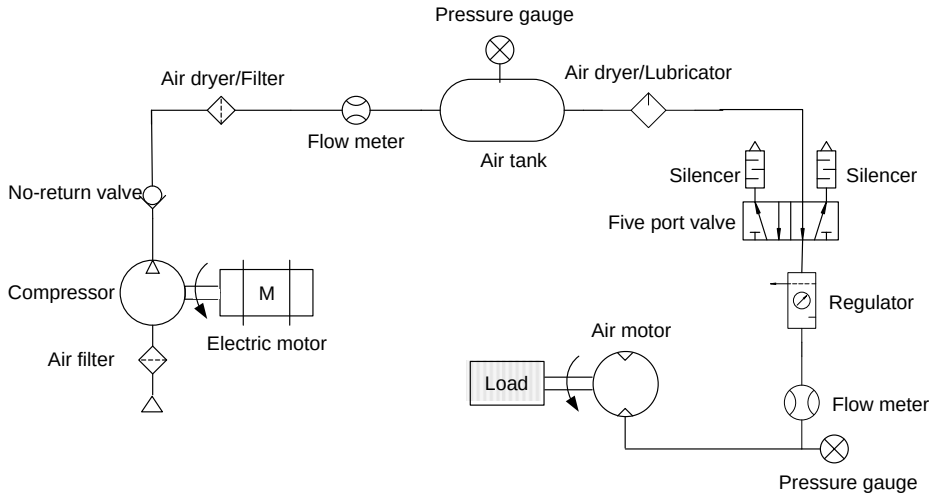

Figure 4.1 Illustration of a typical pneumatic actuator system

Pneumatic Actuators

A pneumatic actuator is a kind of motor that employs compressed air as the energy source. It works by converting the compressed air energy into working energy by the expansion of the air.

There are several types of air motors. Rotary vane, axial and radial piston, and gerotor air motors are most commonly applied in industrial field. These designs operate with high efficiency and longevity from lubricated air. Turbine, V-type, and diaphragm air motor are also available, but they are not widely used (Gast Manufacturing Corporation, 1986). Turbine motors are employed where high rotation velocity and low starting torque are required. While, V-type and diaphragm air motors are used primarily for special applications (Hydraulics & Pneumatics, 2012).

In some instances, pneumatic actuators can replace their counterpart electric actuators, due to their several advantages over electric actuators, especially high power to weight and power to size ratios, wide adaptability, and resistance to environmental

hazards (Pandian, et al., 1999).

Air tanks:

First of all, air tank serves as a storage reservoir. Moreover, it can be used as an intermediate to smoothen pulsating air output - reducing pressure variations from the compressor to actuators. Besides, it can separate moisture and oil vapour, allowing the moisture carried over from the after coolers to precipitate (Lawrence Berkeley National Laboratory, 2003) (United Nations Environment Programme, 2006).

Compressors:

Compressor is a mechanical device that is powered by a prime mover to collect air and increase its pressure. Controls serve to regulate the amount of compressed air being produced. Generally, compressors are classified into 2 categories: positive displacement compressor and dynamic compressor (Lawrence Berkeley National Laboratory, 2003), as described in Figure 4.2. Positive displacement compressors increase the air pressure by reducing its volume. This kind of compressors is further classified into reciprocating and rotary compressors. While, dynamic compressors work to increase the air velocity in order to increase pressure at the outlet end. Most dynamic compressors are centrifugal compressors and can be of radial and axial flow types (United Nations Environment Programme, 2006).

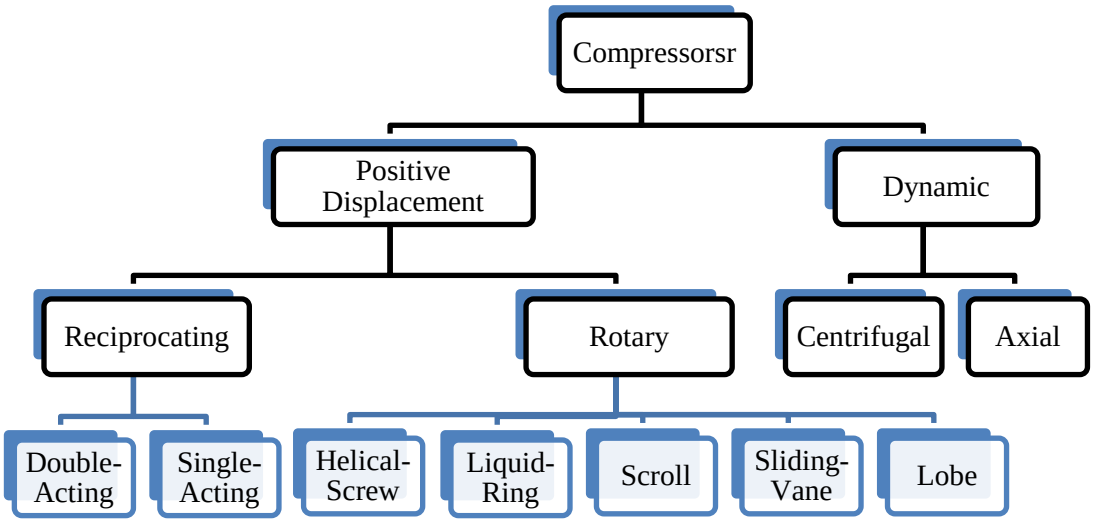

Figure 4.2 Compressor family tree

Intake Air Filters:

Dust and dirt are liable to have harmful effects on compressed air equipment. They may cause sticking valves, scoured cylinders, excessive wear etc. Then the intake air filters are essential to remove dust dirt from entering the compressor.

Air Dryers:

In most cases, air for instrument and pneumatic equipment has to be relatively free of any moisture. The remaining traces of moisture are removed by air dryers using adsorbents like silica gel /activated carbon, or refrigerant dryers, or heat of compression dryers (United Nations Environment Programme, 2006).

Lubricators:

Essentially the pneumatic actuators should be fitted with a lubricator to reduce friction and keep moving parts from wearing excessively. Lubricator is a kind of oil reservoir where a metered amount of oil is fed in mist form into the air stream when air is

flowing. This oil is carried to lubricate all moving parts with the motive air.

Regulators and Valves:

Pneumatic regulators and valves are commonly used to control the gas pressure, flow rate or direction in the system. Based on their different functions, they can be grouped into four categories: 1) direction valves; 2) direction check or non-return valves; 3) flow rate regulators; and 4) pressure regulators (Majumdar, 1996).

Pipeline Network

Similar to wiring in the electrical world—pipeline is essential to interlink the different components in a compressed air system. As it transports compressed air to where it is needed. However, loss of pressure is always accompanied by the piping because of the resistance in pipe fittings and valves, which dissipates energy by producing turbulence. Based on pneumatic system good practice guide, the piping system should be designed for a maximum allowable pressure drop of 5% from the compressed air source to the most distant point of use (United Nations Environment Programme, 2006).

4.2 Mathematical model of vane-type air motors

The key concept of the project is to employ the energy stored in compressed air to help smoothen the wind turbine output in which the compressed air energy is converted to generate mechanical driving torque through an pneumatic drive – air motor in hybrid connection with the wind turbine shaft. The vane-type air motor, the most commonly used rotary pneumatic actuators, is first considered for the hybrid

system. The mathematical model for four-vane-type air motors was described in the paper by Wang *et al* in 1998. The work was extended to the vane-type air motor model with arbitrary number of vanes by Luo *et al.* in 2008. In this project, modelling and simulation study of vane-type air motors are mainly based on the model of air motor with four vanes developed by Wang and Luo.

4.2.1 Working principle of a vane-type air motor

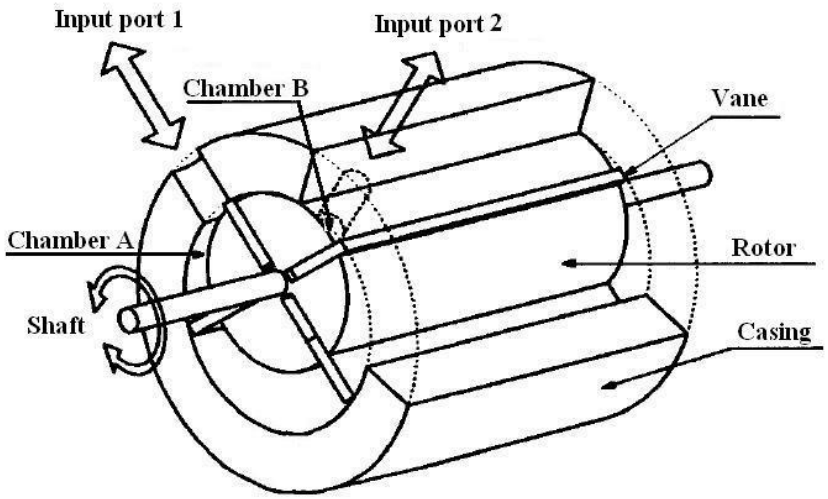

Figure 4.3 Construction of vane-type air motor (Pandian, et al., 1999)

Figure 4.3 shows the structure of a vane-type air motor with four vanes. There is a rotational drive shaft with four slots, each of which is fitted with a freely sliding rectangular vane. When the drive shaft starts rotating, the vanes tend to slide outward due to centrifugal force and are limited by the shape of the rotor housing. Depending on the flow direction, this motor will rotate in either clockwise or counter clockwise directions. The two ports on the two chambers may be alternatively served as inlet and outlet. According to Figure 4.3, input port1 is supposed to be the inlet port, thus,

the rotary direction is counter clockwise. Compressed air is admitted through the input port1 from the valves and fills the cavity between the vanes, housing and rotor. The chamber A which is open to the input port 1 fills up under high pressure. Once the port is closed by the moving vane, the air expands to a lower pressure in a higher volume between the vane and the preceding vane, at which point the air is released via the input port 2. The difference in air pressure acting on the vane results in a torque acting on the rotor shaft. Hence, the higher flow rate and the larger pressure difference will provide larger toque acting on the shaft and result in a higher rotational speed. Figure 4.4 describes the working flowchart of a vane-type air motor.

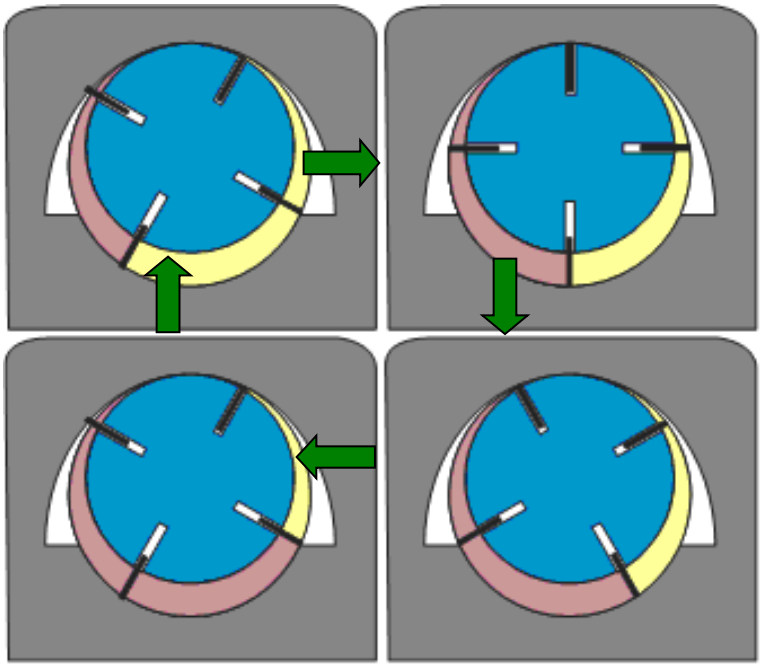

Figure 4.4 Working flowchart of vane-type air motor

4.2.2 Geometric model of a vane-type air motor

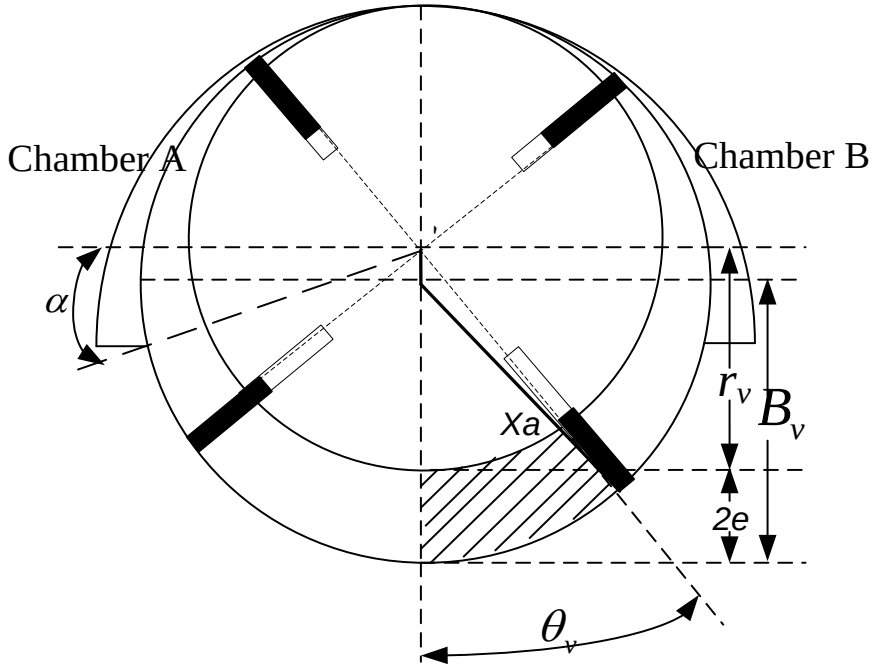

Figure 4.5 Geometric of vane-type air motor

A simplified vane-type air motor structure is shown in Figure 4.5. The vane working radius measured from the rotor centre x_a can be derived by:

$$x_a = e\cos\theta_v \pm \sqrt{B_v{}^2 - e^2\sin^2\theta_v} \tag{4.1}$$

The volume of chamber *A* and chamber *B* are derived as follows (Wang *et al*., 1998), and presented by the subscription v_a and v_b in these equations.

$$V_{v\_a} = \frac{1}{2}L_v(B_v{}^2 - r_v{}^2)(\pi + \theta_v) + \frac{1}{4}L_v e^2\sin 2\theta_v + L_v eB_v\sin\theta_v \tag{4.2}$$

$$V_{v\_b} = \frac{1}{2}L_v(B_v{}^2 - r_v{}^2)(\pi - \theta_v) - \frac{1}{4}L_v e^2\sin 2\theta_v - L_v eB_v\sin\theta_v \tag{4.3}$$

where, B_v is radius of vane-type air motor body; *e* is eccentricity; L_v is vane active length in the axial direction, θ_v is motor rotating angle, r_v means rotor radius. The derivatives of V_{v_a} and V_{v_b} are:

$$\frac{dV_{v\_a}}{dt} = \dot{V}_{v\_a}\frac{d\theta_v}{dt}$$

$$\frac{dV_{v\_b}}{dt} = \dot{V}_{v\_b}\frac{d\theta_v}{dt}$$

with $\dot{V}_{v\_a} = \frac{1}{2}L_v(B_v{}^2 - r_v{}^2) + \frac{1}{2}L_v e^2\cos 2\theta_v + L_v eB_v\cos\theta_v$ and $\dot{V}_{v\_a} = -\dot{V}_{v\_b}$. Since θ_v is a periodic function, it can be seen that $V_{v\_a}, \tilde{V}_{v\_a}, V_{v\_b}$ and $\tilde{V}_{v\_b}$ are also periodic and discontinuous functions. When the chamber A is the drive chamber, θ_v goes from $[-\alpha, -\alpha+\frac{\pi}{2}]$, while chamber B is the drive chamber, θ_v goes from $[\alpha, \alpha-\frac{\pi}{2}]$.

4.2.3 Dynamic model of vane-type air motor

The dynamic relationship with the mass flow rates across the two control ports can be expressed as (Andersen, 1976) (Pu, Moore and Weston, 1991).

$$w_{v\_a} = (p_{v\_a}\dot{V}_{v\_a} + V_{v\_a}\dot{p}_{v\_a}/k)/(R_{air}T_s) \qquad (4.4)$$

$$w_{v\_b} = (p_{v\_b}\dot{V}_{v\_b} + V_{v\_b}\dot{p}_{v\_b}/k)/(R_{air}T_s) \qquad (4.5)$$

The pressure differential of chamber A and B can be derived as (Wang *et al*., 1998):

$$\dot{p}_{v\_a} = -\frac{k\dot{V}_{v\_a}}{V_{v\_a}}p_{v\_a} + \frac{k}{V_{v\_a}}R_{air}T_sC_dC_0A_aX_a f(p_{v\_a}, p_s, p_e) \qquad (4.6)$$

$$\dot{p}_{v\_b} = -\frac{k\dot{V}_{v\_b}}{V_{v\_b}}p_{v\_b} + \frac{k}{V_{v\_b}}R_{air}T_sC_dC_0A_{v\_b}X_{v\_b} f(p_{v\_b}, p_s, p_e) \qquad (4.7)$$

where, T_s is supply temperature, R_{air} C_d C_0 are air constant, A_a is effective port width of control valve, X_a is valve spool displacement, f is a function of the ratio between the downstream and upstream pressures at the orifice. For the convenience of the analysis, the following functions are introduced:

When Chamber A is a drive chamber (Wang *et al*., 1996),

$$f(P_{v\_a}, P_s, P_e) = P_s \tilde{f}(\frac{P_{v\_a}}{P_s}) / \sqrt{T_s}$$
$$f(P_{v\_b}, P_s, P_e) = P_{v\_b} \tilde{f}(\frac{P_e}{P_{v\_b}}) / \sqrt{T_{v\_b}} \quad (4.8)$$

When Chamber B is a drive chamber,

$$f(P_{v\_a}, P_s, P_e) = P_{v\_a} \tilde{f}(\frac{P_e}{P_{v\_a}}) / \sqrt{T_{v\_a}}$$
$$f(P_{v\_b}, P_s, P_e) = P_s \tilde{f}(\frac{P_{v\_b}}{P_s}) / \sqrt{T_s} \quad (4.9)$$

where $\tilde{f}(x)$ is a function on the ratio between the downstream and upstream pressures at the orifice, it equals (Luo *et al*., 2008):

$$\tilde{f}(x) = \begin{cases} 1 & , \quad \frac{P_{atm}}{P_u} < x \le C_r \\ C_k[p_r^{2/k} - p_r^{(k+1)/k}]^{\frac{1}{2}} & , \quad C_r < x \le 1 \end{cases} \quad (4.10)$$

For air $k = 1.4$, $C_r = 0.528$ and $C_k = 3.864$.

The drive torque is determined by the difference of the torque acting on the vane between the drive and exhaust chambers, and is given by:

$$\tau_v = (P_{v\_a} - P_{v\_b})(x_a - r_v) L_v (x_a - r_v) / 2$$
$$= (P_{v\_a} - P_{v\_b})(e^2 \cos\theta_v + 2eB_v \cos\theta_v + B_v{}^2 - r_v{}^2) L_v / 2 \quad (4.11)$$

4.2.4 Simulation study on vane-type air motor dynamics

Based on the differential equations from (4.1) to (4.11), a complete mathematical model for vane-type air motor is implemented. The parameters used for the 4-vane-type air motor model are exactly based on Wang's paper, a well validated model (Wang et al., 1998). In the simulation, the open loop study is conducted. The input is 5×10^5 Pa supply pressure and output is constant 3 N × m mechanical load. The

full set of the parameters is shown in Table 4.1.

Table 4.1 The parameters of 4-vane-type air motor simulation

Symbol	Parameters	Value
r_v	Rotor radius	0.00325 m
B_v	Body radius	0.00365 m
e	Eccentricity	0.0004 m
L_v	Vane active length	0.00445 m
T_s	Supply temperature	293 K
A_a	Effective control valve port width	0.003 m
p_s	Supply pressure	5×10^5 Pascal
J_{am}	Air motor inertia	0.000608 kg$\times$ m^2
F_{am}	Friction coefficient	0.04
	Mechanical Load	3 N$\times$ m
	Simulation time	1 second

Assuming the vane-type air motor rotates clockwise, referring to Figure 4.6. That is the Chamber A is driving chamber while Chamber B stands for Driven chamber. Given the simulation condition in Table 4.2, the simulated dynamics of vane-type air motor are shown in Figure 4.6.

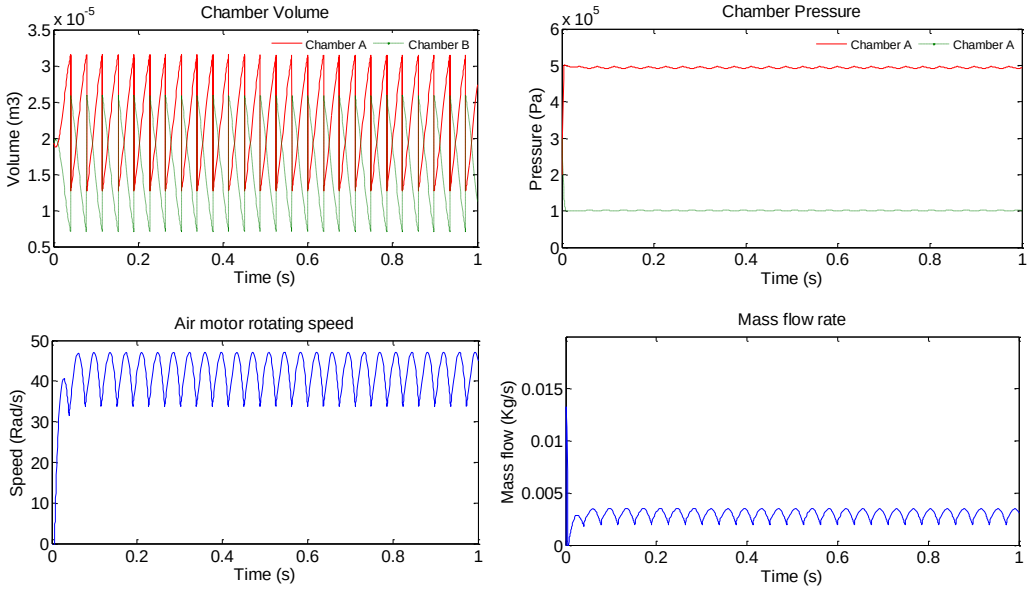

Figure 4.6 Simulated dynamics of vane-type air motor

It is obvious that after the initial start time, the volume, pressure and speed variation are periodic. The periodic fluctuations in the steady stage are originated from the cyclically changed difference between P_{v_a} and P_{v_b} (the pressures in chamber A and chamber B). The mean rotating speed is about 42 rad/s, which is 6.68 Hz in frequency; while the frequency of the fluctuations is approximately 26 Hz. So the cycle time of one fluctuation precisely equals the time that takes the shaft rotates for ¼ cycles; because the whole chamber is divided by 4 vanes.

4.3 Mathematical model of scroll air motors

A scroll type air motor, also known as a scroll expander, is a relatively new concept to pneumatic actuators, which is essentially a refrigeration scroll compressor working backwards. In Power and Control Systems Research Laboratory, University of Warwick, two scroll compressor types regard to different number of scroll wraps are converted into air motors for study. They are TRSA09 with 2.41 wraps and TRSA05 with 2 wraps, both manufactured by Sanden, as shown in Figure 4.7.

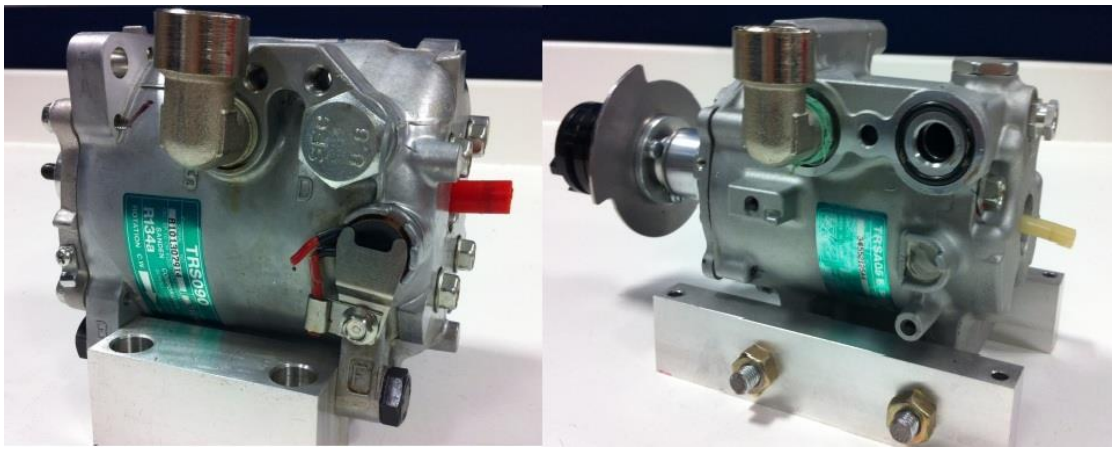

Figure 4.7 Two types of scroll air motor: TRSA09 and TRSA05

4.3.1 Working principle of scroll air motor

A 2.41-wrap scroll air motor in motion is illustrated in Figure 4.8. It illustrates a air motor with both scrolls are circular involutes with 2.41 wraps. The blue scroll represents the moving scroll and the green one is the fixed scroll. The moving scroll travels along the orbit anticlockwise when compressed air comes into centre chamber through the inlet port. Each scroll is fitted to a back plate.

As the moving scroll travels along the circular orbit, these two scrolls keep contacting at some points. Thus the whole inside space is divided into three different types of chambers: the central, the side and the exhaust chambers.

Each chamber will experience three phases during one operating cycle: charging, expansion and discharging phases. First, the charging phase starts as the compressed air flows into the central chamber, as described in the diagram (1) in Figure 4.8. Beyond that, there are two side chambers and one exhaust chambers connected to the atmosphere through the outlet port of the scroll air motor. For the next phases, two side chambers are rotating anticlockwise and they continue expanding along with the

central chamber driven by the expansive force. At one moment after the diagram (4), two side chambers get their maximum volume, and then they will connect to the outlet port and become the new exhaust chamber. Similarly, the central chamber also expands to the maximum. Then it splits into a new smaller central chamber and two new side chambers.

This unique structure features scroll air motors significant advantage in utilizing both transmission and expansion air power, which results in much higher energy efficient performance than conventional pneumatic actuators , such as cylinders, vane-type air motors, etc.

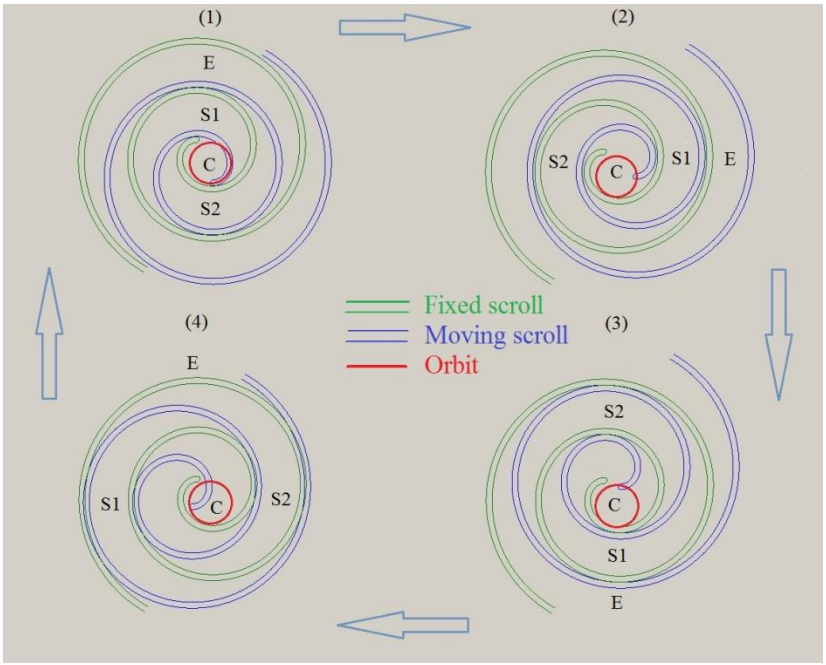

Figure 4.8 Schematic diagram of a scroll-type air motor

The mathematic model of scroll air motors was previously studied in (Yang, 2007) (Luo, 2009), (Wang, 2011) and (Luo, 2012). The geometric mathematical model of a 3-wrap scroll air motor was first reported by (Yang et al., 2007). Then the model is

modified to include the scroll's thermodynamic behaviours, including the consideration of the leakage was reported in (Luo et al., 2009). The complete modelling study with thermal dynamic and efficiency analysis was reported in (Wang et al, 2011). The scroll expander's dynamic characteristics with respect to its shape, number of scroll wraps, inlet and outlet port sizes, etc were studied in details (Luo et al 2012). In this PhD research project, the system power rate is around 1kW-5kW. EIn the practical experiments, the observable temperature change is within 2.6% (for details, see Chapter 7) which will not affect the scroll performance and energy conversion efficiency obviously. So the mathematical model has not considered the thermal dynamic characteristics of a scroll. A mathematical model of a simplified scroll air motor is adopted, with the following assumptions: no air leakage between chambers, using ideal compressed air, neglecting static frictions and working at a constant surrounding temperature. In particular, to match the air expander used in the project, the initial model is further developed to suit a 2.41-wrap scroll air motor.

4.3.2 Geometric model of a scroll air motor

To obtain a complete mathematical model of a scroll air motor, the mechanical geometry features of a scroll air motor has been studied first. The scrolls' model can be derived from the fundamental geometry curve of a spiral. If the initial point of the spiral is at $A_0 = (x_0, y_0), \varphi_s$ is the tangent angle of a point on the spiral and the radius is defined by $\rho_s = \rho_0 + \kappa_s \varphi_s$, as demonstrated in Figure 4.9.

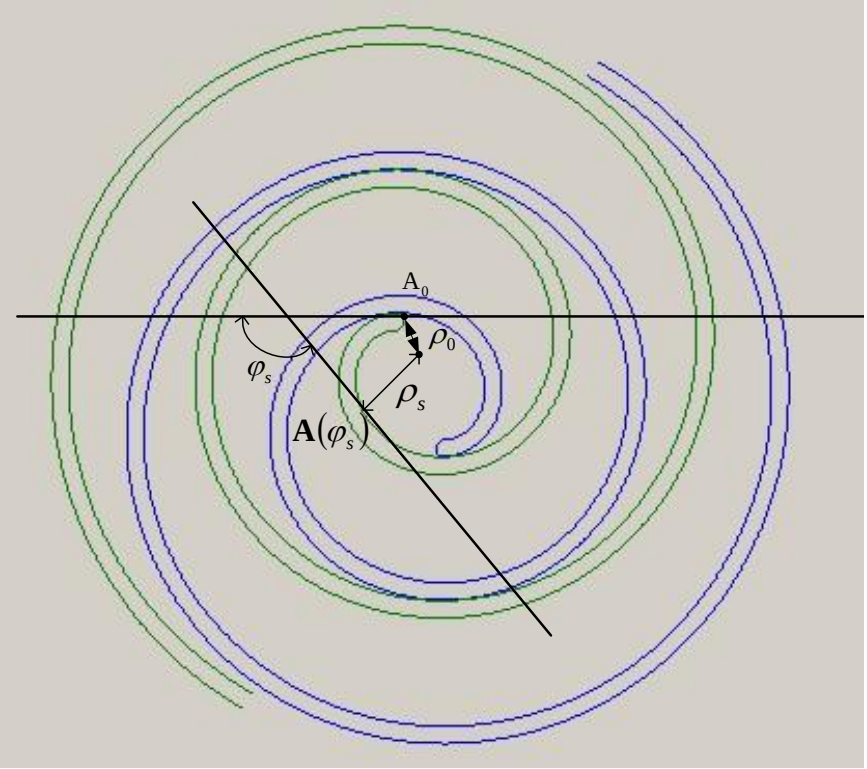

Figure 4.9 Geometric model of a spiral

Therefore, each position of a point on the fixed scroll can be determined by (Yang *et al*., 2007)

$$\mathbf{A}(\varphi_s) = \mathbf{A}_0 + \int_0^{\varphi_s} \left((\rho_0 + \kappa_s u_s)\cos u_s, \quad (\rho_0 + \kappa_s u_s)\sin u_s \right) du_s \tag{4.12}$$

With its horizontal and the vertical position of (Luo, 2011)

$$\begin{aligned} x_{\mathbf{A}}(\varphi_s) &= x_0 + (\rho_0 + \kappa_s \varphi_s)\sin\varphi_s + \kappa_s \cos\varphi_s - \kappa_s \\ y_{\mathbf{A}}(\varphi_s) &= y_0 - (\rho_0 + \kappa_s \varphi_s)\cos\varphi_s + \kappa_s \sin\varphi_s + \rho_0 \end{aligned} \tag{4.13}$$

where κ_s is the ratio between the line segment and tangent angle segment, which determines the shape of a spiral.

While, the family of the moving scroll can be described by

$$A(\varphi_s, \alpha_s) = A(\varphi_s) + D(\alpha_s) \tag{4.14}$$

where $D(\alpha_s)$ is the equation of the orbit.

Then we can derive the equations for the moving scroll (Wang *et al*., 2011):

$$\begin{aligned} x_{\mathbf{A}}(\varphi_s,\alpha_s) &= x_0+(\rho_0+\kappa_s\varphi_s)\sin\varphi_s+\kappa_s\cos\varphi_s-\kappa_s+r_s\sin\alpha_s \\ y_{\mathbf{A}}(\varphi_s,\alpha_s) &= y_0-(\rho_0+\kappa_s\varphi_s)\cos\varphi_s+\kappa_s\sin\varphi_s+\rho_0-r_s\cos\alpha_s \end{aligned} \tag{4.15}$$

α_s is orbit angle of moving scroll and r_s is the radius of the orbit.

Applying Green's Theorem, the volume of the central chamber V_c is given by (Yang *et al*., 2007)

$$\begin{aligned} V_c(\alpha_s) = z_s[&(\kappa_s r_s-\kappa_s{}^2\pi-x_0r_s+x_0\kappa_s\pi)\cos\alpha_s \\ &+(\kappa_s r_s\rho_0\pi-r_s\rho_0-y_0r_s+y_0\kappa_s\pi)\sin\alpha_s \\ &+(\kappa_s r_s\pi+2\kappa_s\rho_0\pi)\alpha_s+\kappa_s{}^2\pi\alpha_s{}^2-\kappa_s r_s+\frac{1}{3}\kappa_s{}^2\pi^3 \\ &-\frac{1}{2}\kappa_s r_s\pi^2+\rho_0 r_s\pi+\frac{1}{2}r_s{}^2\pi+\rho_0^2\pi] \end{aligned} \tag{4.16}$$

where z_s stands for the depth of the scroll.

For the case of scroll air motor with more than 2 pairs of side chambers, the area of one of the i^{th} $(i=1,2,3\cdots)$ pair of side chambers is:

$$V_{si}(\alpha_s,i)=\pi r_s{}^2+2\pi r_s(\rho_0+\kappa_s(\alpha_s+\pi+2(i-1)\pi)) \tag{4.17}$$

The volume of the exhaust chamber can be described by

$$V_e(\alpha_s)=V_{total}-V_c(\alpha_s)-V_{si}(\alpha_s) \tag{4.18}$$

where V_{total} stands for the total control volume of the scroll air motor.

4.3.3 Dynamic model of scroll air motor

Similar as Equation (4.4) and (4.5), the dynamic relationship with the mass flow rates across the scroll air motor can be expressed as (Luo et al., 2009):

$$w_c=(p_c\dot{V}_c+V_c\dot{p}_c/k)/(R_aT_s) \tag{4.19}$$

$$w_{si}=(p_{si}\dot{V}_{si}+V_{si}\dot{p}_{si}/k)/(R_aT_s) \tag{4.20}$$

And the pressures in different chambers can be obtained by:

In centre chamber,

$$\dot{p}_c = -\frac{\dot{V}_c}{V_c}\gamma p_c \omega_s + \frac{1}{V_c}\gamma R_{air} C_d C_0 C_k A_i p_s f(p_s / p_c)\sqrt{T_s} \tag{4.21}$$

In the first pair of side chambers,

$$\dot{p}_{si} = -\frac{\dot{V}_{si}}{V_{si}}\gamma p_{si} \omega_s \tag{4.22}$$

In case of the i^{th} (i=1, 2, 3…) pair of side chambers

$$\dot{p}_{sii} = -\frac{\dot{V}_{sii}}{V_{sii}}\gamma P_{sii} \omega_s \tag{4.23}$$

In the exhaust chamber,

$$\dot{p}_e = -\frac{\dot{V}_e}{V_e}\gamma p_e \omega_s + \frac{1}{V_e}\gamma R_{air} c_d c_0 c_k A_o p_e f(p_e / p_{atm})\sqrt{T_s} \tag{4.24}$$

The torque generated by a scroll air motor τ_s is the sum of the torques on all driving segments, it can be derived as:

$$\begin{aligned}\tau_s = z_s r_s [&(2\rho_0 + 2k_s\alpha_s + k_s\pi)(p_c - p_{si1}) \\ &+ \sum_{i=2,3,4...}(2\rho_0 + 2k_s\alpha_s + (4i-3)k_s\pi)(p_{sii} - p_{si(i-1)}) \\ &+ (2\rho_0 + 2k_s\alpha_s + (4i+1)k_s\pi)(p_e - p_{sii})]\end{aligned} \tag{4.25}$$

where, p_s is the supply pressure; p_{atm} is the pressure of atmosphere; T_s is the supply air temperature; R_{air} C_d C_0 C_k are air constant; $\gamma = 1.4$ is the ratio of specific heats; A_i A_o are the effective area of inlet and outlet valves; ω_s is the rotating speed of scroll air motor; f is a function of the ratio between the downstream and upstream pressures at the orifice. Combine Equation 4.10, It can be described below:

$$f(p_s / p_c) = P_s \tilde{f}(\frac{P_c}{P_s}) / \sqrt{T_s}$$
$$f(p_e / p_{atm}) = P_e \tilde{f}(\frac{P_{atm}}{P_e}) / \sqrt{T_e} \quad (4.26)$$

4.3.4 The relationship between wrap numbers and side chamber pairs

For the simulation study, the main problem is to determine the reset point, which expresses when the side chambers are shifted to the exhaust chamber meanwhile the side chambers are created from the central chamber. Currently, there are different air motors with varying wraps numbers, resulting to varying pairs of side chambers. For example, TRSA09 scroll air motor has 2.41 wraps with one pair of side chambers, while TRSA05 has 2 wraps with one pair of side chambers. Additionally, (Yang et al., 2007) reported a 3 wraps model with 2 pairs of side chambers.

Here, it is assumed that for the moving scroll at a particular orbit angle α_s, the fixed scroll $\mathbf{B}(\phi_s)$ touches the moving scroll at $\mathbf{A}(\varphi_s, \alpha_s)$, that is, $\mathbf{A}(\varphi_s, \alpha_s) = \mathbf{B}(\phi_s)$ at the particular points. From the definitions of scrolls and the theorem defined in (Wang et al., 2011), the moving scroll touches the fixed scroll at the points $\varphi_s = \phi_s + j\pi$, where *j* is an arbitrary integer. While, for the envelope of the family of moving scrolls, $\alpha_s = \varphi_s + j\pi$.

It can be deduced that, for a scroll air motor with *n* wraps, the end point of fixed scroll is $\mathbf{B}(2n\pi)$. During one moving cycle $\alpha_s \le 2\pi$, $\mathbf{B}(2n\pi)$ will contact the moving scroll at the point $\mathbf{A}(2n\pi - \pi, \alpha_s)$; meanwhile, $\mathbf{B}(2n\pi - 2k\pi)$ contacts to the moving scroll at the point $\mathbf{A}(2n\pi - (2k+1)\pi, \alpha_s)$, $2n\pi - (2k+1)\pi \ge 0$, where *k* is a

natural number. There is one pair of side chamber between two adjacent contact points. So the number of side chamber pairs could be marked as $floor(2n-2)$, where $floor$ is a function in Matlab. In this equation, it rounds $2n-2$ to the nearest integers less than or equal to $2n-2$.

That is, to create at least one pair of side chambers $floor(2n-2)=1$, the scroll air motor must has at least 1.5 wraps. Practically, due to the air leakage between the fixed and moving scrolls, 1.5-wrap cannot be perfectly sealed to form any side chamber.

For 2-wrap scroll air motor, it has one pair of side chambers, at the point $\mathbf{A}(3\pi,\pi)$, the central chamber create a new pair of side chambers, and the previous side chambers start to merge to the exhaust phase.

For a 2.41-wrap scroll air motor, it also has one pair of side chamber and its reset point is $\mathbf{A}(3.82\pi,1.82\pi)$.

To compare 2.41 and 2-wrap scroll air motor, even they have same amount of side chambers, the volumes vary according to the different reset points. It is easier to achieve higher expansion ratio on 2.41-wrap scroll air motor.

4.3.5 Simulation study on scroll motor dynamics

The complete mathematical models for scroll air motors presented in Section 4.3 are implemented in Matlab/Simulink environment. In the simulation study, the scroll parameters of TRSA09, manufactured by SANDEN, are shown in Table 4.2. This scroll air motor mathematical model had been validated in the research laboratory and the air motor mechanism is also employed for building the overall hybrid system, which will be described in Chapter 6. The same pressure used for vane- type air motor

simulation study and test are used for the scroll air motor with the input is 5×10^5 Pa supply pressure and a constant 3 N× m mechanical load.

Table 4.2 The parameters of scroll air motor (TRSA09) simulation

Symbol	Parameters	Value
ρ_s	Radius of the curvature	0.0054 m
r_s	Radius of the orbit	0.00517 m
z_s	Height of the scroll	0.0333 m
r_h	Radius of the housing body	0.055 m
δ_s	Thickness of the moving and fixed scroll	0.0046 m
T_s	Supply temperature	293 K
A_i	Effective open area of inlet	0.00005 m^2
A_o	Effective open area of outlet	0.00008 m^2
p_s	Supply pressure	5×10^5 Pascal
J_{am}	Air motor inertia	0.000908 kg× m^2
F_{am}	Friction coefficient	0.001
	Mechanical Load	3 N× m

The results indicate that the implemented model can predict the main dynamic features of scroll air motor with its chamber volume and pressure variations. Figure 4.10 and 4.11 shows the volume and pressure change of different chambers.

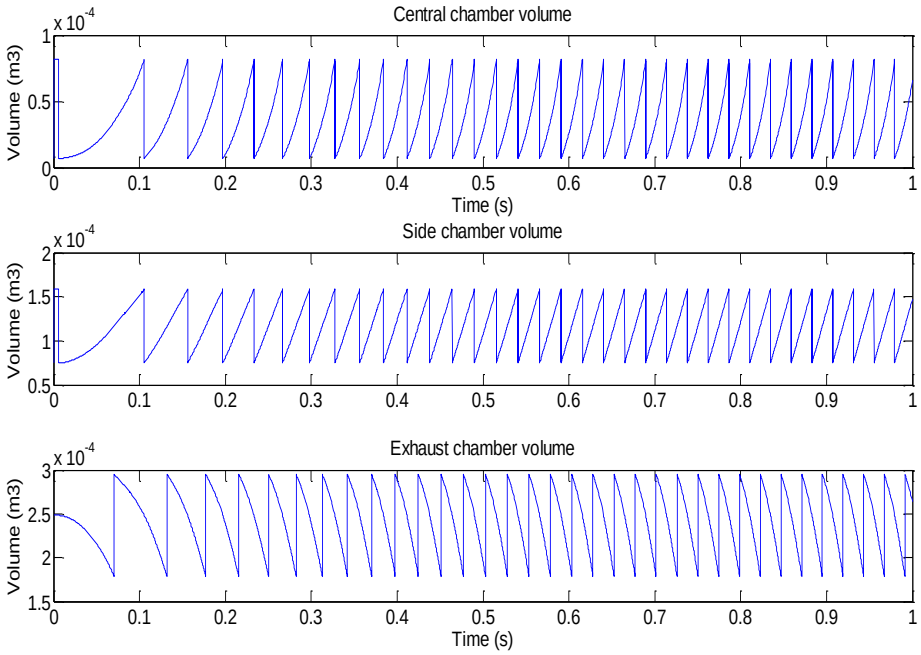

Figure 4.10 Simulated chamber volumes of scroll air motor

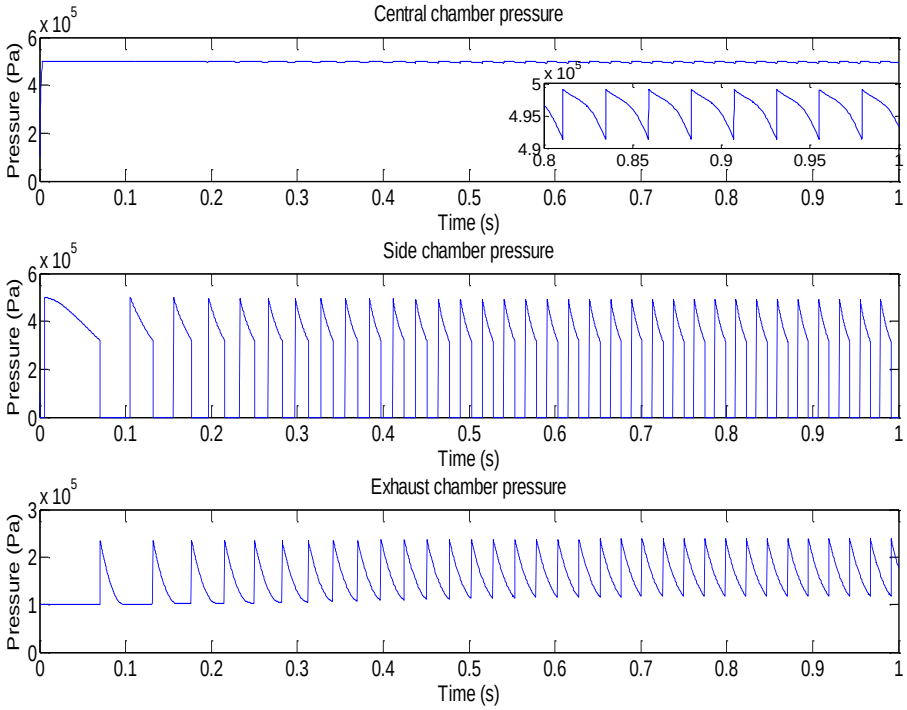

Figure 4.11 Simulated chamber pressures of scroll air motor

The simulation results of the rotating speed and mass flow rate are given in Figure 4.12. Considering Figure 4.10 and 4.11, it is clear that the volume and pressure

variations are associated with the angular speed.

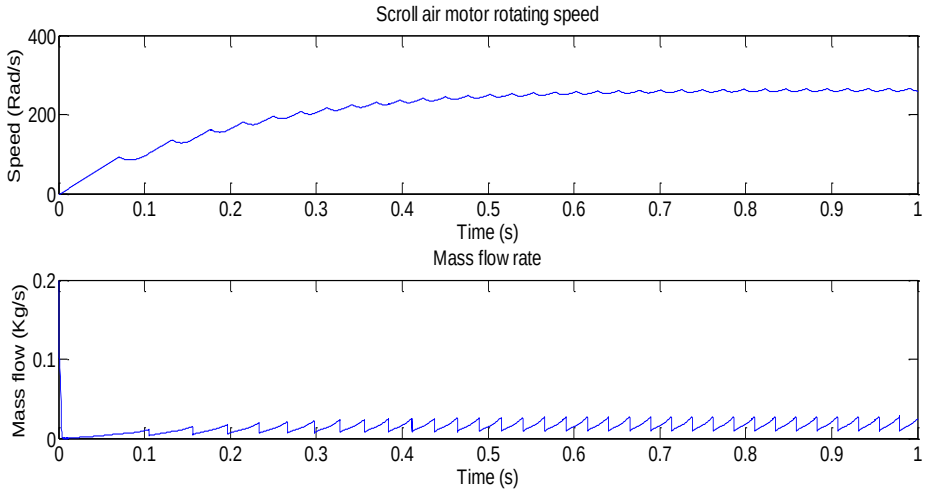

Figure 4.12 Simulated speed and mass flow rate of scroll air motor

4.4 Energy efficiency analysis of vane and scroll type air motors

To serve as the air-electricity transformer in hybrid wind turbine system, the energy efficiency is principally considered. Compared with other types, scroll air motor has higher energy efficiency which is the main factor for the team to select this device. From the reported research (Yang et al., 2007; Luo et al., 2009; Luo et al., 2011;Wang et al., 2011), its unique structure allows the scroll air motor to utilise both the transmission and expansion air power much more efficiently. This section will analyse the energy conversion ability of scroll and most common, vane-type air motor to provide constructive explanations. The analysis is conducted based on the well-validated mathematical models in Matlab/Simulink.

Energy efficiency is the ratio between the useful output of an energy conversion machine and the total intake energy. For the air motor system, the input energy is the energy stored in the compressed air; and the output energy is counted by the work done to drive the load.

Therefore, the energy efficiency of air motors is defined as:

$$\eta_{am} = \frac{E_{load}}{E_{air\_in}} = \frac{\int \tau_{load}.\omega_{am} dt}{\int P_{air\_in} dt} \times 100\% \tag{4.27}$$

where E_{load} stands for the work done to drive the load, E_{air_in} is the energy from the input compressed air, which is a function of the mass flow, τ_{load} is the mechanical load torque, ω_{am} is the air motor rotating speed, and P_{air_in} is the power of the input compressed air, which is a function of the mass flow rate.

In this case the exhaust air energy is not considered, as the downstream is directly opened to the atmosphere. That is the exhaust pressure is equal to atmospheric pressure. Practically, the system energy efficiency could be evidently increased with the instrumentality of exhaust recycle (Luo et al., 2012).

According to the 4-vane-type air motor model in Section 4.2 and 2.41-wrap scroll air motor model in Section 4.3, the simulation performances can be compared. Two types of air motors are tested under the same working conditions, inputting the same supply air pressure and load torque. The input pressure and torque are within the common operation conditions. The mass flow rate indicates input power scale; the rotational speed reveals the output power scale. Table 4.3 and Table 4.4 show the simulated results. It is worth to note that the results are the steady state average value, so the energy efficiency could be converted into the power efficiency under this

circumstance.

Table 4.3 The simulation results of 4 vane-type air motor

Supply pressure (bar)	Load torque (N×m)	Rotational speed (Rad/s)	Mass flow rate (kg/s)
4	0.5	76.13	3.80×10^{-3}
4	1	64.58	3.23×10^{-3}
4	1.5	52.50	2.66×10^{-3}
4	2	39.90	2.09×10^{-3}
4	2.5	27.30	1.43×10^{-3}
4.5	0.5	93.14	4.94×10^{-3}
4.5	1	95.34	4.28×10^{-3}
4.5	1.5	66.15	3.71×10^{-3}
4.5	2	54.60	3.14×10^{-3}
4.5	2.5	42.53	2.38×10^{-3}
4.5	3	29.40	1.71×10^{-3}
5	0.5	100.80	6.08×10^{-3}
5	1	89.25	5.32×10^{-3}
5	1.5	78.75	4.75×10^{-3}
5	2	67.20	4.18×10^{-3}
5	2.5	55.65	3.33×10^{-3}
5	3	44.10	2.47×10^{-3}
5	3.5	31.50	1.90×10^{-3}
5.5	0.5	112.35	7.41×10^{-3}
5.5	1	102.90	6.65×10^{-3}
5.5	1.5	91.88	6.18×10^{-3}
5.5	2	80.85	5.42×10^{-3}
5.5	2.5	69.30	4.75×10^{-3}
5.5	3	57.75	4.09×10^{-3}
5.5	3.5	47.25	3.33×10^{-3}
5.5	4	34.65	2.47×10^{-3}
6	0.5	33.10	2.38×10^{-3}
6	1	123.90	8.84×10^{-3}
6	1.5	113.40	8.08×10^{-3}
6	2	92.40	6.65×10^{-3}
6	2.5	81.90	5.99×10^{-3}
6	3	71.40	5.23×10^{-3}
6	3.5	60.90	4.56×10^{-3}
6	4	49.35	3.71×10^{-3}
6	4.5	36.75	2.85×10^{-3}

Table 4.4 The simulation results of 2.41-wrap scroll air motor

Supply pressure (bar)	Load torque (N×m)	Rotational speed (Rad/s)	Mass flow rate (kg/s)
4	0.5	766.50	2.85×10^{-2}
4	1	604.80	2.38×10^{-2}
4	1.5	468.30	1.90×10^{-2}
4	2	343.35	1.33×10^{-2}
4	2.5	200.55	7.60×10^{-2}
4.5	0.5	819.00	3.33×10^{-2}
4.5	1	660.45	2.57×10^{-2}
4.5	1.5	527.10	2.28×10^{-2}
4.5	2	412.65	1.90×10^{-2}
4.5	2.5	305.55	1.38×10^{-2}
4.5	3	178.50	7.13×10^{-2}
5	0.5	867.30	4.09×10^{-2}
5	1	710.85	3.33×10^{-2}
5	1.5	579.08	2.85×10^{-2}
5	2	466.20	2.33×10^{-2}
5	2.5	368.55	1.85×10^{-2}
5	3	287.10	1.33×10^{-2}
5	3.5	197.70	9.12×10^{-2}
5.5	0.5	910.35	4.75×10^{-2}
5.5	1	756.00	3.99×10^{-2}
5.5	1.5	626.85	3.71×10^{-2}
5.5	2	515.55	2.76×10^{-2}
5.5	2.5	418.95	2.38×10^{-2}
5.5	3	334.43	1.85×10^{-2}
5.5	3.5	249.90	1.43×10^{-2}
5.5	4	145.95	8.55×10^{-2}
6	0.5	950.25	5.23×10^{-2}
6	1	799.05	4.66×10^{-2}
6	1.5	670.43	3.80×10^{-2}
6	2	560.70	3.61×10^{-2}
6	2.5	464.63	2.85×10^{-2}
6	3	380.63	2.38×10^{-2}
6	3.5	304.50	1.90×10^{-2}
6	4	228.90	1.43×10^{-2}

Based on Equation 4.27, the power efficiency of both air motors can be obtained. Then scroll air motor's power efficiency improvement upon vane-type's can be defined as:

$$\eta_{imp} = \frac{E_{scroll} - E_{vane}}{E_{vane}} \times 100\% \tag{4.28}$$

Through comparison, it is obvious that scroll air motor holds a significant advantage under any conditions, as described in Table 4.5 (n/a means dead zone condition). It is shown that the efficiency improvement can be as high as 32% in this simulation. And therefore, the high efficiency scroll air motor is selected for the hybrid wind turbine system.

Table 4.5 Scroll air motor's power efficiency improvement

Efficiency improvement		Supply pressure (P) 4	4.5	5	5.5	6
Load torque (N×m)	0.5	21.47%	18.21%	15.87%	14.37%	18.08%
	1	15.24%	4.46%	15.30%	10.79%	10.74%
	1.5	12.99%	17.15%	10.88%	2.88%	13.67%
	2	22.35%	12.83%	12.73%	13.40%	1.14%
	2.5	24.62%	12.08%	7.55%	9.39%	7.79%
	3	n/a	31.84%	2.31%	15.54%	6.11%
	3.5	n/a	n/a	18.75%	11.65%	8.57%
	4	n/a	n/a	n/a	10.09%	9.11%
	4.5	n/a	n/a	n/a	n/a	22.14%

4.5 Mathematical model of compressor

The compressors in CAES systems are purely powered by the excess energy from the grid, which is not a constant energy source. So the compressor has to run at part load much of the time during the CAES charging phase. In this case, reciprocating compressors are significantly more efficient. Compared with the common screw compressor, at part load, the reciprocating compressor enjoys a higher efficiency due to the cylinder unloaders (Almasi, 2009) (Stoecker, 1998). In this project, the most common type of compressor-reciprocating compressor is taken into account. Many

modern industrial air compressors are sold "packaged" with the compressor, drive motor, and many of the accessories mounted on a frame for ease of installation. However, the power may be written in a simpler form for an adiabatic process:

$$P_{cm}\eta_C = w_C c_p T_{atm}(\beta_C^{\frac{k-1}{k}} - 1) \tag{4.29}$$

(Ueno et al., 2003) (Arsie et al., 2005)

where P_{cm} is the power of the compressor motor, η_C is the compressor efficiency, w_C is the mass flow rate of the compressor, c_p is the specific heat of air at constant pressure and $\beta_C = \frac{p_C}{p_{atm}}$ is the compression ratio. The derived equation is based on the following assumptions: 1) compression process in the compressor cylinder is adiabatic; 2) pressure drops across the suction and discharge lines are negligible (Ueno et al., 2003).

Considering the effects of part-load operation, the ratio between actual and maximum adiabatic efficiency has been expressed as a function of the ratio between actual and maximum power, as shown in Figure 4.13. It can be seen that the compressor can only achieve the maximum efficiency within a certain power rating range (60%-90% of the full power).

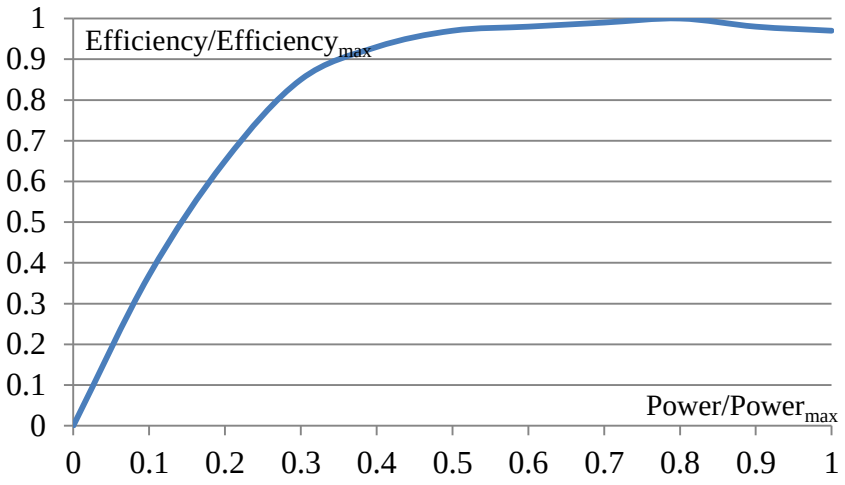

Figure 4.13 Effect of compressor power ratio on efficiency (Arsie et al., 2005)

4.6 Mathematical model of air tank

For the model of an air tank, a constant volume steel tank has been assumed. There are two ports for the tank, one is to get the air in from compressor (increase of internal tank pressure), and the other is to discharge the air to the air motor. Without consideration of heat losses and flow dynamics via pneumatic valves, the inside air pressure during charging and discharging phases can be derived by mass flow based on the gas state equations.

$$\frac{d}{dt}\left(\frac{p_t}{T_t}\right) = \frac{d}{dt}\left(\frac{m_t R_{air}}{V_t}\right) = \frac{w_t R_{air}}{V_t}$$

that is

$$\dot{p}_t = \frac{(w_C - w_{am})R_{air}}{V_t} \tag{4.30}$$

where p_t is the internal tank pressure, V_t is the tank volume and w_C, w_{am} are the mass flow rate of compressor and air motor, respectively.

4.7 Summary

This chapter focuses on the fundamental principles and modelling of different components of CAES systems. The structure of the pneumatic system is described in terms of different subsystems, of how they are functioned. Based on the thermodynamic and geometric study, the complete dynamic models have been derived, including two types of air motors, compressor and air tank. The new 2.41 wrap scroll air motor is modelled and the relationship between the wrap number and mathematical model is introduced. Through the simulation results comparison, the high efficiency of scroll air motor is confirmed. The efficiency improvement can reach up to 32% under the given simulation conditions.

Chapter 5

Modelling and simulation study of a hybrid wind turbine system

With the mathematical models of wind turbines and compressed air systems developed in the previous chapters, a complete small scale hybrid system model is built with consideration of the practical restrictions. This chapter starts from the design of the hybrid integration mechanisms. A novel hybrid wind turbine structure with direct mechanical connection is presented. The overall system mathematical model is derived and the simulation studies are conducted and the results are presented with the charging and discharging phases. At last, the efficiency analysis based on the model is carried out in order to evaluate the system operating performance and explore the strategies for further improvement.

5.1 Two schematics of hybrid systems with CAES

There are two possible system structures for integrating a wind turbine system with compressed air energy storage. The first one is the existing utility scale CAES system. The utility-scale has been demonstrated as an economical solution for hours' timescale energy storage applications. The energy storage system schematic diagram is illustrated in Figure 5.1.

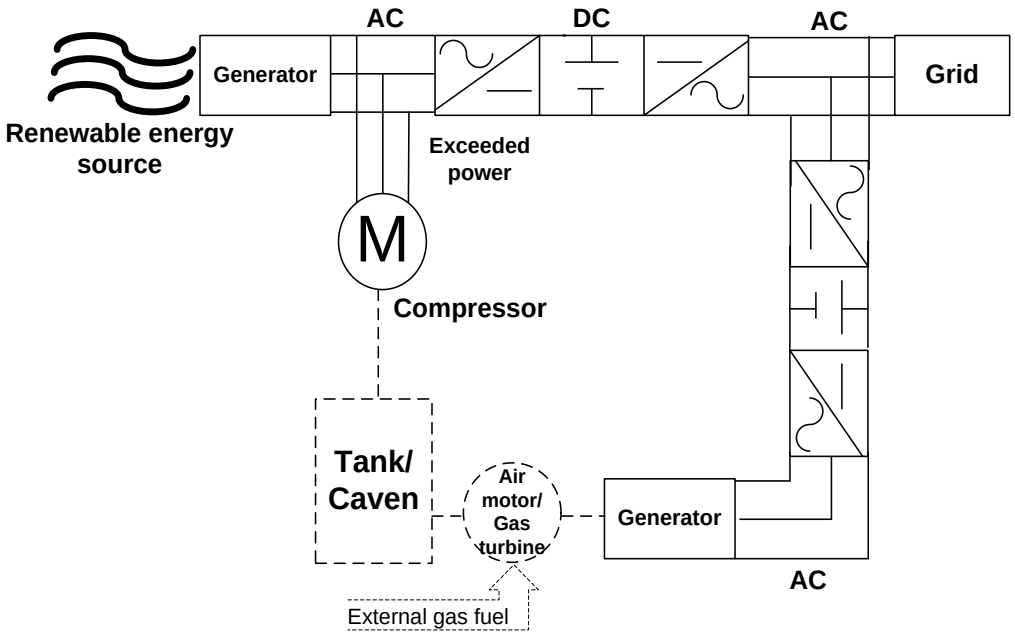

Figure 5.1 Utility-scale CAES application's diagram

The utility-scale CAES systems are successfully implemented in Hantorf in Germany, McIntosh in Alabama, Norton in Ohio; a municipality in Iowa, in Japan and under construction in Israel (Daneshi et al., 2010) (Denholm et al., 2009) (Wolf et al., 2011). The CAES produces power by storing energy in the form of compressed air in an underground cavern. Air is compressed during off-peak periods, and is used on compensating the variation of the demand during the peak periods to generate power with a turbo-generator/gas turbine system. However, this system implementation seems to be limited as it needs a large space to store compressed air, such as large underground carven for large scale power facilities.

This hybrid technique is similar to the series hybrid powertrain in HEV, as the primary energy source and energy storage are hybrid electrically. The non-mechanical structure gives the flexibility to the driving rotor to operate within it power efficient area, independent from torque and speed of the generator. However, the overall

efficiency decreases due to two energy conversions (Gurkaynak et al., 2009).

Inspirited by the parallel hybrid drive train in HEV (Du et al., 2011) (Yang et al., 2011), the second method, a novel direct electromechanical integration is proposed, which will hybridise the wind power and the power from CAES in a parallel manner, as described in Figure 5.2. The concept behind the proposed the structure is that the air motor will be connected to the wind turbine shaft through a mechanical transmission mechanism to provide assistant driving force to smooth the short term transient fluctuations. Also, the driving force provided by the CAES may provide a direct compensation to the torque variation of the wind turbine which is expected to alleviate the stress imposed onto the wind turbine mechanical components, such as the shaft. Based on the current available capacity of scroll air motors, the system structure is more suitable for small-scale wind turbine power generation.

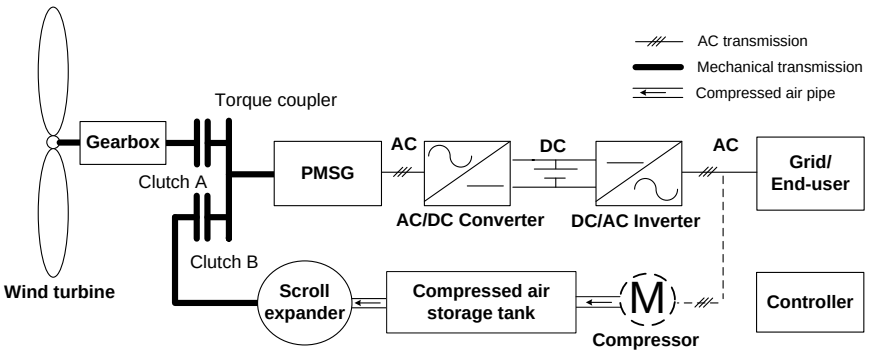

Figure 5.2 Small scale hybrid wind turbine with CAES

The power transmission is able to engage the scroll air motor to the wind turbine shaft. A clutch is placed to the system for conditional switching on and off the CAES and providing a speed match between the scroll and the wind turbine shaft speed. The scroll air motor used in the research laboratory is obtained by modifying a vehicle

scroll compressor (model -TRS090). Thus, for this compressor, there has been a set of existing technical equipment to achieve a similar objective, as shown in Figure 5.3.

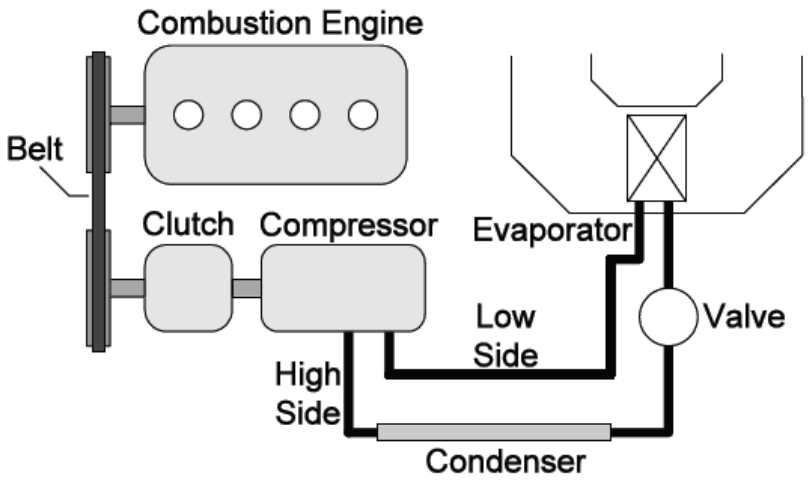

Figure 5.3 Basic structure of typical automobile air conditioning system

In an automobile air conditioning system, the compressor is driven by the engine of the vehicle. The clutch in Figure 5.4 is an electromagnetic clutch which is integrated with most compressors. The whole unit temperature will be controlled by switching the on and off position of the clutch. This structure is simple and easy for maintenance (Yeung etc., 2009). The power transmission system is designed to have a reciprocal structure, as described below:

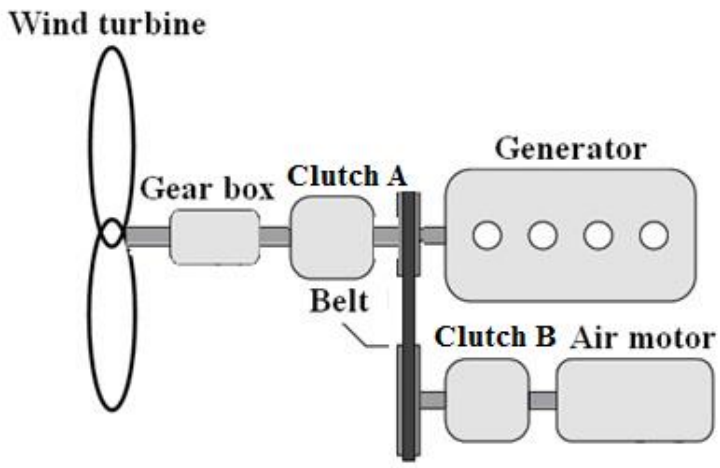

Figure 5.4 Structure of the power transmission system in hybrid wind turbine

In most cases, clutch A is engaged. That is, the generator is driven by the wind turbine blades fully or at least partially. When the wind speed is extremely low, under the cut-in wind speed, the clutch A is open. In this case, the generator is exclusively driven by the scroll air motor. For the simplicity of process modelling, the extreme low wind speed condition is not included in the overall system. That is, the clutch A is always engaged.

The power transmission has three working modes that are described as follows:

Mode 1: When the wind speed is sufficient to match the generator load, the wind turbine operates at its stand-alone mode; clutch B remains open.

Mode 2: When the wind power generation exceeds the generator load demand, the compressor starts to compress air to the storage, which is named the charging mode. The air tank internal pressure will continuously increase along with more compressed air pushed in. Because the compressor is not mechanically connected to the main powertrain, its operation is independent from original running characteristic of the wind turbine system.

Mode 3: When the wind speed is low and the power generated is not enough to match the load demand, the compressed air in the air tank will be released to power the air motor through opening the pneumatic control valve; then the air motor will start rotating to compensate the deficit of the power demand. Simultaneously, the clutch B is engaged. The hybrid wind turbine operates at discharing mode. Thus the pneumatic system and a typical wind turbine are integrated rigidly. Meanwhile, the two plates of the designed belt transmission have different diameters to play the function as a gearbox. In this case, the wind turbine mechanical characteristics will be affected due to the mechanical integration.

The main issue for modelling the whole power transmission is that it presents three different configurations:

Mode 1: In this mode, the disengaged clutch B can be considered completely separated. Both the active plate and the passive plate of the belt transmission can be considered as an extra inertia load, so the total equivalent inertia will be:

$$J_{belt} = J_{pas} + J_{act}\varsigma_b^{\,2} \tag{5.1}$$

where J_{belt} J_{pas} and J_{act} are the inertias of the belt, passive plate and active plate respectively, is ς_b is the speed ratio of the belt.

Mode 2: During the charging phase, Clutch B remains disengaged. Besides Equation 5.1, the difference between the wind power generated and load demand is used to compress air. Referring to Chapter 4.5, the output mass flow rate from a reciprocating compressor can be obtained.

$$(P_G - P_{load})\eta_C = w_C c_p T_{atm}(\beta_C^{\frac{k-1}{k}} - 1) \tag{5.2}$$

Mode 3: During the discharging phase, once the clutch is engaged with the two sides, the active plate and clutch B are considered as one equivalent mass. The dynamic equations are as follows:

$$\begin{aligned}
&\tau_{am} - M_f \omega_{am} - \tau_{act} = (J_{am} + J_{cb} + J_{act})\dot{\omega}_{am} \\
&\tau_{pas} = \varsigma_b \eta_b \tau_{act} \\
&\tau_H + \tau_{pas} - \tau_{emf} - F_G \omega_G = \dot{\omega}_G (J_G + J_{pas}) \\
&\omega_{am} = \varsigma_b \omega_G
\end{aligned} \tag{5.3}$$

where, τ_H is the input torque of wind turbine high speed shaft; η_b is the transfer efficiency of the belt; J_{am} is the air motor inertia; J_{cb} is the clutch B inertia; τ_{am} is the air motor drive torque; M_f is the air motor friction coefficient; $\dot{\omega}_{am}$ represents the angular acceleration.

For the simulation of the hybrid system, the maximum time step has to be tightened (10^{-6} seconds) to improve the accuracy of scroll air motor modelling. There comes the problem that the wind turbine power electronic system built in Simpower occupies most of available resources during the running time, making the simulation extremely slow and time-consuming. Thereby, the power electronic system is simplified to have a pure resistance load for a smoother simulation. The simulation structure is demonstrated in Figure 5.5.

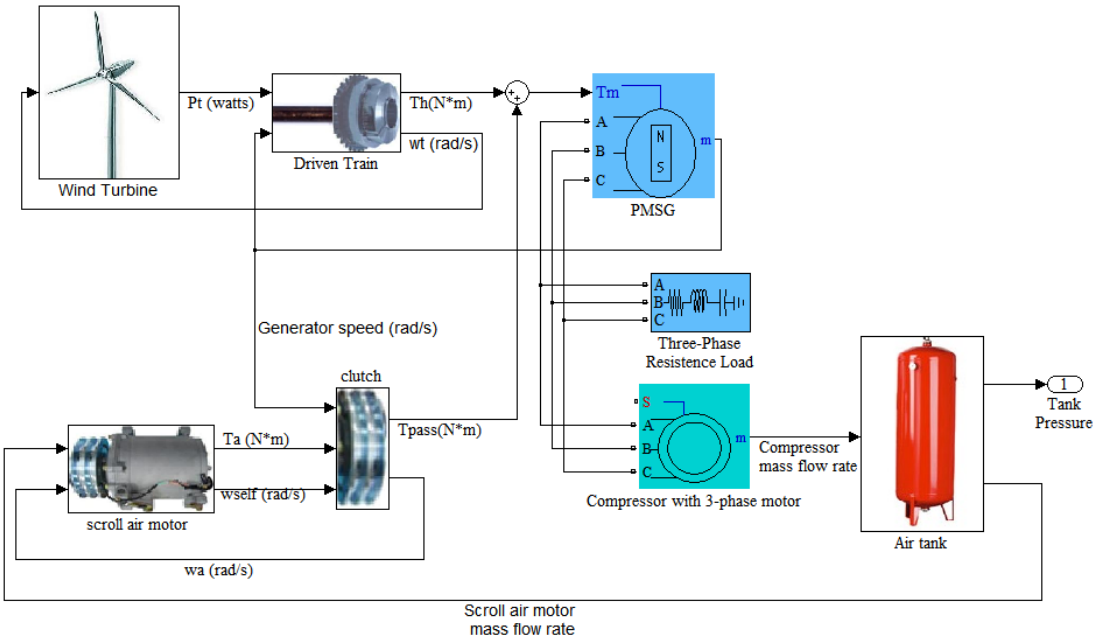

Figure 5.5 Simulation structure of the hybrid wind turbine system

For the scroll air motor based hybrid system, the overall state space model is presented below. The system state variables are chosen as x_1 generator rotor angle, x_2 generator angle velocity, x_3: current in d axis, x_4: current in q axis, x_5: pressure in centre chamber, x_6: pressure in the first pair of side chambers, x_7: pressure in exhaust chamber, x_8: pressure in air tank; and input variables u_1: pitch angle, u_2: supply pressure. Integrating the wind turbine, driven train and generator models, the state functions of the unengaged hybrid wind turbine system can then be described by:

$$\dot{x}_1 = x_2$$

$$\dot{x}_2 = \frac{1}{J_G + J_{pass} + J_T \varsigma_T{}^2 \eta_T}[\frac{\eta_T}{2x_2}\rho_a \pi r_T{}^2 v_w^3 C_p(u_1) - B_{eq}\varsigma_T{}^2 \eta_T x_2 - 1.5 p_G(\varepsilon x_4 + L_d x_3 x_4 - L_q x_3 x_4) - F_G x_2]$$

$$\dot{x}_3 = \frac{U_d}{L_d} - \frac{R_s}{L_d} x_3 + \frac{L_q}{L_d} p x_2 x_4$$

$$\dot{x}_4 = \frac{U_q}{L_q} - \frac{R_s}{L_q} x_4 - \frac{L_d}{L_q} p_G x_2 x_3 - \frac{\varepsilon p_G x_2}{L_q}$$

$$\dot{x}_8 = \frac{w_C R_{air}}{V_t}$$

During stand-alone mode, $w_C = 0$.

while the state space model of the engaged system is:

$$\dot{x}_1 = x_2$$

$$\dot{x}_2 = \frac{1}{J_G + J_{pass} + J_T \varsigma_T{}^2 \eta_T + (J_{am} + J_{cb} + J_{act})\varsigma_b{}^2 \eta_b}[\frac{\eta^{'}}{2x_2}\rho \pi r^2 v_w^3 C_p(u_1)$$
$$- B_{eq}\varsigma_T{}^2 \eta_T x_2 + \varsigma_b \eta_b \tau_{am} - M_f \varsigma_b{}^2 \eta_b x_2 - 1.5 p_G(\varepsilon x_4 + L_d x_3 x_4 - L_q x_3 x_4) - F_G x_2]$$

$$\dot{x}_3 = \frac{U_d}{L_d} - \frac{R_s}{L_d} x_3 + \frac{L_q}{L_d} p x_2 x_4$$

$$\dot{x}_4 = \frac{U_q}{L_q} - \frac{R_s}{L_q} x_4 - \frac{L_d}{L_q} p_G x_2 x_3 - \frac{\varepsilon p_G x_2}{L_q}$$

$$\dot{x}_5 = -\frac{\dot{V}_c}{V_c}\gamma x_5 \frac{x_2}{\varsigma_b} + \frac{1}{V_c}\kappa R_{air} C_d C_0 C_k A_i u_2 f(u_2 / x_5)\sqrt{T_s}$$

$$\dot{x}_6 = -\frac{\dot{V}_{s1}}{V_{s1}}\gamma x_6 \frac{x_2}{\varsigma_b}$$

$$\dot{x}_7 = -\frac{\dot{V}_e}{V_e}\gamma x_8 \frac{x_6}{\varsigma_b} + \frac{1}{V_e}\kappa R_{air} c_d c_0 c_k A_o x_8 f(x_8 / p_{atm})\sqrt{T_s}$$

$$\dot{x}_8 = \frac{-w_c R_{air}}{V_t}$$

where $J_{am}, J_{act}, J_{pas}, J_{cb}, J_G, J_T$ is the inertia of the scroll air motor, belt active plate, passive plate, clutch B, generator, turbine, respectively; M_f is the friction coefficient; V_c is the volume of the centre chamber, V_{s1} is the volume of the side

chamber; $\kappa = 1.4$ is the ratio of specific heats, $c_0 = 0.04$; $c_r = 0.528$; $c_d = 0.8$, A_i, A_o are the effective area of inlet and outlet valves, p_s is the supply pressure, p_e is the exhaust pressure, p_{atm} is the pressure of atmosphere (Yang Li, 2006); w_C and w_c are the mass flow rate of compressor and scroll air motor central chamber, V_t is the internal volume of air tank; r_T is the turbine radius, v_w is the wind speed, C_p is the power coefficient of turbine, which is a function of pitch angle, η_T and i_T mean the efficiency and ratio of the turbine gearbox, B_{eq} is the equivalent damping coefficient of wind turbine; F_G means the combined viscous friction of generator rotor, L is inductance, R_s is resistance of stator windings, p_G is the number of pole pairs, ε is the amplitude of the flux induced by the permanent magnets of the rotor in the stator phases.

5.2 Simulation study of the hybrid wind turbine system

The system consists of a fixed pitch angle 2 KW wind turbine equipped with a three-blade rotor. And the scroll air motor employed is originated from the scroll compressor TRSA090. The parameters of the system are listed in Table 5.1.

Table 5.1 Parameters of the simulated wind turbine

Symbol	Description	Value
J_T	inertia of turbine blades	4 kg × m^2
ρ_a	Air density	1.25 kg/ m^3
r_T	Blade radius	1.7 m
ς_T	Speed ratio of turbine shaft transmission	5

$\eta_{T.}$	Efficiency of turbine shaft transmission	0.95
β_C	Compression ratio	10
P_{Cn}	Rated compressor power	1000 W
V_t	Volume of air tank	10 m^3
p_{t_in}	Initial air tank pressure	10×10^5 Pa
η	Efficiency of hybrid transmission	0.95
r	Orbit radius of the scroll	5.40×10^{-3} m
z	Depth of the scroll chambers	3.33×10^{-2} m
V_{total}	Total control volume of the scroll	2.50×10^{-4} m^3
p_G	The number of pole pairs	6
R_s	Resistance of the stator windings	1.31 Ohm
L_d	Inductance on d axis	2.075 mH
L_q	Inductance on q axis	2.075 mH
λ	Flux amplitude induced by permanent magnets	0.171Wb

To study the dynamic response of the hybrid system, the simulation considers the scenario when the input mean wind speed steps down within a 90 seconds' time series observation window. A typical random wind speed profile composing the nonstationary turbulence is modelled using the Equation 2.1 and 2.2. Figure5.6 shows the simulated wind speed profile for simulation study. In this profile figure, the mean wind speed drops from 12 m/s to 10 m/s at the time of 30 second and then to 8 m/s at 60 second, which demonstrates the major wind speed change within a certain period.

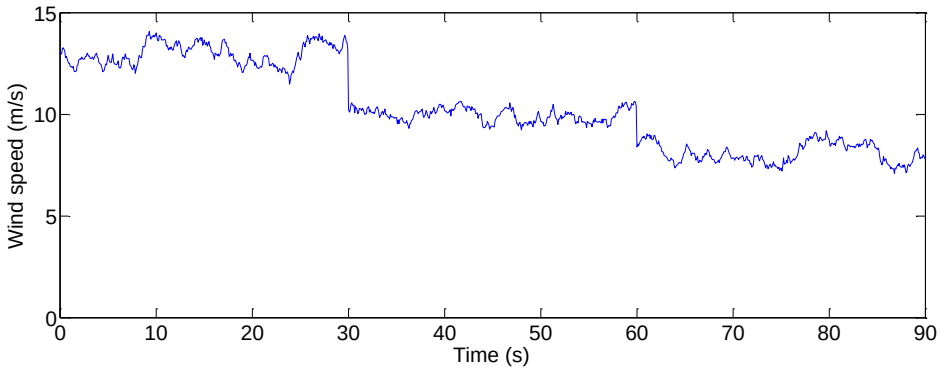

Figure 5.6 Simulated random wind speed profile

The first 30 seconds is charging stage. During this period, the compressor motor is driven by the excess generator power, which equals the difference between the current and rated wind turbine power. From 30 to 60 second, the wind turbine runs under the rated wind speed. Mostly it operates at stand-alone mode, only if there is excess power. Form 60 second, the wind turbine meets wind speed shortage. And then air motor is started to compensate the overall system. The supply pressure to the scroll air motor is set at 5.0×10^5 Pa and the speed ratio between air motor and generator is 1:2.The power compensation system is engaged at the moment of 60 second after the input valve is in its operation.

The simulation results are shown in Figure 5.7, which shows a significant difference of power generation between the hybrid and stand-alone wind turbine status, which in turn changes the load power rating. It can be seen that the hybrid power solution can stabilize the power output on the side of load demand effectively. In this way, the excess power during rich wind period is shifted to overcome the energy shortfall at the lower wind speed.

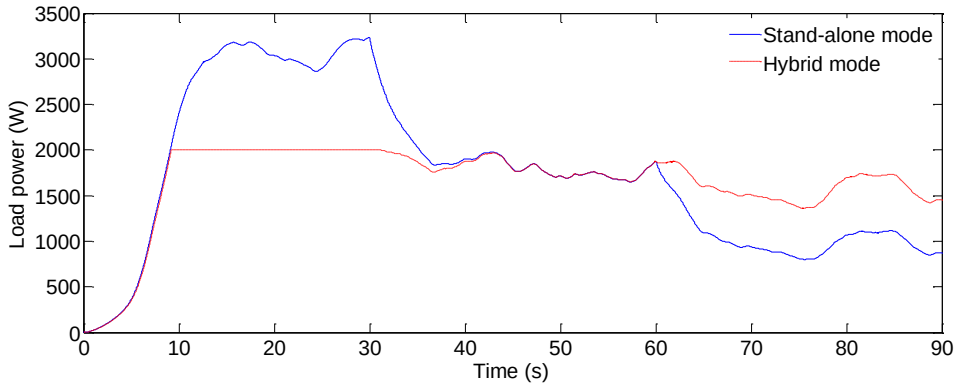

Figure 5.7 Simulation results of the responses of load power

Likewise, the stabilization effect of hybrid operation is apparent on the generator operation patterns, as shown in Figure 5.8. At the high wind speed, the compressor works as an extra load to the generator, thus to reduce the running speed. While when the wind speed is low, the generator is compensated additional driving torque from pneumatic system.

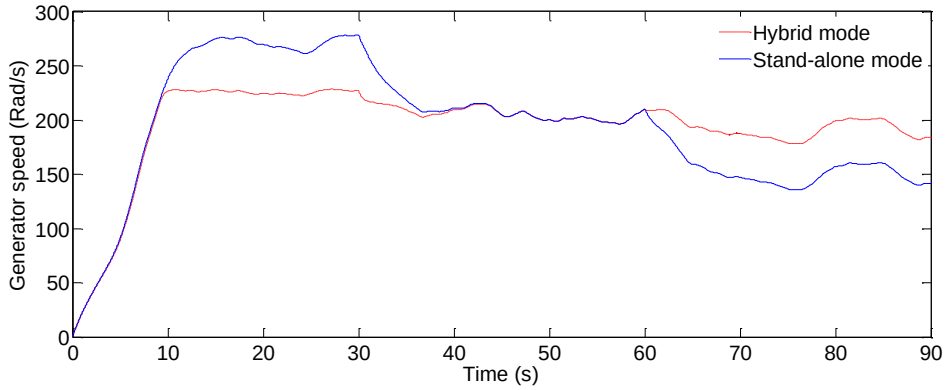

Figure 5.8 Simulation results of the responses of wind turbine generator speed

Figure 5.9 displays the mass flow rate of compressor. When there is surplus power from the load demand, the compress can continuously produce constant 10 bar compressed air as energy storage.

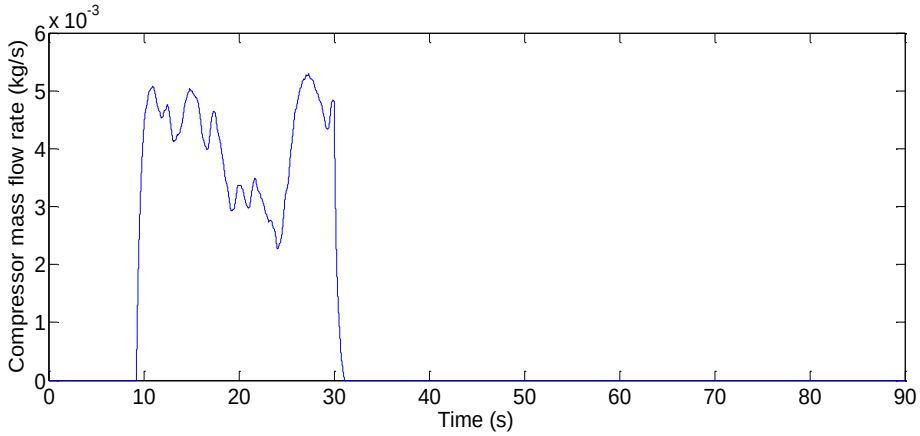

Figure 5.9 Simulation results of the responses of compressor output

The simulation results of scroll air motor operations are revealed in Figure 5.10. The air motor started at the time of 60 second, and joined the wind turbine system rapidly owing to its fast response characteristic. It is worthwhile to note that the air motor is not working steadily under the constant supply pressure. Only because of the hybrid transmission, the air motor running coaxially with the wind turbine, sharing the fluctuation resulted from the variable wind speed.

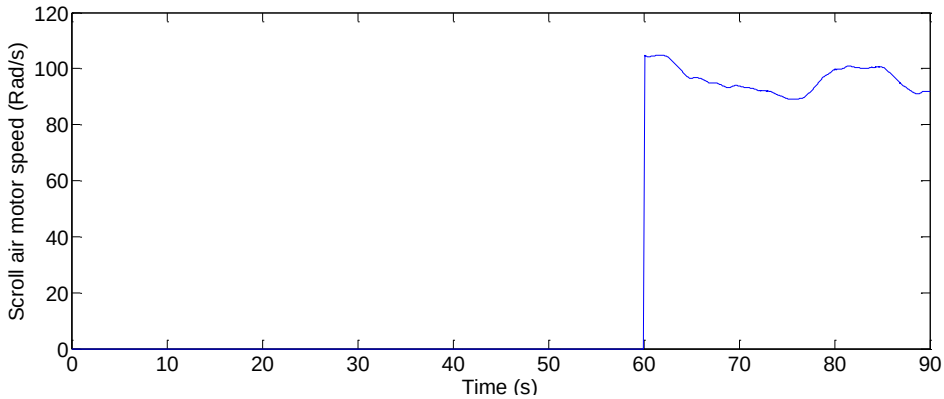

Figure 5.12 (a) Simulation results of the scroll air motor speed

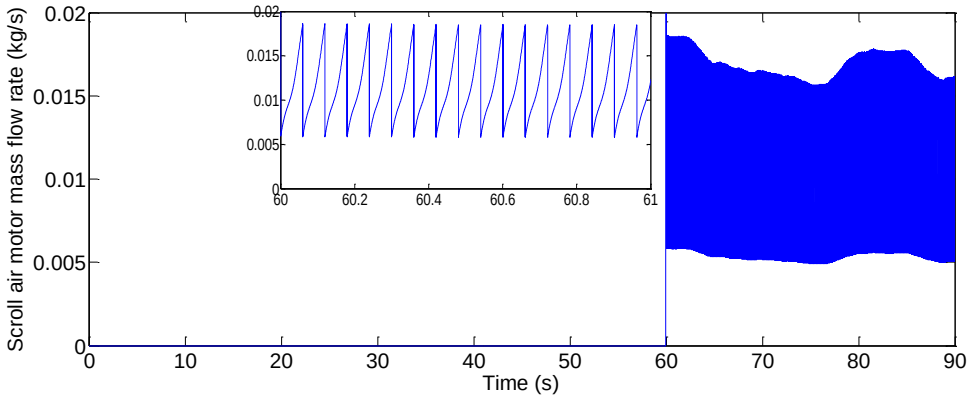

Figure 5.10 (b) Dynamic response of the scroll air consuming mass flow rate

Figure 5.11 shows the air tank internal pressure. From the dynamic pressure, it is easy to distinguish the charging and discharging phases.

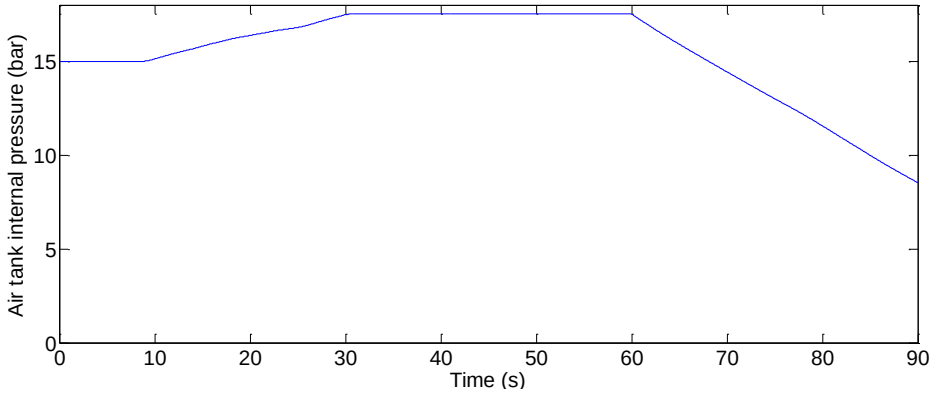

Figure 5.11 Dynamic response of air tank internal pressure

5.3 Energy efficiency analysis based on the simulation results

The energy transmission and conversion of the hybrid mechanism can be schematically illustrated in Figure 5.12.

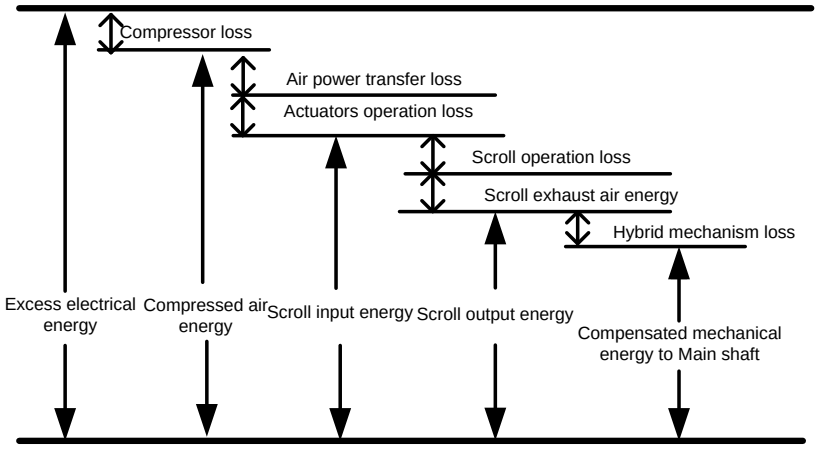

Figure 5.12 Energy transmission and conversion diagram

In almost all cases, the efficiency of charging phase is determined by the compressor. It is highly suggested to keep the compressor running at or at least near its full capacity to obtain an optimised performance. While in this project, the efficiency of discharging phase is focused

As it is difficult to evaluate the efficiency of the belt transmission from simulation, this value of losses is set at a constant for simplicity. In this case, the efficiency of scroll air motor plays a key role in the hybrid system performance. The air motor efficiency can be defined as the ratio between the output mechanical power and input air power. Thus it is necessary to find out how much air power/energy contained in the compressed air input to the system. As described in Chapter 3, a well-accepted approach is adopted for calculating the input air energy:

$$E_{air} = m_{in} R_a T_{atm} [\ln \frac{p}{p_{atm}} + \frac{\kappa}{\kappa + 1} (\frac{T - T_{atm}}{T_{atm}} - \ln \frac{T}{T_{atm}})] \tag{5.4}$$

where, E_{air} is available energy of compressed air, p is pressure, V is volume, κ (heat ratio of air) equals 1.4, T is temperature, subscript atm means atmosphere

condition. Substituting this equation and $T_{in} = T_{atm}$ into Equation 5.4, air power at atmospheric temperature can be reduced to:

$$\dot{E}_{air} = w_c R_a T_{atm} \ln \frac{p_{in}}{p_{atm}} \tag{5.5}$$

Besides the pneumatic system efficiency, considering its feedback effort on the whole system, the turbine efficiency C_p is also taken into account. With the model described by Figure 5.7, Table 5.2 presents the simulation results of the turbine and air motor efficiency for the cases at different air supply pressures and speed ratios. For the wind turbine, a profile with constant 8 m/s wind speed is applied for a steady state analysis. Under this situation, the energy efficiency is the equivalent of power efficiency. The pressures and speed ratios are chosen as coordinate elements as they reveal the upstream and downstream factors on the pneumatic system.

Table 5.2 Simulation results of the hybrid wind turbine system

Speed ratio	Inlet pressure (bar)	Mass flow rate (kg/s)	Inlet air power (w)	Air motor power (w)	Air motor efficiency	Turbine efficiency Cp
1:2	3	0.0018	170.26	80	46.99%	0.42
1:2	3.5	0.00205	221.12	105	47.49%	0.44
1:2	4	0.0022	262.59	130	49.51%	0.42
1:2	4.5	0.0029	375.55	158	42.07%	0.41
1:2	5	0.0032	443.43	180	40.59%	0.39
1:2	5.5	0.0038	557.76	220	39.44%	0.36
1:2	6	0.0040	617.08	240	38.89%	0.35
1:1	5	0.0095	1316.4	820	62.31%	0.34
1:1.5	5	0.0050	692.8	345	49.79%	0.37
1:2	5	0.0032	443.4	180	40.59%	0.39
1:2.5	5	0.0026	360.3	114	31.62%	0.40
1:3	5	0.0020	277.1	77	27.83%	0.41

Figure 5.15 demonstrates the simulated system efficiency via different supply

pressures. The desired speed ratio between air motor and the wind turbine generator is set at 1:2. It can be easily seen that, different inlet pressures will result in different air motor efficiency. Within the simulation condition range, Figure 5.13 shows that the maximum efficiency reaches 49.51% at the 4 bar supply pressure.

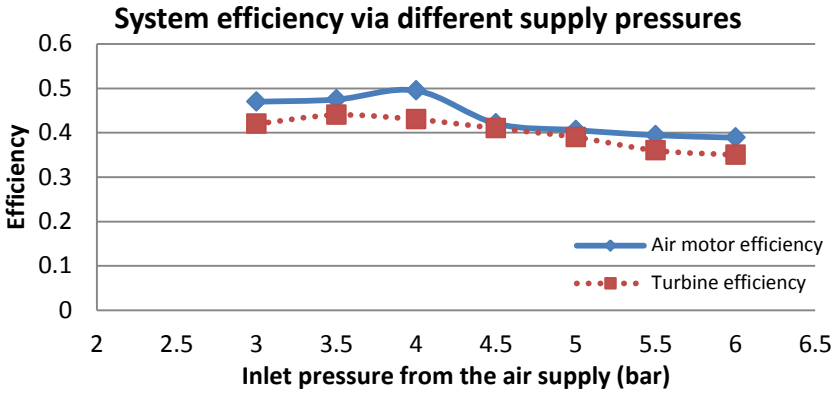

Figure 5.13 Simulated system efficiency via different supply pressures

Figure 5.14 illustrates the simulated efficiency of the system varies with different speed ratios that represents different load levels. In other words, lower ratio indicates higher speed, lower torque load; conversely higher ratio means lower speed and higher torque load. It is shown that the scroll air motor efficiency will greatly increase while the air motor speeds up; the maximum value could exceed 60% with the lowest speed ratio. When the rotation is slowing down, the air expansion power could not get fully employed, that in turn, results in a low efficiency.

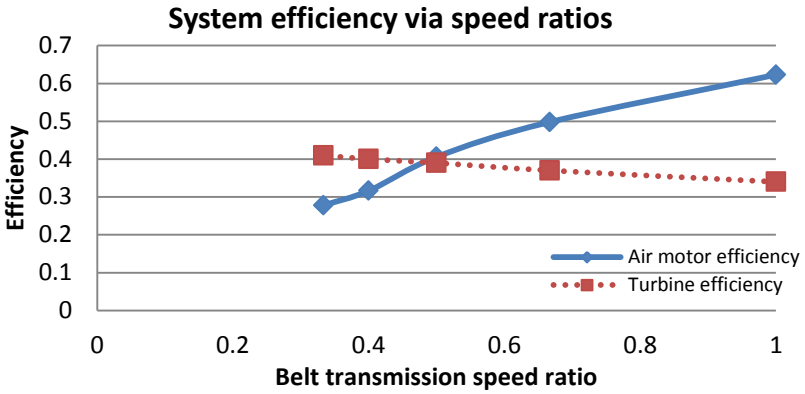

Figure 5.14 Simulated system efficiency via different speed ratios

However, for the turbine efficiency C_p, it has no direct relationship with the system working conditions. In real wind turbine operations, pneumatic compensation is only integrated when the wind speed drops. Then the air motor's driving force contribution will bring the turbine speed higher than that in stand-alone mode. Thus the tip-speed ratio $\lambda = \omega_T \cdot r_T / v_w$ will definitely increase, usually the high λ value results in the low C_p value, as show in Figure 2.5. That should be considered as adverse feedback to the hybrid system. Further work on aerodynamic based turbine blade research needs to be conducted to gain better understanding to this "loop effect".

5.4 Summary

This chapter starts from learning the current hybrid transmission strategies. Two main structures are introduced and studied. Inspired by these, novel hybrid integration for small-scale wind turbine system is presented, which is a direct electro-mechanical transmission. The operation of this hybrid transmission is described as multi-mode, including the charging, stand-alone, discharging phases. The simulation study on the hybrid wind turbine system shows the encouraging stabilization ability for the load

demand. The proposed hybrid system enables the hybrid wind turbine operates at a relatively steady speed profile, which in turn will improve the overall system reliability. Additionally, the simulation-based energy efficiency analysis reveals that the hybrid transmission design has significant impact on the energy efficiency. The overall system efficiency is proportional to the inlet pressure and inverse proportional to the belt transmission speed ratio. And some characteristics on typical wind turbines are changed due to the integration of energy storage system. The simulation results indicate that the wind turbine efficiency C_p is lower than that in stand-alone mode.

Chapter 6

Multi-mode control strategy for the hybrid wind turbine system

The mathematical model of hybrid wind turbine in the last chapter is built with only on-off switch control. To maintain a more accurate operation status, closed-loop control is required. The design of hybrid wind turbine controller is more difficult than the control of typical stand-alone system, because the complete hybrid system is an integrated system that consists of many sub-systems and multi-mode operations. Each sub-system is also a complex system that has its own functionality and desired performance. Such high order nonlinear control system is far too complicated and multi modes operations exist (Utkin and Chang, 2002). It needs to determine the optimal operating mode among three possible modes, such as stand-alone mode, charging mode and discharging mode. Therefore, to coordinate each sub-system in an optimal manner and regulate the whole system's power output, a suitable management or decision making strategy is essential and a multi-mode control is required to cover all the operation modes.

The main objective of the multi-mode control strategy design is to develop a steady and practical power management strategy that determines the proper CAES engagement time to either charge or discharge the stored compressed air; meanwhile, it also satisfies the following constraints:

• to meet the load power demand at all time;

• to maintain a steady power output under the variable wind speed;

• to protect the wind turbine from over-speed at high wind speed.

A supervisory hybrid system controller sits at the top to manage the operation of the hybrid powertrain system. The supervisory powertrain controller is designed to include the following functions: wind turbine pitch control, air motor supply pressure control and CAES engagement control. To ensure that the multi-mode controller achieves a guaranteed level of performance and robustness, a model-based design process was adopted (Lin et al., 2003).

6.1 Wind turbine pitch control

In the most general cases, the control system is an essential part in a wind turbine system. Control systems can be broadly grouped into two major categories: open-loop control and close-loop control. Open-loop control, also known as non-feedback control, is a simple control solution; as it does not use feedback for decision making if its output has achieved the desired objective of the input. While closed loop control can counteract against disturbances (negative feedback) and self-adjust accordingly (Christian, 2005). The closed loop controller is able to automatically adjust the operational state of the whole system, in order to track some pre-defined operation curve or characteristics, thus to achieve real automatic control.

Nowadays, closed loop controller plays a main role in modern wind power industry automatic control area.

As described in the wind turbine model chapter, the power coefficient C_P is the figure-of-merit and is defined as the ratio of actual power delivered to the free stream power flowing through a similar but uninterrupted area, and tip speed ratio λ is the ratio of turbine speed at the tip of a blade to the free stream wind speed. C_P is a nonlinear function of and the pitch angle β (in degrees). Figure 2.5 visualize C_P - λ curve family via the different pitch angle θ_p .

There are two control schemes for permanent magnetic synchronous generator to achieve the two control goals: pitch control and speed control. The pitch control is implemented to adjust the aerodynamic power extracted from the wind. The pitch controller plays the role of a governor in a conventional generator system, which is used to prevent the generator from exceeding its rated power. This goal is achieved by monitoring either speed or power feedback. The speed control is applied to drive the machine to follow the target speed curve. This goal is achieved by controlling the full power converter on the machine side (Yin et al., 2007).

Compared with generator speed control, pitch control is relatively fast, and can be better used to regulate power flow especially when near the high speed limit. While the system speed change is relatively slow because of the large inertia involved. This makes it difficult to use the power converter to control the generator speed in highly variable wind applications. For pitch control, two conditions are discussed respectively (Muljadi and Butterfield, 2001).

1. Below and around the rated operation

At low and medium wind speeds, the goal is to maximize the power extraction with

an optimal power coefficient and so constant tip speed ratio (Lackner, 2009). The pitch control is rarely actuated and only set to the optimum value, for example $0^{o,}$ depending on different individual characteristic.

2. Above the rated operation

As the wind speed increases, the power generated by the wind turbine also increases. Once the maximum rating of the power converter is reached, the pitch control is use to help control average power. In practice, turbine blades are pitched towards incoming wind to decrease the angle of attack and thereby shed the aerodynamic power. As a result, the wind turbine operates at lower efficiency.

The developed control system has integrated a fuzzy logical controller for speed control of the generator that can limit the captured energy at high wind speeds. Fuzzy control provides a systematic way to incorporate human experience about how to control a nonlinear system, which usually has uncertain factors and inaccurate property. The controller is structured under Simulink environment, as shown in Figure 6.1:

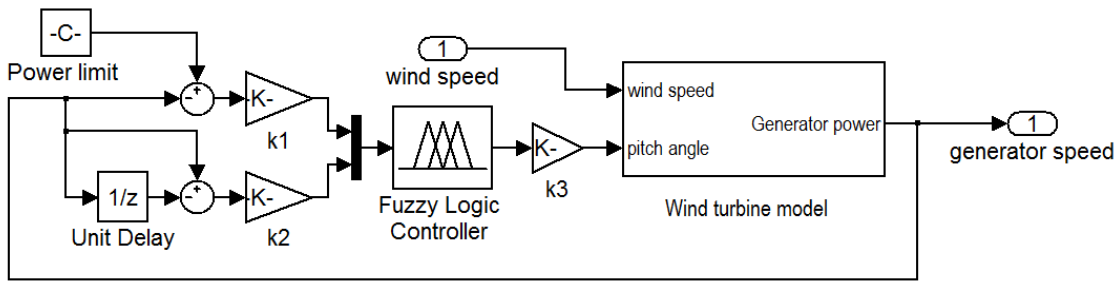

Figure 6.1 Fuzzy logical pitch controller diagram

Choosing the generator speed error v_e (difference between running and reference

generator speed), the generator speed increment v_i and pitch angle control value θ_p as the linguistic variables. v_e and v_i are inputs of the fuzzy controller, θ_p is the controller output value. The linguistic values of v_e and θ_p both are: [NB NM NS ZO PS PM PB], which means negative big, negative middle, negative small, zero, positive small, positive middle, and positive big respectively; The linguistic values of v_i are: [N Z P], that means negative, zero, positive.

Standard triangular membership functions have been used for both the inputs and the output of the fuzzy controller. The control law of a fuzzy controller is represented by a set of heuristically chosen fuzzy rules. The designed fuzzy rules used in this model are given in Table 6.1.

Table 6.1 Rule base for proposed fuzzy controller

θ_p		v_i		
		N	Z	P
v_e	NB	PB	PB	PM
	NM	PB	PM	PS
	NS	PM	PS	ZO
	ZO	PS	ZO	NS
	PS	ZO	NS	NM
	PM	NS	NM	NB
	PB	NM	NB	NB

Given the rules and membership functions, the fuzzy controller produces the crisp and continuous nonlinear input/output map, as shown below：

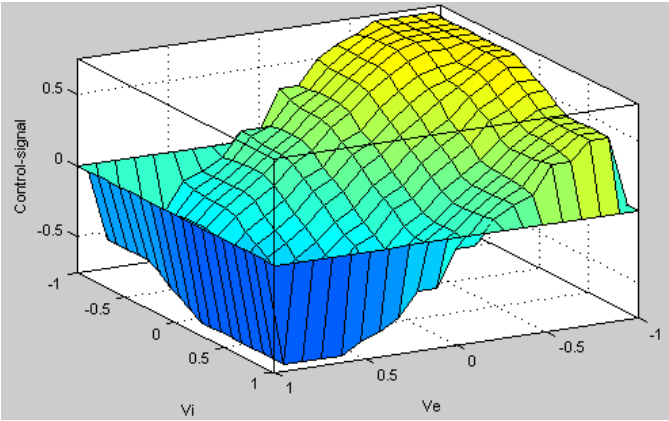

Figure 6.2 Fuzzy logical controller nonlinear input & output map

The fuzzy map indicates that numerous nonlinearities are designed to enhance the controller's ability to drive the system to the set point. Soft and nonlinear control actions resulted from the fuzzy rules can improve the wind turbine performance (Prats et al., 2000).

An immediate and easy understanding of the controller logic can be obtained as following considerations:

1) If v_e is negative big and v_i is also negative, the output angle is too small and its amplitude is dropping, consequently current pitch angle must be quickly increased.

2) If v_e is negative big while v_i is positive, the output is lower than its reference, but since its amplitude is increasing, pitch angle increment must be small.

3) If v_e is small, pitch angle variation must be smoothed because too large variations excite oscillatory modes (Zhang et al., 2008).

6.2 Air motor supply pressure control

To achieve global speed objective, the scroll air motor is controlled to achieve a specified output. In this application the PID-type control is used. Considering the

limited volume of the scroll central chamber, traditional PID valve displacement control is not quite efficient for scroll air motor. Proportional pressure regulator based PID control is applied to adjust the overall performance of the hybrid system. Proportional-integral-derivative (PID) control is certainly the most widely used control strategy today. It is estimated that over 90% of control loops employ PID control, quite often with the derivative gain set to zero (PI control). Over the last half-century, a great deal of academic and industrial effort has focused on improving PID control, primarily in the areas of tuning rules, identification schemes, and adaptation techniques. It is appropriate at this time to consider the state of the art in PID control as well as new developments in this control approach (Knospe, 2006). A major advantage of the PID controller is that its parameters have a clear physical meaning. Indeed, increasing the proportional gain leads to an increasing of the bandwidth of the system and therefore a faster but more oscillatory response should be expected. Conversely, increasing the integral time constant, for example decreasing the effect of the integral action) leads to a slower response but to a more stable system. Finally, increasing the derivative time constant gives damping effect, although much care should be taken in avoiding to increase it too much as an opposite effect occurs in this case and an unstable system could eventually result (Visioli, 2006). The PID control system in this study is depicted in Figure 6.3.

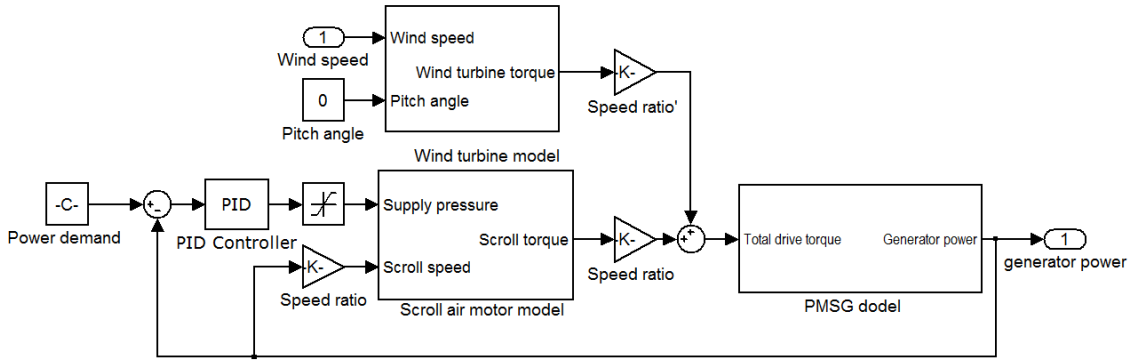

Figure 6.3 PID pressure controller diagram

The tracking error is defined as

$$e = \omega_{ref} - \omega_G \tag{6.1}$$

in which ω_{ref} represents the reference generator velocity. The PI control law can be represented as:

$$U_{PID} = U_P + U_I + U_D = K_P e + K_I \int e + K_D \frac{de(t)}{dt} + C_{initial} \tag{6.2}$$

where U_P is a proportional controller; U_I is an integral controller; U_D is an differential controller; K_P K_I and K_D are the corresponding control gains; and $C_{initial}$ means the initial condition.

6.3 CAES engagement control

According to the introduction in Chapter 5, the CAES engagement control strategy can be simply described as: When the wind speed is low and the turbine cannot generate sufficient electricity to match the load demand, the compressed air in the air tank will be released into the scroll air motor through opening the pneumatic control valve; then the air motor will start rotating to compensate the deficit of the power demanded. While during the high wind speed, the excess electrical power over load

demand will be used to drive the compressor, and then the hybrid system enters the charging phase.

For the purpose of avoiding mechanical damage, the mechanical clutch should be engaged only when the turbine and the scroll air motor operates at the same speed. However, due to the fast response nature of scroll air motor, it could easily meet and surpass the demand speed in an instant, which is hard to be observed and controlled. And if the operate time of electro-magnetic coil is considered, this task will be much more difficult. For the electromagnetic clutch applied in this project, the common control strategies include:

1. Coil current control

In vehicle technology, the electromagnetic clutch is usually controlled by its coil current (Wu et al., 2009). Because the transmission torque of the electromagnetic clutch is linear to the coil current. In this way, the clutch can be jointed within variable speed ranges smoothly. However, this requires power electronic devices, and permits relative rotation between the connected members.

2. Simple switch control

One simple way is "connect once start", that means clutch will be engaged once the air motor starts to run. Although, the mechanical shock may be unavoidable in this way, the torques shock of both air motor and generator vary in an acceptable range.

From Newton's Second Law of Motion, in stand-alone state, we have:

$$\tau_e = \tau_H - (J_G + J_{pass} + J_T \frac{\eta_T}{\varsigma_T^{\ 2}})\dot{\omega}_G - B_{eq} \frac{\eta_T x_2}{\varsigma_T^{\ 2}} \tag{6.3}$$

While in hybrid state,

$$\tau_e = \tau_w + \frac{\eta_b}{\varsigma_b}\tau_{am} - [J_G + J_{pass} + J_T \frac{\eta_T}{\varsigma_T^2} + (J_{am} + J_{cb} + J_{act})\frac{\eta_b}{\varsigma_b^2}]\dot{\omega}_G - B_{eq}\frac{\eta_T x_2}{\varsigma_T^2} - M_f \frac{\eta_b x_2}{\varsigma_b^2} \quad (6.4)$$

According to these 2 equations, the air motor factors are not so influential except the added drive torque—$\frac{\eta_b}{\varsigma_b}\tau_{am}$. That is resulted from the tiny air motor friction and inertia compared with the whole system. So that is why the mechanical shock is limited. It can be concluded that "connect once start" strategy should be acceptable.

3. Master plate speed control

During vehicle starts, as well known, the maximum torque also varies with the engine throttle opening, so taking them as control target, the joint process of the clutch can be shorten, then friction loss will be decreased more (Wu et al., 2008).

To the scroll air motor, the supply pressure can be adjusted until the rotational speed of master plate is same as that of the slave one. Then the clutch can be engaged steadily. By the same token, it could be hard to implement owing to the scroll's instant start nature.

For conclusion, the advantage and disadvantages of different control strategies can be summarised:

Table 6.2 Comparisons between different clutch control strategies

	Coil current control	Simple switch control	Master plate speed control
Complexity	High	Low	Medium
Mechanical shock	Low,	Medium w	Low
Noise and friction	High	Medium	Low

In this project, the simple switch control is employed both in simulation and experiment mainly because of simple structure and acceptable performance.

6.4 Simulation study of the hybrid system with multi-mode control

With the designed control strategy, the flow chart can be illustrated in Figure 6.4. The strategy consists of judgements, modelling, and closed-loop control processes. When the generator power is above the limit, there is the fuzzy logical pitch control. Within the limit power and rated power, the hybrid system is in charging mode. Around the rated power, the wind turbine is running in stand-alone mode. Besides, the pneumatic system is discharging when the wind power is under the rated value.

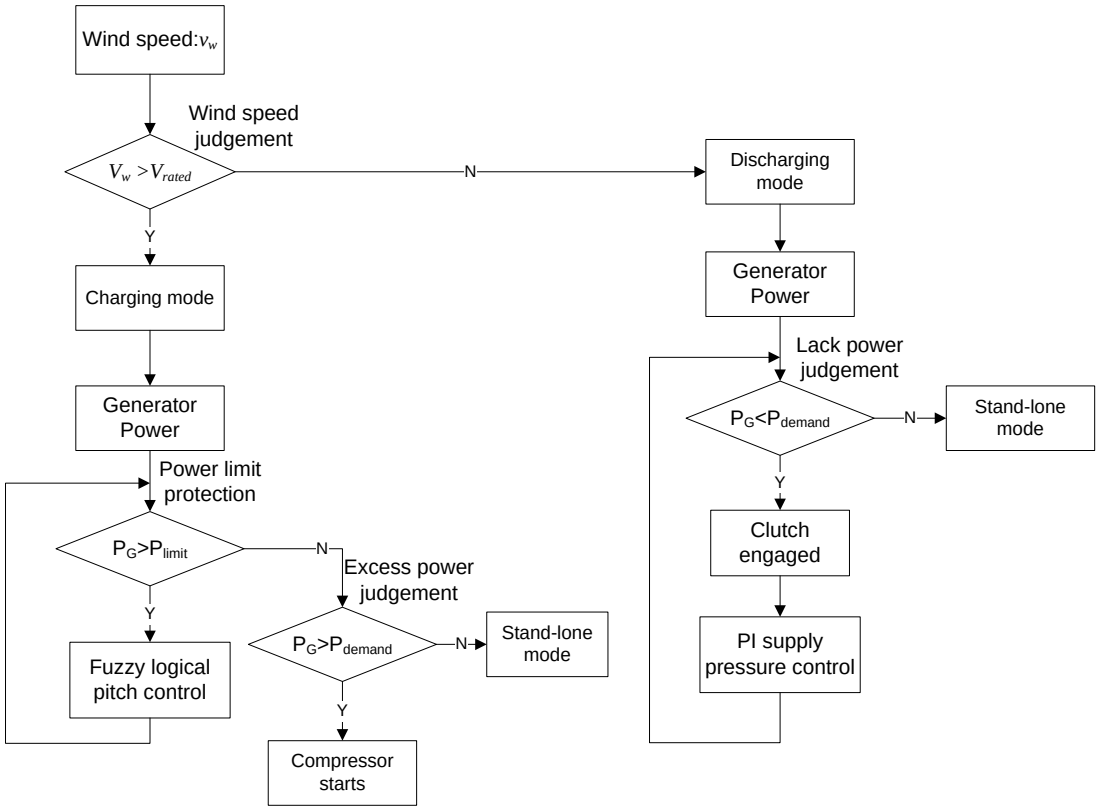

Figure 6.4 Multi-mode control diagram

The output of the power management strategy is the compressor switch command and air motor switch command, which are designed for the purpose of energy storage. Moreover, the design procedure is required to be systematic, accommodating multiple objectives and cost-effectiveness. In this study, a model based design approach is applied based on the simulation programme. The control strategy could be tested and tuned in a hardware-in-the-loop (HIL) simulation test in a fast and cost-effective way. The mathematical model for the controlled hybrid wind turbine system is derived, and Figure 6.5 describes the block diagram of the overall system model in Simulink.

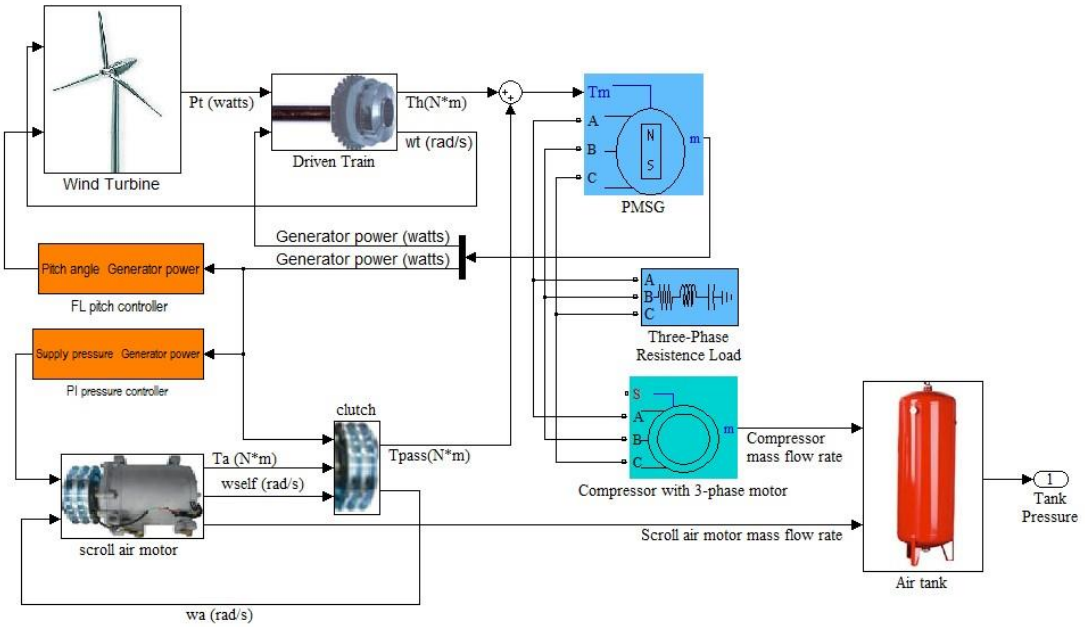

Figure 6.5 Block diagram of multi-mode controlled hybrid wind turbine system

For comparison, the parameters used for the wind turbine and CAES are exactly the same as those that used in Chapter 5 (referring to Table 5.1). The power limit for the wind turbine generator is set to be at 3000 W and the load power demand is 2000 W. Then the developed model for the controlled hybrid system is implemented for the simulation studies.

The simulation results are shown in Figure 6.6 to 6.8 in comparison with the uncontrolled system performance in Chapter 5. In Figure 6.6, the generator power under two situations is demonstrated, that is with or without the control strategy.

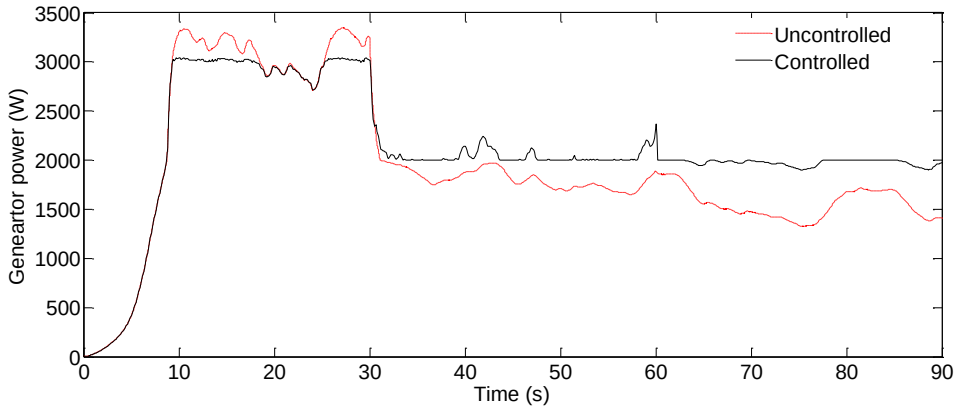

Figure 6.6 Simulation results of hybrid wind turbine generator power

During the first 30 seconds high wind speed period, the wind turbine pitch controller is activated at the over power moment. The power generation over 3000 W is shed due to the fuzzy logical pitch controller. The pitch angle will increase while the wind power is extremely surplus. Consequently, the excess power used to compress air is also reduced, revealed in the compressor mass flow rate, as show in Figure 6.7. However, it is still essential to provide the wind turbine over power protection.

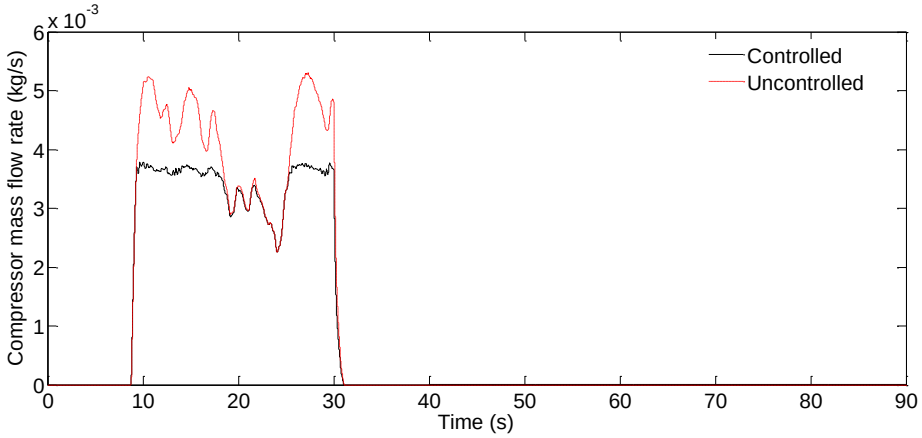

Figure 6.7 Simulation result of compressor mass flow rate

While, under or around rated wind speed, the generator power can still maintain a

steady output near the desired level. This illustrates that the scroll air motor can operate properly to alleviate the impact of low and variable wind speed. The supply pressure is adjusted according to the current extracted wind power, then to determine how much power is compensated to the load demand.

As with the generator power, the simulated generator speed has similar changing tendency, shown in Figure 6.8. Compared with the uncontrolled simulation, the controlled generator operates steadier without major disturbances. In turn, this will alleviate the mechanical stress imposed onto the wind turbine.

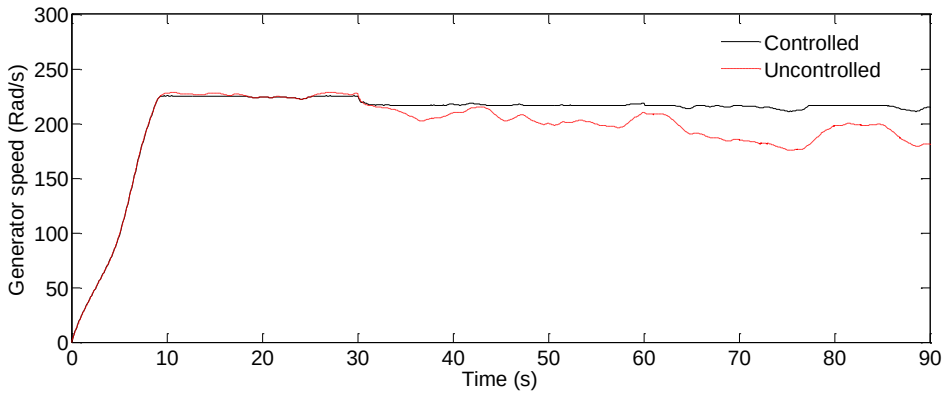

Figure 6.8 Simulation results of hybrid wind turbine generator speed

Figure 6.9 shows the controlled variables in multi-mode system. (a) is pitch angle value, which fluctuate to maintain a steady extracted wind power during high wind speed, and then decline to 0 degree for a maximum when wind speed is low. (b) describes the supply pressure curve. It starts to increase when there is lack of generator power and then is controlled to adjust the compensated power from the pneumatic system.

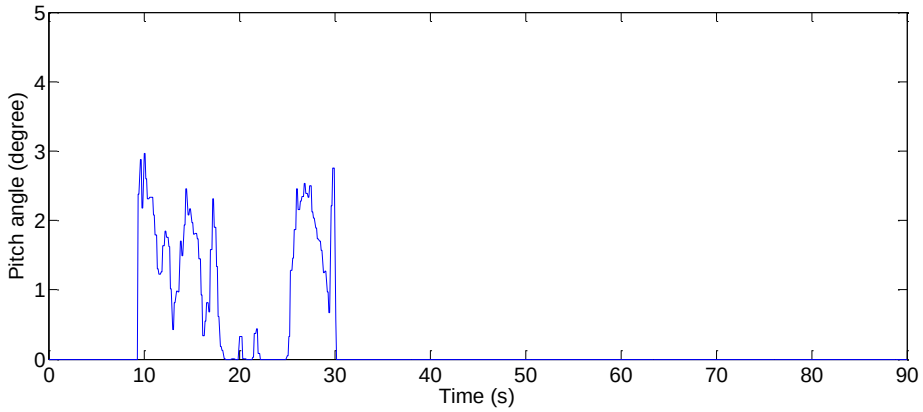

Figure 6.9(a) Simulation result of controlled hybrid wind turbine pitch angle

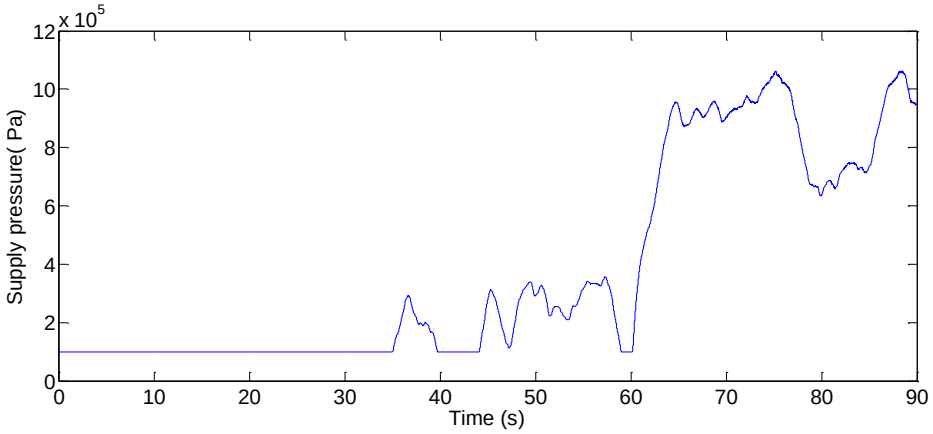

Figure 6.9(b) Simulation result of controlled hybrid wind turbine supply pressure

6.5 Summary

In this chapter, the achievement on the multi-mode control strategy for the hybrid wind turbine is reported. The complete model for the whole system is derived and implemented in Simulink for simulation study. The use of fuzzy logical pitch control can improve mechanical power response performance of wind turbine. It is shown that the wind turbine can still maintain a steady statue at varying wind speed of 12-10 m/s. The PI pressure control could compensate the appropriate power to fulfil the power gap during the low wind speed period. However the performance is it is not so accurate, due to the highly nonlinear pressure dynamic characteristics resulted from

the compressibility of air. Based on the simulation of the overall system with the proposed controller, the experiment method and conditions are prepared.

Chapter 7

Hybrid wind turbine experiment system

The design of the hybrid wind turbine system, together with the multi-mode control strategy, is a novel research field. Although the simulations have brought encouraging performance, still they are not enough and need to be tested in practice, which require experimental setups.

The chapter describes the creation of such an experimental setup. A test rig associated with the proposed hybrid wind turbine system is built in the research laboratory. For the convenience of lab work, the experimental is based on a wind turbine simulator that is functioned by dual DC motors driving system. The design of the overall test rig can be divided into a number of subdesigns, which will extensively be discussed in the following sections. The test rig can perform most functions as a real hybrid wind turbine under the dSPACE real-time supervision. Unfortunately because of the insufficient time, the final stage of the setup did not include a charging phase. This chapter has embodied the recent experimental work, including the experimental system design and result analysis.

7.1 Wind turbine simulator design

7.1.1 Introduction of wind turbine simulator

Since a real wind turbine may not always be available; and due to the nature of wind,

the testing environment is not controllable, which is not very convenient for an early stage development (Gong and Xu, 2008). For the research on wind power technology, it is necessary to build a simulator to simulate the dynamic behaviour of wind turbine and generator, without reliance on natural wind resources (Liu, Wang and Zhang, 2010). It was noticed that the existence of an equipment to accomplish most of the tests in indoor lab scale, as close as possible of the actual values encountered in the field, could bring lower cost design and non-time consuming tests having as a consequence, more efficient and practical solutions (Farret, Gules and Marian, 1995).

A wind turbine simulator system should have the same characteristics as a real wind turbine has, by which to design, estimate and test the real wind energy conversion system. The research and development on wind turbine simulator technologies encompasses three major topics: wind speed simulation (Nichita et al., 2002), variable-pitch dynamic simulation (Jin et al., 1998) and turbine characteristic simulation. Considering the hybrid wind turbine is designed for small scale, there have been many studies focusing on turbine characteristic simulation based on different types of driving motors, including induction motor (Kojabadi, Chang and Boutot, 2004) (Jia, Wang and Yang, 2007), permanent magnet synchronous machine (PMSM) (Xu et al., 2007), DC motor (Battaiotto, Mantz and Puleston, 1996) (Ovando, Aguayo, and Cotorogea, 2007). The strategy of a wind turbine simulator operation can be summarized as: giving the exactly same driven load, the wind turbine torque command is calculated based on a given wind speed profile, either online or offline; the driving motor is controlled following this command to output as the real wind

turbine does.

7.1.2 Overall test rig schematic

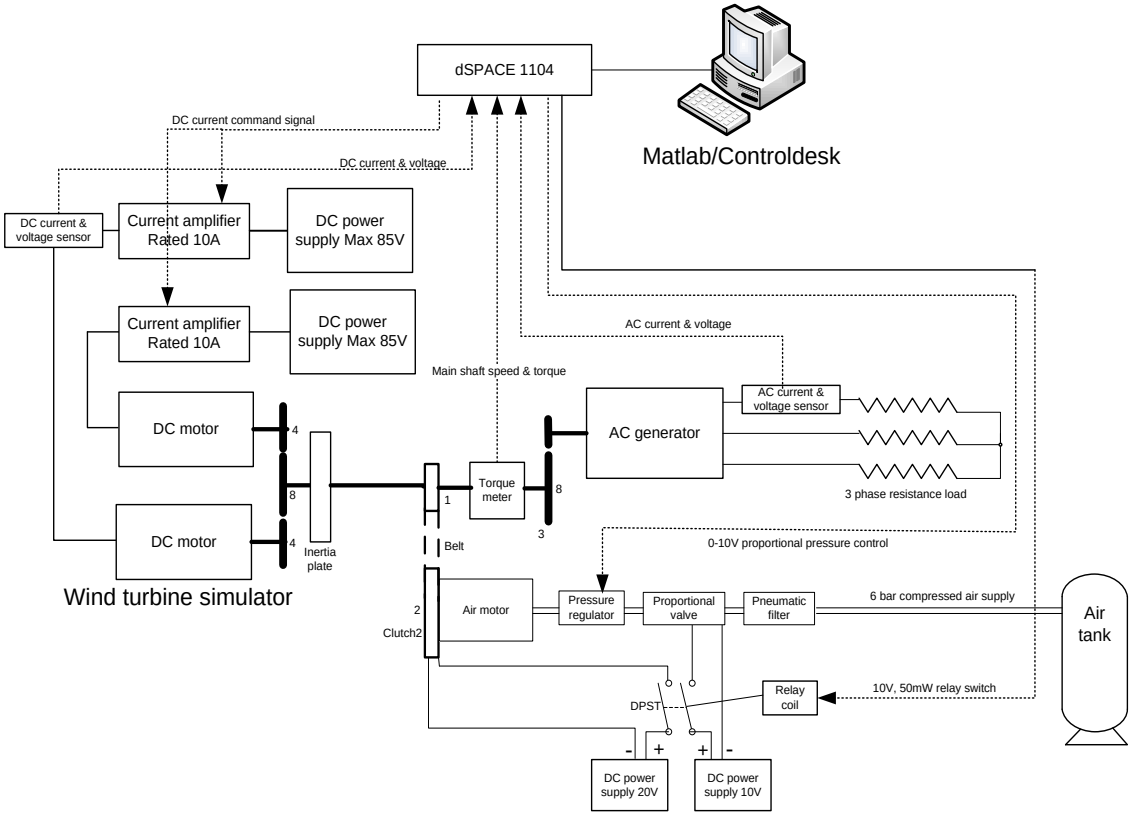

Figure 7.1 Hybrid wind turbine prototype test rig

Based on this wind turbine simulator, a 1 kW hybrid wind turbine prototype is set up in the research lab to test and verify the hybrid wind turbine concept, as shown in Figure 7.1. A novel electromechanical integration is applied to engage CAES to wind power generation. The whole system is mainly composed by hardware and software two parts. The hardware includes: main control computer, dual DC motors & current amplifiers, inertia compensation, sensors, permanent magnet synchronous generator (PMSG) & electrical load, scroll expander, belt transmission and magnetic clutch; while the software comprises wind speed profile, motor command program; sensor

data collection program. The real-time control design has been implemented in Simulink/dSPACE environment. Due to the lab current limit, dual DC motors is coupled in parallel to double the capacity.

7.2 Mechanical setups

All drawings are made with AutoCAD 2004. The main test rig body consists of dual-DC motor, DC motor side gearbox, main shaft, main shaft clutch, PMSG side gearbox, PMSG, belt transmission, side shaft clutch, side shaft, scroll air motor, bearings and brackets. The overall assemble diagrams are shown in Figure 7.2, in which (a) is the front view and (b) is the vertical view.

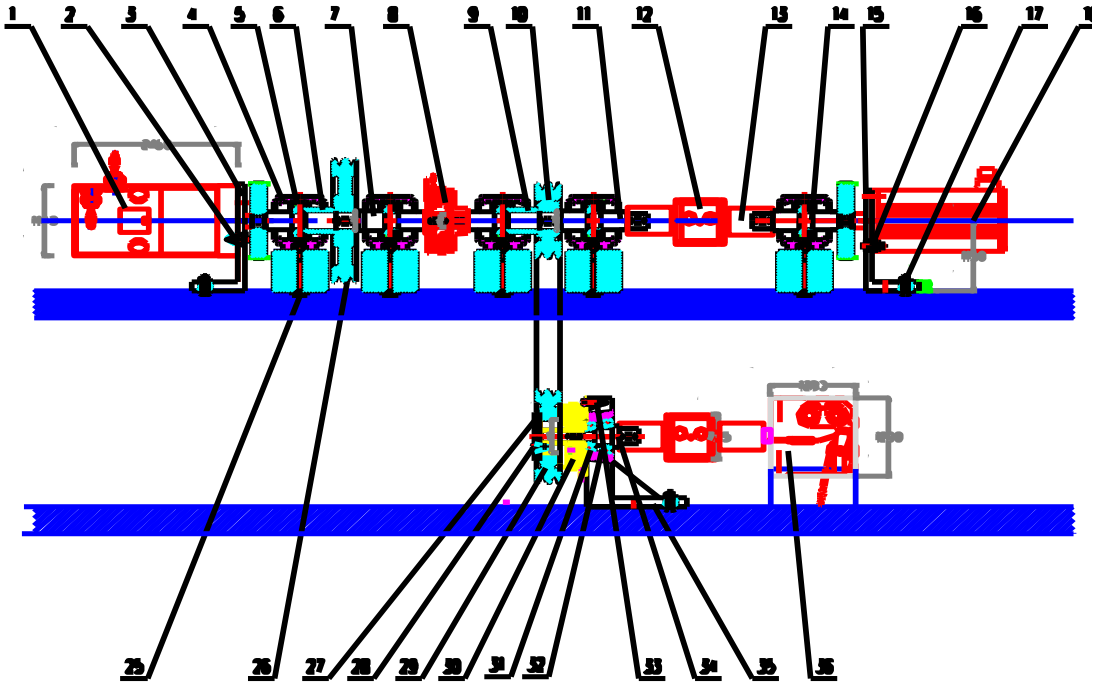

Figure 7.2 (a) Front view of the test rig plan

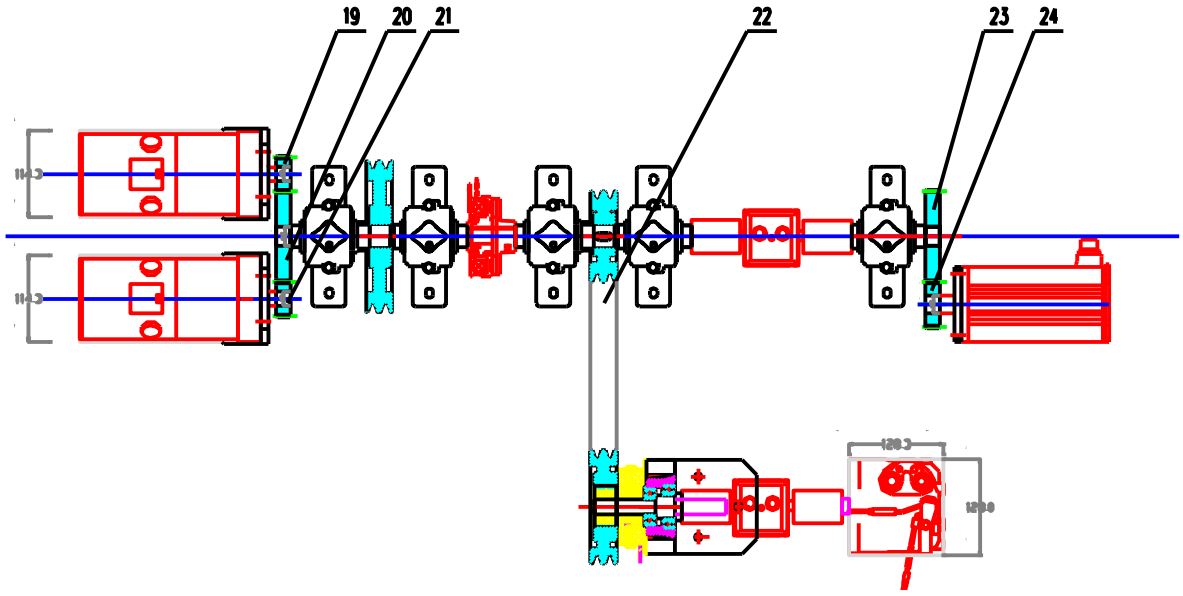

Figure 7.2 (b) Vertical view of the test rig plan

In this system, the maximum main shaft speed is limited to 1500rpm. In this way, the operation noise could be reduced and also the security in lab is improved. The gearboxes are applied as speed devices to ensure every actuator can work at its optimised condition. The speed ratios are determined by the actuators rated speed, which can be found from the specifications. For mounting all the other components, which was the first important step in creating the experimental setup, the frame must be stiff, to prevent unwanted vibrations and movements of the construction during operation. In this project, the baseplate chosen is made out of aluminum, since this material is easy to process, relatively light and reasonably stiff. It provides excellent attachment to concrete foundations and inertia blocks assuming the anchor bolts are installed properly. Besides, Machinery can be placed onto the baseplate prior to installation and roughly aligned in the lateral and axial directions to ensure that the

foot bolt locations are drilled and tapped precisely to prevent an incorrect shaft end to shaft end spacing or bolt bound condition before installing (Piotrowski, 2006).

The diagram of test rig mounted on the frame is shown in Figure 7.3.

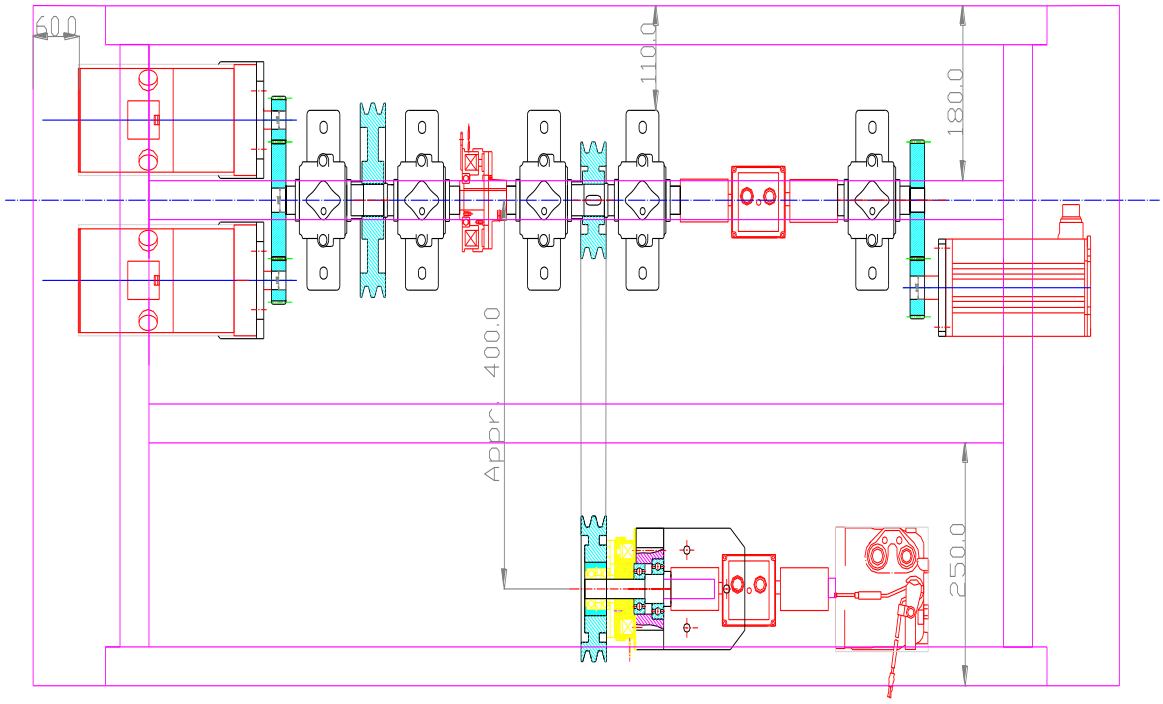

Figure 7.3 Vertical view of the test rig assemble with frame

In Figure 7.3, the belt distance is approx. 400mm; the greater distance with stretch will cause a large drop on belt tension, creating slip and power transmission inefficiency. The tension of belt transmission is virtually required. This means that the distance between both belt plates should be adjustable, thus to ensure the belt is always tightened.

The mechanical setup also includes the design of various parts, like pinch suspension and paper conduction, to connect these components to the frame and the location of

these parts in the frame. The part involved in Figure 7.1 (a) is listed in Table 7.1. Some components for the mechanical setups are provided by external suppliers, including the V-belt, clutches, electric machines, etc. All other parts described in this section need to be specially designed to connect these components to the basic mechanical frame. Some important dimensions of components are given in Appendix.

Table 7.1 Mechanical part list

Number	Name	Quantity	Model number
1	DC motor	2	M4-2952X-2100t-000, Callan Technology
2	Screw bolt	8	M6
3	DC motor flanges	2	Refer to Figure A.1
4	Bearing	5	SN206
5	Bearing ring	5	6206
6	Bearing balls	50	
7	Inertia plate	1	Outer diameter 200mm
8	Shaft 1	1	Refer to Figure A.7
9	Clutch 1	1	CS-10-31G 24V, Mikipulley Ltd.
10	Belt plate 1	1	Outer diameter 120mm
11	Shaft 2	1	Refer to Figure A.8
12	Toque meter	1	RWT 310, Sensor Technology Ltd.
13	Gear coupling	4	
14	Shaft 3	1	Refer to Figure A.9
15	PMSG flange	1	Refer to Figure A.2
16	Screw bolt and nut	4	M6
17	Screw bolt and nut	3	M8
18	PMSG	1	SGMSS-20A, Yaskawa Ltd.
19	Spur cylindrical gears	1	Diameter 48mm,Refer to Figure A.5
20	Spur cylindrical gears	1	Diameter 120mm,Refer to Figure A.4
21	Spur cylindrical gears	1	Diameter 48mm,Refer to Figure A.5
22	V-belt	2	Type A
23	Spur cylindrical gears	1	Diameter 120mm,Refer to Figure A.4
24	Spur cylindrical gears	1	Diameter 60mm,Refer to Figure A.6
25	Screw bolt and nut	2	M8
26	Block	5	Refer to Figure A.12
27	Screw bolt and nut	10	M12
28	Belt plate washer	1	Refer to Figure A.11
29	Screw bolt	4	M4

30	Belt plate	1	Outer diameter 150mm
31	Clutch 2	1	101-10-15G 24V, Mikipulley Ltd.
32	Rolling bearings	1	6304
33	Rolling bearings	1	6206
34	Clutch 2 flange	1	Refer to Figure A.3
35	Shaft 4	1	Refer to Figure A.10
36	Screw bolt and nut	3	M12
37	Screw bolt and nut	4	M6
38	Bushing 1	1	Inner diameter 45mm
39	Bushing 2	1	Inner diameter 45mm
40	Scroll air motor	1	Modelled from TRSA09, Sanden Ltd.

Because of safety concerns, the whole test rig is sealed by a wooden cage, it can only be open when the electricity is totally switched off, controlled by a stroke switch. With respect to visibility, the top of the cage is made of transparent strong plastic. The final view of the test rig is pictured as below:

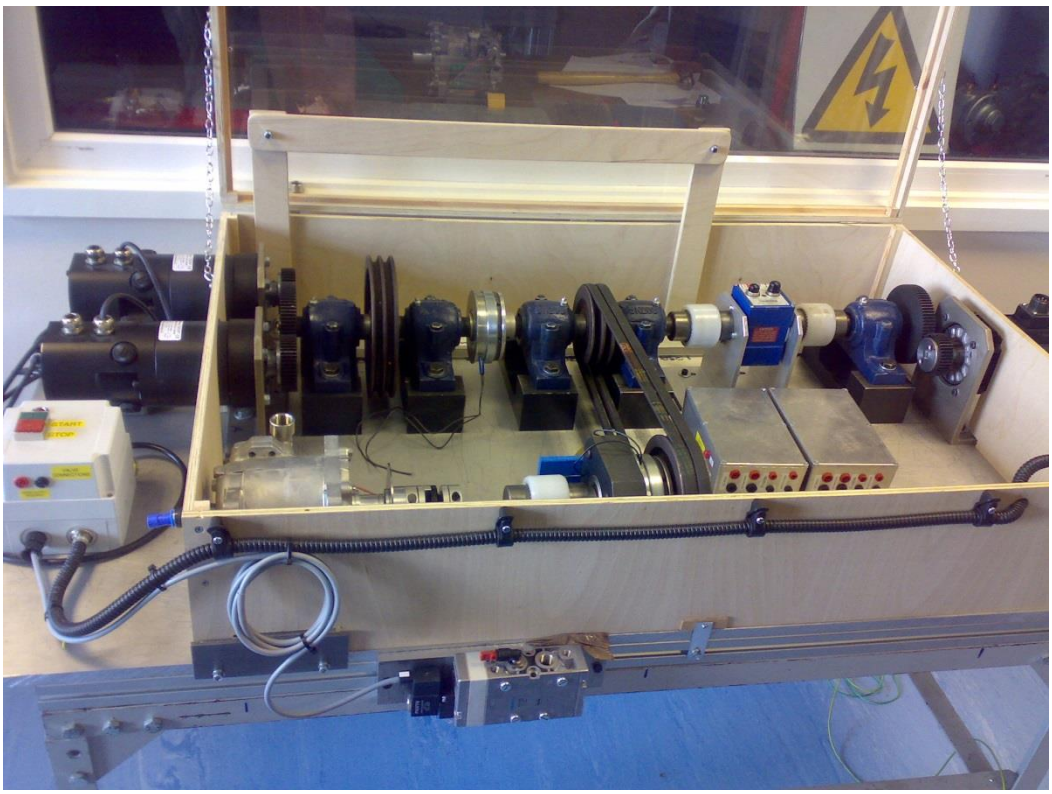

Figure 7.4 Hybrid wind turbine test rig in the laboratory

7.3 Description of hardware-in-the-loop (HIL) system

Hardware-in-the-Loop Simulation allows the rig to be tested in a simulated environment in closed-loop (Hanselmann, 1996). It can address properly the complex system integration issues and to validate performance specifications. Figure 7.1 already shows a block diagram of the experimental setup of hybrid wind turbine test rig with the analog signal interconnections between the dSPACE system and the sensors. Among these, a dSPACE real-time controller card (model: DS/rti1104) is the core component.

The DS1104 R&D Controller Board is a standard board that can be plugged into a PCI slot of a common computer. The DS1104 is specifically designed for the development of high-speed multivariable digital controllers and real-time simulations in various areas. It can link external signals from the 100-pin I/O connector on the board to Sub-D connectors using an adapter cable. Specific interface connector panels provide easy access to all the input and output signals of the DS1104 R&D Controller Board (dSPACE GmbH, 2012).

As the data acquisition card, dSPACE1104 have 7 analogue inputs. They are DC motor current & voltage measurement, PMSG load current & voltage measurement, main shaft torque & speed measurement and supply air pressure measurement. The analogue input voltage range for each connector is±10V.

As the control board, dSPACE1104 have 5 analogue outputs. One for DC amplifier control signal, 2 clutches switch signal, pneumatic valve switch signal and pressure regulator control signal. The voltage and current ranges of the output is ±10V and

±5mA. The details of the dSPACE1104 specifications can be found in the "DS1104 R&D Controller Board: Hardware Installation and Configuration" from dSPACE GmbH.

As a part of the HIL system, varies of sensors and control actuators are employed. They are list in the following table.

Table 7.2 Sensors for the hybrid wind turbine test rig

Sensors	Description	Manufacturer
Voltage transducer	SN: LV 25-P Measurement range: ±10V to ±250V	LEM
Current transducer	SN: LTSR 15-NP Measurement range: ±15A	LEM
Torque sensor	SN: RWT310 Speed measurement range: 0 - 2000 RPM Torque measurement range 0 – 1.1 to 0 - 20	Sensor technology Ltd.
Pressure sensor	SN:SDE1-D10-G2-W18-L-PU-M8 Measurement range: 0 to 10 bar	Festo
DC power supply	Voltage: 90 Vdc Current: 0 to 10Adc	TRM International Ltd
DC amplifier	SN:10/100 Amplifier DC SUPPLY VOLTAGE: 24 to 100 Vdc Peak Current: 10Adc	TRM International Ltd
Air supply	6 bar constant pressure supply	University of Warwick
Pneumatic valve	SN:MYPE-5-1/4-010-B Operating pressure: 0 to 10 bar	Festo
Proportional pressure regulator	SN: VPPM-6L-L-1-G18-0L10H-V1N Operating pressure: 0 to 10 bar	Festo
Signal relay	SN: IM26TS Coil Current: 4.2mA, Coil Voltage12VDC Control On Voltage (max): 10.2 VDC	Tyco Electronics
Flow meter (High flow rate)	SN:MS6 SFE-F5-P2U-M12 Measurement range:200-500 L/min	Festo
Flow meter (Low flow rate)	SN:SFE-LF-F200-HQ8-P21-M12 Measurement range:0.5-200 L/min	Festo
Temperature sensor	K-type thermocouple Measurement range:-50 ^{o}C to 250 ^{o}C	RS

According to Figure 7.1, the pneumatic valve is applied to switch on/off the air supply to the air motor. The proportional pressure regulator can control the air supply pressure by the analogue signal from the dSPACE board. And the relays are employed to switch on/off the clutches and pneumatic valve. For further air power calculation and power efficiency analysis, flow meters and temperature sensor are also involved in the experiment.

7.4 PMSG and scroll air motor model validation

Most parameters of the system components are available in the associated handbook or data sheets. The unknown parameters for models, such as the PMSG and scroll air motor, can be identified using intelligent computational algorithms together with laboratory data (Wei, Wang and Wu, 2007).

The case of PMSG validation is tested in the following ways. First, drive the PMSG with pure resistance load by an electrical motor and records the torque & speed on the driving shaft, and current & voltage value on the PMSG load. All the results are in the time domain. And then use the recorded torque value as input to run the PMSG model. At last, compare the simulated speed and voltage curves with the experimental data. Figure 7.5 (a) shows the measured torque on main shaft, which is used as the input to PMSG in simulation. Figure 7.5 (b)-(c) illustrate the comparison of simulation and experimental results of main shaft speed and generator single phase voltage RMS value. So the mathematical model built for the PMSG should be able to represent the dynamic features of the generators in a real wind turbine. However, there is still some

error between the simulated and experimental voltage curve. This might be caused by the heating effects of the resistance load.

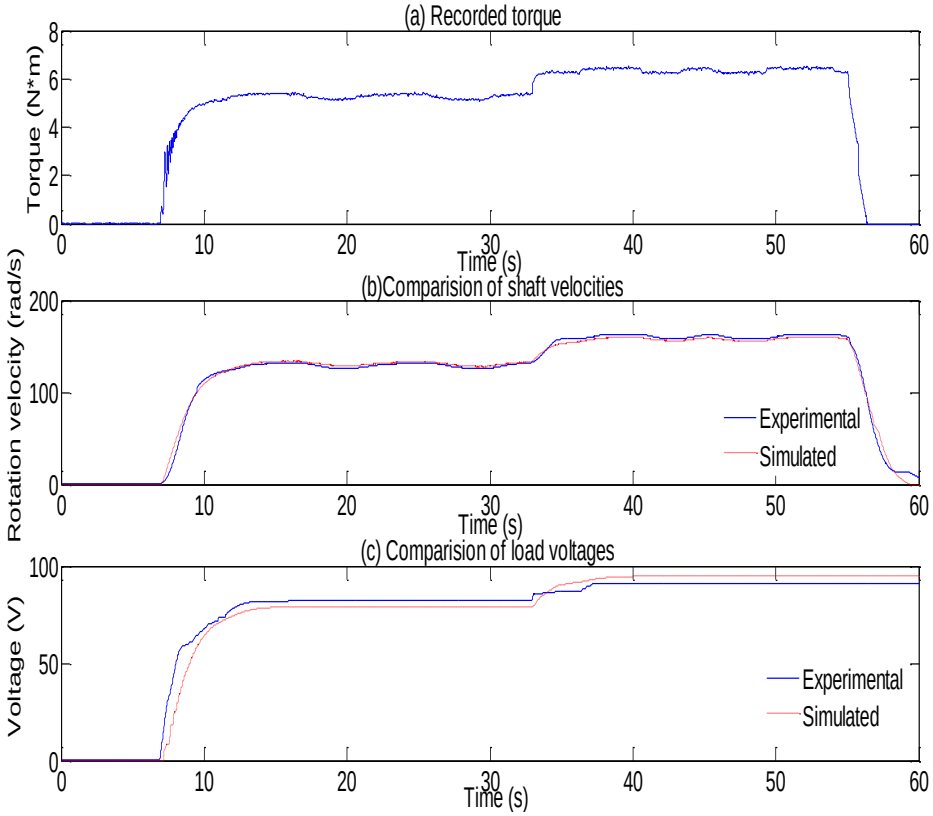

Figure 7.5 Comparison of simulated and experimental results for PMSG validation

The validated PMSG parameters are shown in Table 7.3.

Table 7.3 Parameters of the validated PMSG model

Symbol	Description	Value
p	The number of pole pairs	2
R_s	Resistance of the stator windings	0.4578 Ohm
L_d	Inductance on d axis	3.34 mH
L_q	Inductance on q axis	3.34 mH
λ	Flux amplitude induced by permanent magnets	0.171Wb
F_G	Friction factor	0.0003035 N×m×s

Similar to the case of PMSG model validation, the 2.41-wrap scroll air motor can be

verified by the comparing the simulated and experimental speed curve, using the same input supply air pressure. Figure 7.6 (a) shows the measured supply air pressure at the inport. Figure 7.6 (b) describes the comparison of simulation and experimental results of air motor main shaft speed.

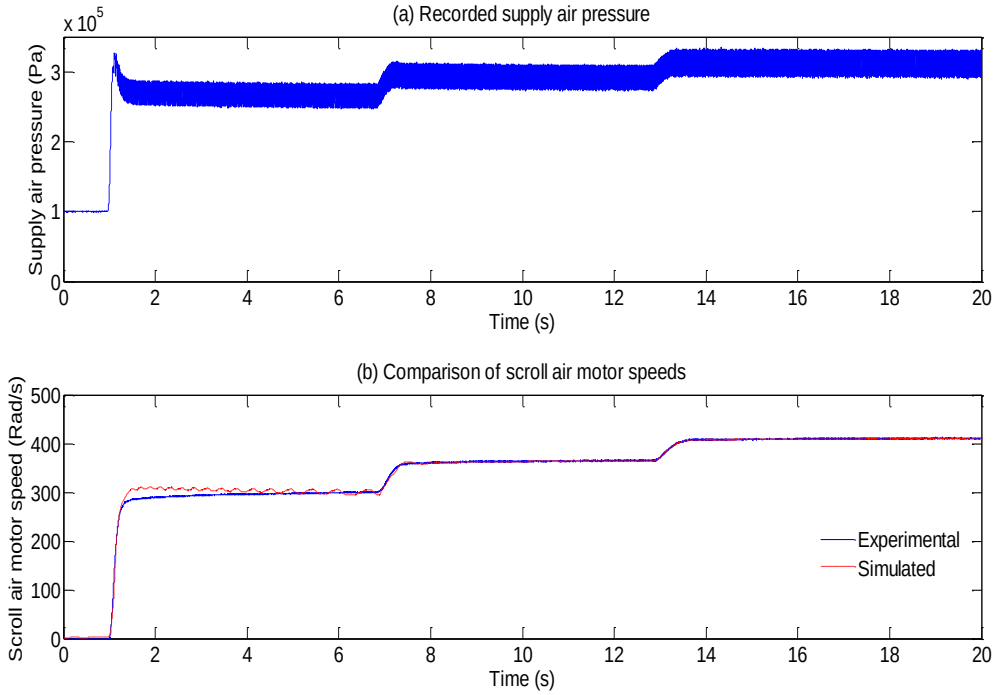

Figure 7.6 Comparison of simulated and experimental results for scroll air motor validation

From the validation results given in above figure, the simulated result shows fair agreement with the experimental curve. It is proven that the scroll air motor model is able to reveal the dynamic responses of the practical one. The validated scroll air motor parameters have been already reported in Table 4.2

7.5 Test study of the hybrid wind turbine system

7.5.1 Study of the stand-alone test system

Two scenarios for the stand-alone wind turbine simulator test are constructed. After the tests, the command data to current amplifier is recorded, which is applied in the next step hybrid test to ensure that the comparison is under the same condition.

First is the dynamic test based on random wind speed profile, where the nonstationary turbulence component is modelled using a shaping filter with white noise input (Welfonder, Neifer and Spanner, 1997). Figure 7.7 shows the simulated random wind speed profile for experiment. In this figure the mean wind speed drops from 10 m/s to 8 m/s at 30 second, thus to demonstrate the wind speed change in a certain period.

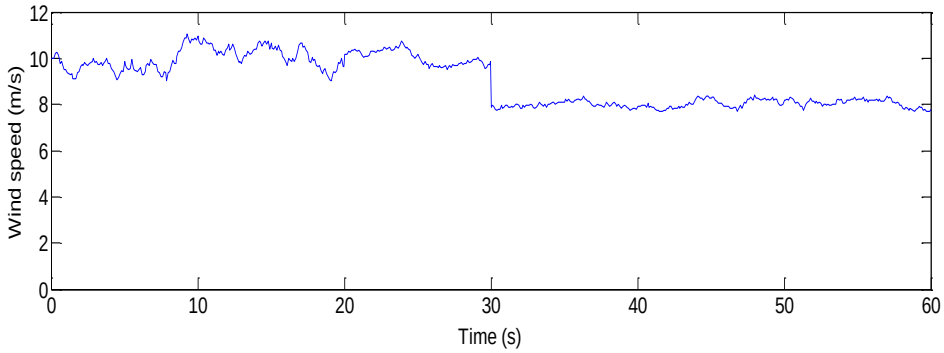

Figure 7.7 Simulated random wind speed profile

In this case, the DC motors are controlled by a classical torque-current closed loop to meet the static and dynamic torque requirements. While, the torque command signal is generated by a typical fixed pitch angle wind turbine model (Sun, Wang and Luo, 2011). The control strategy is described in Figure 7.8.

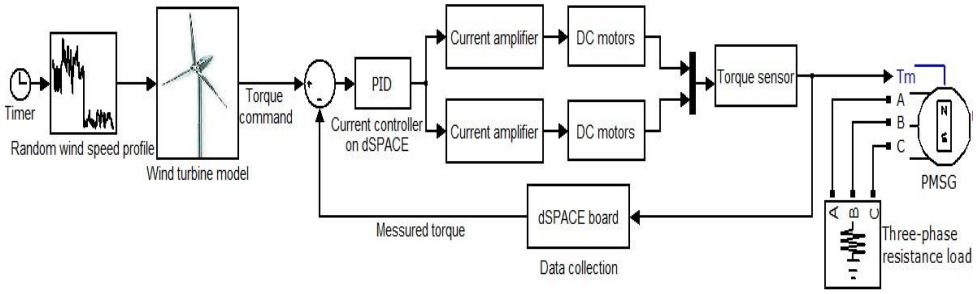

Figure 7.8 Control strategy for random wind speed based dynamic test

The experimental results are given in Figure 7.9. (a) is compared torque curve, (b) is the speed curves; and (c) is the control signal that sent to DC amplifier. It can beeb seen that the torque (a) and speed (b) characteristics of the wind turbine simulator fit well to those of the real wind turbines. Thus it can be proven that the simulator can meet the requirements of the laboratorial wind power generation system.

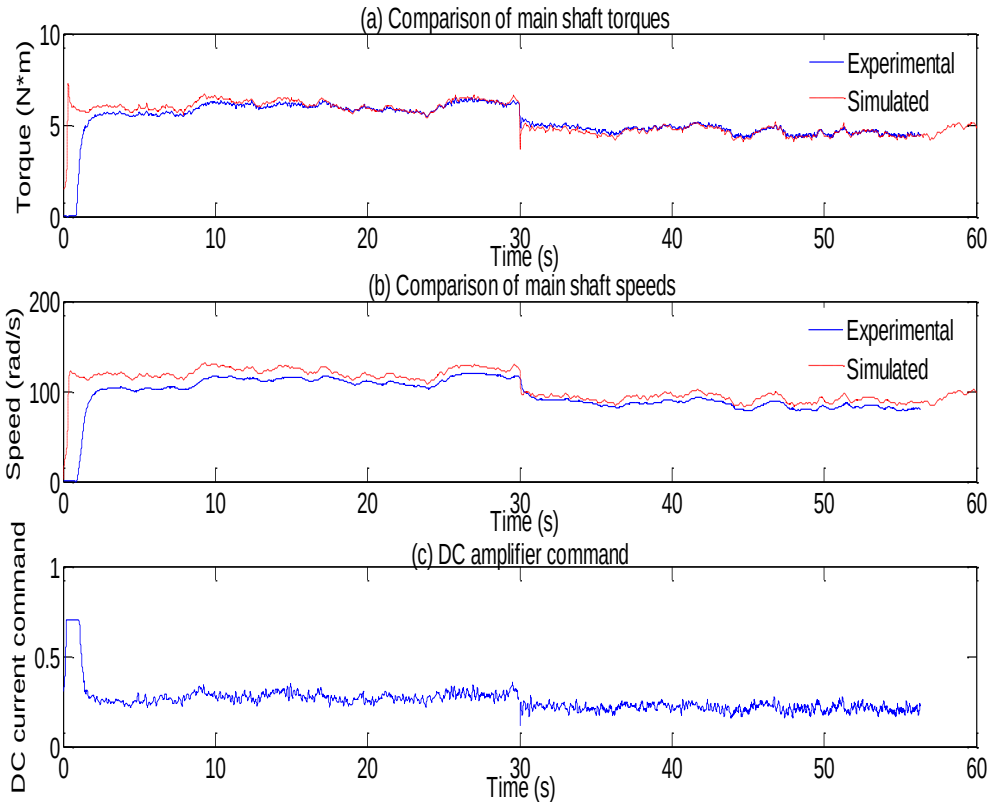

Figure 7.9 Comparison of simulated and experimental results for stand-alone system

The second scenario is constant mechanical power test, which is carried out for the hybrid system efficiency analysis. The control method applied is similar as that in random wind speed dynamic test. A fixed power- current close loop controller is built to command the DC motor output. Three groups of power scale for the single motor are tested, in which a power drop at 30 second is adopt in each group, and they are 600-500 W, 600-400 W and 600-300 W respectively. The main shaft mechanical power is calculated from the measured torque and rotation velocity, as shown in the figures below:

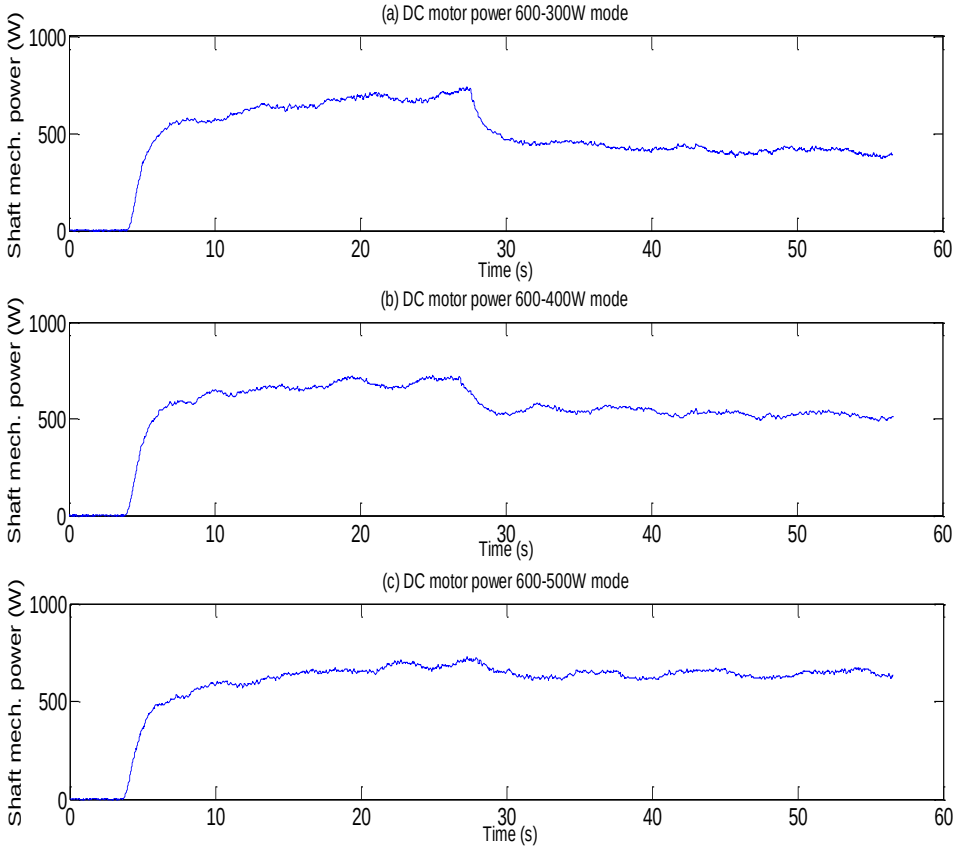

Figure 7.10 Fixed mechanical power tests on different motor driving mode

7.5.2 Study of the hybrid system test integrated with CAES system

There are also 2 scenarios built for the hybrid system test, in contrast with stand-alone test and fixed mechanical power test, respectively.

A combined control strategy is proposed based on the dynamic stand-alone wind turbine system test, that is, the open loop current control is used to achieve the equal power output as that in stand-alone mode, and the PID air pressure control is applied for the scroll expander system, which is shown in Figure 7.11. The magnetic clutch and on-off valve will be activated during the low wind speed period, and then the torque on the main shaft will maintain at around a desired value due to the pressure regulation. The objective is to observe the dynamic response at the engagement moment and the control performance of the pneumatic power compensation.

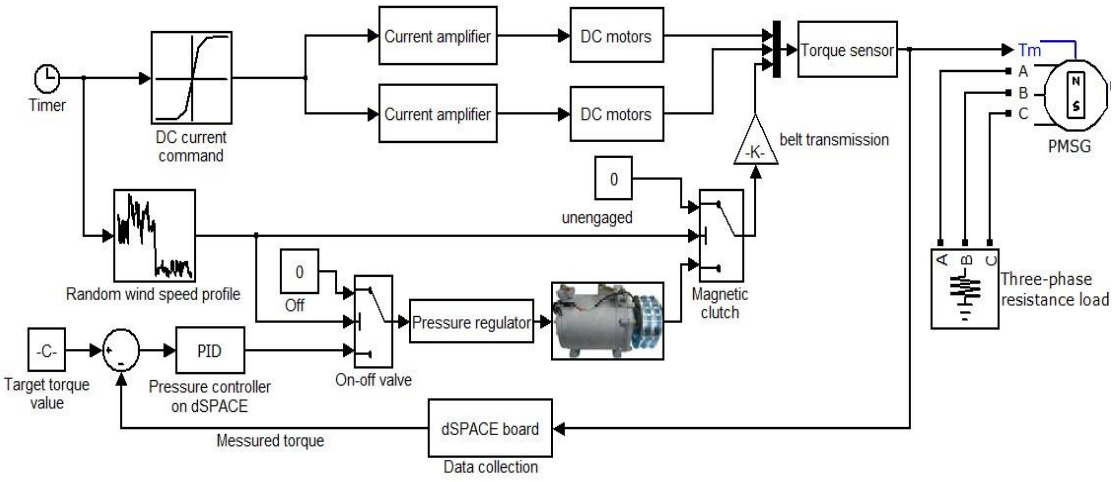

Figure 7.11 Control strategies for hybrid wind turbine simulator test

Figure 7.12 shows the experimental results of the overall hybrid system with proposed control strategy, in comparison with the results in stand-alone test, where the target value for torque is set to 6 N×m. The experiment results shown in Figure 7.12

thoroughly verify that the idea works properly in terms of system performance. The pneumatic system can contribute stable and controllable power to this hybrid system. Additionally, it is noticed that, during the clutch engagement, there will be slight slump mainly due to the rigid integration between two different speeds.

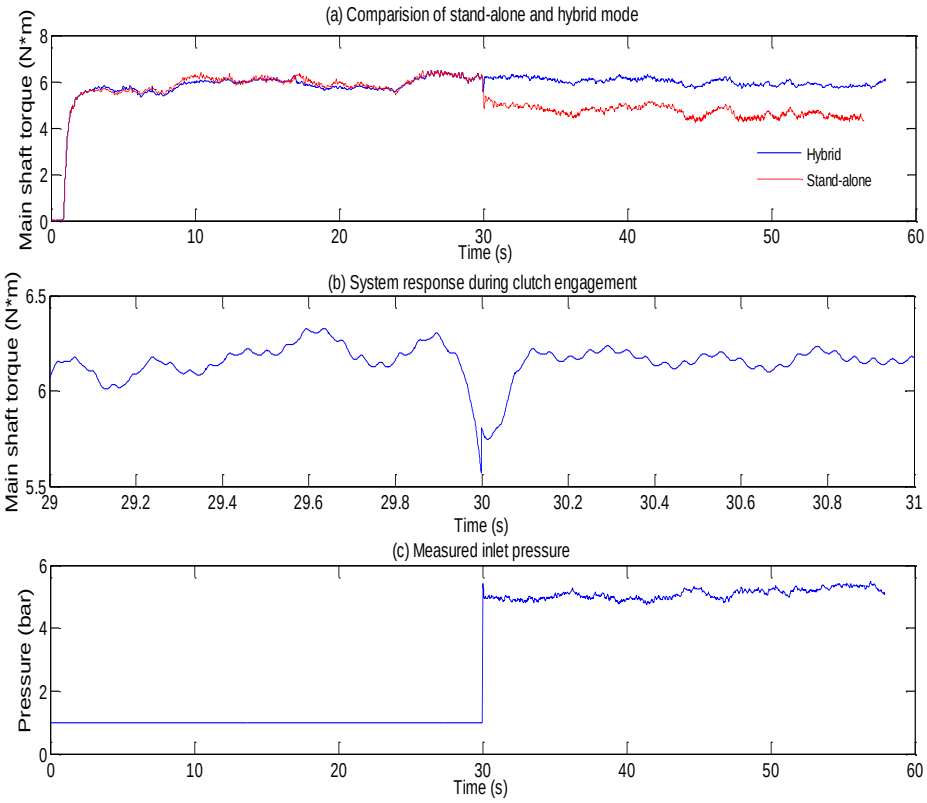

Figure 7.12 Dynamic performance of hybrid wind turbine simulator

7.6 Power efficiency analysis of hybrid wind turbine test rig

The Power efficiency analysis for the whole system is conducted in extension of fixed mechanical power test. While the energy transmission and conversion can be schematically illustrated in Figure 7.13

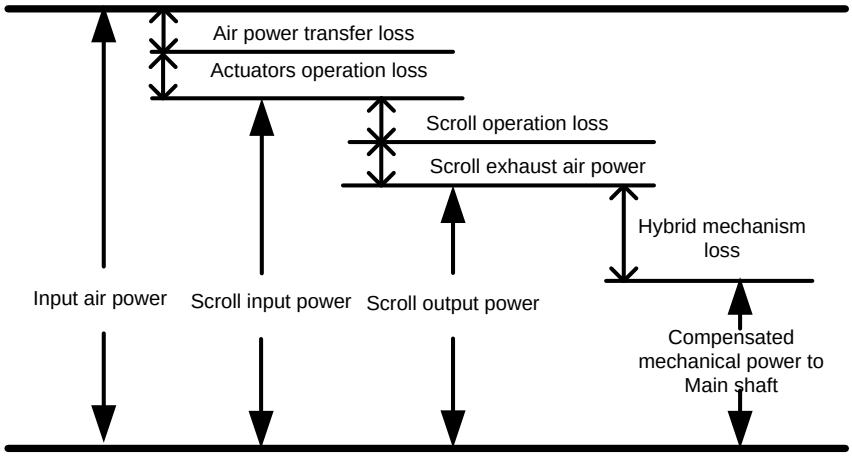

Figure 7.13 Power transmission and conversion diagram

Because it is difficult to measure the torque and speed on the scroll air motor branch, the scroll output power cannot be obtained directly. While, as shown in Figure 7.13, the first and last part of power can be calculated from the data acquisition. Here the pneumatic compensation efficiency can be defined as the ratio between the compensated mechanical power and input air power. Thus it is necessary to find how much air power/energy contained in the compressed air input to the system. Using Equation 3.1, air power at atmospheric temperature can be calculated with the flow rate measurement.

For the compensated mechanical power could be considered as the power difference between hybrid and stand-alone mode. Three groups of stand-alone results in fixed mechanical power test are applied to explore the relationship between rotation velocity and efficiency. Meanwhile, for each group on the basis of speed, tests under different supply air pressure states are recorded as well. The test results are shown in

Table 7.4 in details:

Table 7.4 Power efficiency analysis under different conditions

Rotation velocity (rad/s)	Inlet pressure (bar)	Exhaust pressure (bar)	Flow rate (L/min)	Inlet temperature (centigrade)	Outlet temperature (centigrade)	Stand-alone power	Hybrid power	efficiency
110	5.76	1.0	335	17	24.5	640	980	34.76%
110	4.90	1.0	255	17.5	24.5	640	950	45.87%
110	3.95	1.0	230	18	24.5	640	900	49.34%
98	5.75	1.0	340	17.2	24.5	510	925	41.84%
98	4.88	1.0	250	17.6	24.5	510	875	55.27%
98	3.90	1.0	220	18.1	24.5	510	780	54.07%
85	5.73	1.0	320	17.2	24.5	390	800	44.01%
85	4.90	1.0	245	17.7	24.5	390	690	46.20%
85	3.90	1.0	205	18.1	24.5	390	610	47.28%

It is obvious that the results indicate that the efficiency varies inversely as the input air pressure. It is suggested to supply lower pressure compressed air to achieve higher transmission efficiency. However, the overall efficiency is not of a reassuring nature, the highest value is only around 50%. It should be pointed out that the efficiency approach used here covers quite a lot of actuators, as the efficiency value decrease along the procedure is inevitable. Despite the efficiency of scroll air motor, the expected efficiency of separate hybrid transmission could reach around 70%. However, compared with the exiting reports on the power efficiency of CAES plants, the achieved value is still acceptable. Because its structure is quite simple, does not involve any exhaust or thermo energy recycle auxiliaries. In other words, the hybrid wind turbine test rig should have large space for efficiency improvement.

7.7 Summary

The proposed hybrid wind turbine test rig is successfully constructed in the author's group. The system design and functions are reported in detail. The experimental test confirmed that the wind turbine simulator can work well to demonstrate the dynamic response of the real one and the pneumatic system can contribute indeed to the overall system through hybrid transmission. Applying dSPACE real-time supervision, the multi-mode control runs stably and reliably, reach to the effect anticipative. Through the experimental results study, the power conversion efficiency is not optimistic, around 40%-50%. It is still acceptable for a prototype test. The efficiency improvement is feasible with a suitable future modification.

Chapter 8

Conclusions and future work

This chapter summarises the major achievements of the presented PhD research work in the field of a new hybrid wind turbine system. Possible directions for further work are also recommended in this chapter.

8.1 Conclusions

The research project was carried out with the support from Birmingham Science City Energy Efficiency & Demand Reduction project. It presents a new small scale hybrid wind turbine system, which integrates the CAES system with a typical 3-balde wind turbine. The main contributions of this PhD project are summarized as follows:

1) A typical wind turbine system has been introduced including the descriptions of each subsystem and the relevant functions. The simulation for the mathematical model under random wind speed input is conducted. The simulation results indicate the impact of the wind's intermittence onto the wind power generation. The generator power output fluctuates evidently as the wind speed varies. Furthermore, this wind turbine model can be used to build the wind turbine simulator in the research laboratory as the command source. The encouraging experiment results prove that this small scale model is capable for both simulation and experiment analysis.

2) A comparative review and investigations on different energy storage technologies have been conducted. Different technologies have different performances and are applied in different circumstances. In this small scale research project, CAES does have demerits of power/energy efficiency and energy density. However, it is well balanced with key advantages such as high cost-effectiveness, easy maintenance and long expectance.

3) The core components of the designed hybrid system, the pneumatic actuators are introduced based on how they are functioned, including compressor, air motor and air tank. Two types of air motors have been studied through the previous research project, including vane and scroll type. The new 2.41 wrap scroll air motor is modelled and the relationship between the wrap number and mathematical model is presented. Then the multi wraps scroll type air motor can be derived in the extensive model study. The model has been evaluated and validated by comparing the simulation results with a series of experiment data obtained from prototype test rig. To confirm the high efficiency of scroll air motor, the simulation results based comparison has been conducted between vane and scroll type air motors. Under the given simulation condition, the efficiency of scroll air motor is significantly up to 32% higher than that of vane type.

4) The new hybrid system is developed, inspired by Hybrid Electric Vehicle (HEV) structures. Based on the analysis of different operation phases, the hybrid powertrain is modelled in multi-mode, consisting of the charging, stand-alone, discharging phases. A complete mathematical model for the proposed hybrid

system is derived by composing all the above mentioned subsystems. The simulation results show that the proposed hybrid system has the encouraging stabilisation ability for the load demand. It enables the hybrid wind turbine operates at a relatively steady speed profile no matter how much the wind speed is, which in turn will improve the overall system reliability. In addition, the simulation results reveal that the hybrid transmission design has significant impact on the energy efficiency. The round-trip system efficiency is proportional to the inlet pressure and inverse proportional to the belt transmission speed ratio. Besides, the wind turbine efficiency C_p is lower than that in stand-alone mode, which could be considered as the side effect of the engaged CAES.

5) Through the simulation results, it can be obtained that a proper control strategy for the overall system is necessary. A new multi-mode control is introduced to the system. It combines fuzzy-logical pitch control, PID pressure control and CAES engagement control according to multi operation phases. The simulation studies are carried out by comparing the non-controlled and controlled systems. Through the comparison, it is demonstrated that the hybrid system can still maintain an accurate statue at varying wind speed of 12-8 m/s.

6) A prototype test rig of hybrid wind turbine is introduced from the design to the final drawings. With the test rig, the wind turbine generator and air motor models are evaluated and validated by comparing the simulation results with a series of experiment data. dSPACE 1104 control board with its interface is employed in the experimental work as both data acquisition card and host controller. The test

rig can execute most functions of a real wind turbine under the dSPACE HIL control. From both the simulation and test results, the hybrid wind turbine system can generate reliable steady power output with the compensation from CAES. It can be concluded that the proposed hybrid system of wind turbine and CAES is feasible with a great potential for future industrial applications. The energy conversion efficiency from the compressed air energy to the electrical power output has been investigated with various operation conditions. The system test results indicated that the efficiency can be up to 55% under a well-controlled operation condition, which is higher than the typical pneumatic actuator efficiency. The findings have provided essential evidences and information for the next stage of research which will lead to the hybrid system with improved efficiency and reliability.

8.2 Recommended future work

According to the current research on the hybrid wind turbine system, some future works could be conducted for the further improvement as follows:

1) The complete hybrid wind turbine system has the ability to utilise the excess wind power. In future studies, the charging phase will be involved in the experiment work, including the compressor and its related equipments. Hence, the conventional compressor control strategy are also desired to be included, i.e. switch and power flow control.
2) The current experimental study is based on the wind turbine simulator. In the

future, the real wind turbine based hybrid system will be constructed. It will be a horizontal 3-blade wind turbine with 2kW power capacity. The field test can be conducted within the campus, and its associated controlling and data monitoring functions are implemented by dSPACE 1104 board.

3) Furthermore, the optimisation of the hybrid transmission mechanical structure will be developed. It has been expected that a more complicated and efficient planetary gearbox can be deployed into the system to achieve high power transmission efficiency.

Reference

[1]. Agrawal, J.P., 2001. *Power electronic systems: theory and design.* Stephen Hellba, ed., Prentice-Hall.

[2]. Airuser, 2012. Air-powered generator system installed at Stockport Pyramid. Retrieved from: http://www.airuser.com/stories/articles/-/2012/aug_2012/air_powered_generator_system_installed_at_stockport_pyramid/ [Accessed September 10, 2012].

[3]. Akhmatov, V., 2002a. Variable-Speed Wind Turbines with Doubly-Fed Induction Generators, Part I: Modelling in Dynamic Simulation Tools. *Wind Engineering*, 26(2), pp.85–108. Retrieved from:http://dx.doi.org/10.1260/030952402761699278.

[4]. Akhmatov, V., 2002b. Variable-speed wind turbines with doubly-fed induction generators. II. Power system stability. *Wind Engineering*, 26(3), pp.171–188. Retrieved from: http://dx.doi.org/10.1260/030952402762056081.

[5]. Almasi, A., 2009. Reciprocating Compressor Optimum Design and Manufacturing with respect to Performance, Reliability and Cost. In *Proceedings of World Academy of Science*.

[6]. Ananthaswamy, A. & Michael L. P., 2012. Power paradox: Clean might not be green forever. *New Scientist*.

[7]. Arsie, I. et al., 2005. A Model of a Hybrid Power Plant with Wind Turbines and Compressed Air Energy Storage. *ASME Conference Proceedings*, 2005(41820), pp.987–1000. Retrieved from: http://dx.doi.org/10.1115/PWR2005-50187.

[8]. Andersen B. W., 1976. *The Analysis and Design of Pneumatic Systems*, Krieger Pub Co.

[9]. Barth, E. & Riofrio, J., 2004. DYNAMIC CHARACTERISTICS OF A FREE PISTON COMPRESSOR. In *2004 ASME International Mechanical Engineering Congress and Exposition*. Anaheim, California USA.

[10]. Battaiotto, P.E., Mantz, R.J. & Puleston, P.F., 1996. A wind turbine emulator based on a dual DSP processor system. *Control Engineering Practice*, 4(9), pp.1261–1266. Retrieved from: http://www.sciencedirect.com/science/article/pii/0967066196001323.

[11]. Bolund, B., Bernhoff, H. & Leijon, M., 2007. Flywheel energy and power storage systems. *Renewable and Sustainable Energy Reviews*, 11(2), pp.235–258. Retrieved from: http://linkinghub.elsevier.com/retrieve/pii/S1364032105000146.

[12]. Van den Bossche, P., Van Mierlo, J. & Maggetto, G., 2002. Energy sources for hybrid electric vehicles: comparative evaluation of the state of the art. In *AECV conference*. Noordwijkerhout.

[13]. British Wind Energy Association, 2005. Briefing Sheet-Wind Turbine Technology. Retrieved from: http://www.bwea.com/energy/briefing-sheets.html.

[14]. Bullough, C. et al., 2004. Advanced Adiabatic Compressed Air Energy Storage for the Integration of Wind Energy. In *Proceedings of the European Wind Energy Conference*. London.

[15]. Burns, S., 2009. *Hypoid vs. Worm Gear Efficiencies*,

[16]. Cai, M. & Kagawa, T., 2001. Design and application of air power meter in compressed air systems. *Environmentally Conscious Design and Inverse Manufacturing, 2001. Proceedings EcoDesign 2001: Second International Symposium on*, pp.208–212.

[17]. Cericola, D. et al., 2010. Simulation of a supercapacitor/Li-ion battery hybrid for pulsed applications. Journal of Power Sources, 195(9), pp.2731–2736. Retrieved from: http://linkinghub.elsevier.com/retrieve/pii/S0378775309019818.

[18]. Chapman, S., 2005. *Electric machinery fundamental*. Fourth edition. McGraw-Hill.

[19]. Chen, H. et al., 2009. Progress in electrical energy storage system: A critical review. *Progress in Natural Science*, 19(3), pp.291–312. Retrieved from: http://www.sciencedirect.com/science/article/pii/S100200710800381X.

[20]. Cheung, K.Y. et al., 2002. *Large-Scale Energy Storage Systems*, Imperial College London.

[21]. ConvenEnergy Storage & Power LLC, 2012. CAES Technology. Retrieved from: http://www.enstpo.com [Accessed October 10, 2012].

[22]. Crotogino F., Mohmeyer, K. and Scharf, R., 2001. *Huntorf CAES: More than 20 Years of Successful Operation*, Orlando, Florida, USA. Retrieved from:http://www.uni-saarland.de/fak7/fze/AKE_Archiv/AKE2003H/AKE2003H_Vortraege/AKE2003H03c_Crotogino_ea_HuntorfCAES_CompressedAirEnergyStorage.pdf.

[23]. Daneshi, A. et al., 2010. *Wind power integrated with compressed air energy storage*, IEEE.

[24]. Daneshi, H., Srivastava, A.K. & Daneshi, A., 2010. Generation scheduling with integration of wind power and compressed air energy storage. In *IEEE PES T&D 2010*. IEEE, pp. 1–6. Retrieved from: http://ieeexplore.ieee.org/articleDetails.jsp?arnumber=5484430&contentType=Conference+Publications [Accessed August 17, 2012].

[25]. Davidson, B.J. et al., 1980. Large-scale electrical energy storage. *Physical Science, Measurement and Instrumentation, Management and Education - Reviews, IEE Proceedings A*, 127(6), pp.345–385.

[26]. Department of Energy and Climate Change, 2010. *Feed-in Tariffs: Government's Response to the summer 2009 Consultation*, Retrieved from: http://www.decc.gov.uk/assets/decc/Consultations/Renewable Electricity FinancialIncentives/1_20100204120204_e_@@_FITsconsultationresponseandGovdecisions.pdf.

[27]. Deglaire, P. et al., 2007. Experimental results from a 12 kW vertical axis wind turbine with a direct driven PM synchronous generator. In *Most*. pp. 1–10.

[28]. Denholm, P., 2004. Life cycle energy requirements and greenhouse gas emissions from large scale energy storage systems. *Energy Conversion and Management*, 45(13-14), pp.2153–2172. Retrieved from:http://linkinghub.elsevier.com/retrieve/pii/S0196890403003200.

[29]. Denholm, P. & Kulcinski, G.L., 2003. *Net energy balance and greenhouse gas emissions from renewable energy storage systems*, Energy Center of Wisconsin.

[30]. Denholm, P. & Sioshansi, R., 2009. The value of compressed air energy storage with wind in transmission-constrained electric power systems. *Energy Policy*, 37(8), pp.3149–3158. Retrieved from:http://www.sciencedirect.com/science/article/pii/S0301421509002328.

[31]. Díaz-González, F. et al., 2012. A review of energy storage technologies for wind power applications. *Renewable and Sustainable Energy Reviews*, 16(4), pp.2154–2171. Retrieved from:http://linkinghub.elsevier.com/retrieve/pii/S1364032112000305.

[32]. dSPACE GmbH, 2012. *DS1104 R&D Controller Board： Hardware Installation and Configuration*.

[33]. Edwards, P.P. et al., 2008. Hydrogen and fuel cells: Towards a sustainable energy future. *Energy Policy*, 36(12), pp.4356–4362. Retrieved from: http://www.sciencedirect.com/science/article/pii/S0301421508004503.

[34]. Energetix, 2012. Compressed Air UPS Systems. Retrieved from: http://www.pnu-power.com/.

[35]. Energetix Group Ltd., 2012. Pnu Power - Compressed Air UPS systems. Retrieved from: http://www.pnu-power.com [Accessed October 26, 2012].

[36]. Energy Efficiency & Renewable Energy, 2007. Shell and Luminant to Build the World's Largest Wind Farm in Texas. Retrieved from:http://apps1.eere.energy.gov/states/news_detail.cfm/news_id=11131 [Accessed November 10, 2012].

[37]. Environmental change institute of Oxford University, 2005. *Wind power and UK wind resource*, Retrieved from: http://www.eci.ox.ac.uk/publications/downloads/sinden05-dtiwindreport.pdf.

[38]. Farret, F.A., Gules, R. & Marian, J., 1995. Micro-turbine simulator based on speed and torque of a DC motor to drive actually loaded generators. *Devices, Circuits and Systems, 1995, Proceedings of the 1995 First IEEE International Caracas Conference on*, pp.89–93.

[39]. Fitzgerald, A., Kingsley, C. & D.Umans, S., 1992. *Electric Machinery* fifth., McGraw-Hill.

[40]. FUJITSU Semiconductor Ltd., 2011. *Space Vector Pulse Width Modulation*,

[41]. Gasch, R. & Twele, J., 2012. *Wind Power Plants Fundamentals, Design, Construction and Operation.* Second edition. Springer.

[42]. Gast Manufacturing Corporation, 1986. *Air motors handbook.* Revised edition. Gast Manufacturing Corporation.

[43]. Gong, B. & Xu, D., 2008. Real time wind turbine simulator for wind energy conversion system. *Power Electronics Specialists Conference, 2008. PESC 2008. IEEE*, pp.1110–1114.

[44]. Gonzalez-Longatt, F.M., Wall, P. & Terzija, V., 2011. *A simplified model for dynamic behavior of permanent magnet synchronous generator for direct drive wind turbines*, IEEE. Retrieved from: http://ieeexplore.ieee.org/xpls/abs_all.jsp?arnumber=6019425.

[45]. Grauers, A., 1996. Efficiency of three wind energy generator systems. *IEEE Transactions on Energy Conversion*, 11(3), pp.650–657. Retrieved from: http://ieeexplore.ieee.org/lpdocs/epic03/wrapper.htm?arnumber=537038.

[46]. Greenblatt, J.B. et al., 2007. Base load wind energy: modeling the competition between gas turbines and compressed air energy storage for supplemental generation. *Energy Policy*, 35(3), pp.1474–1492. Retrieved from:http://www.sciencedirect.com/science/article/pii/S0301421506001509.

[47]. Guangchen, L., Shengtie, W. & Jike, Z., 2010. Design and Realization of DC Motor and Drives Based Simulator for Small Wind Turbine. *Power and Energy Engineering Conference (APPEEC), 2010 Asia-Pacific*, pp.1–4.

[48]. Gurkaynak, Y., Khaligh, A. & Emadi, A., 2009. State of the art power management algorithms for hybrid electric vehicles. *Vehicle Power and Propulsion Conference, 2009. VPPC'09. IEEE*, pp.388–394.

[49]. Hanselmann, H., 1996. Hardware-in-the-loop simulation testing and its integration into a CACSD toolset. *Computer-Aided Control System Design, 1996, Proceedings of the 1996 IEEE International Symposium on*, pp.152–156.

[50]. Hansen, A. & Michalke, G., 2007. Fault ride-through capability of DFIG wind turbines. *Renewable Energy*, 32(9), pp.1594–1610. Retrieved from: http://linkinghub.elsevier.com/retrieve/pii/S096014810600276X.

[51]. He, X., Parten, M. & Maxwell, T., 2005. Energy Management Strategies for a Hybrid Electric Vehicle. *Vehicle Power and Propulsion, 2005 IEEE Conference*, pp.536–540.

[52]. Heier, S. & Waddington, R., 2006. *Grid Integration of Wind Energy Conversion Systems.* Second edition. Wiley.

[53]. Helwig, A. & Ahfock, T., 2009. Ultra-capacitor assisted battery storage for remote area power supplies: A case study. *Power Engineering Conference, 2009. AUPEC 2009. Australasian Universities*, pp.1–6.

[54]. Hemeida, A.M., Farag, W.A. & Mahgoub, O.A., 2011. Modeling and Control of Direct Driven PMSG for Ultra Large Wind Turbines. *World Academy of Science, Engineering and Technology*, 59.

[55]. Hydraulics & Pneumatics, 2012. Air motor selection and sizing.

[56]. Ibrahim, H., Ilinca, A. & Perron, J., 2008. Energy storage systems—Characteristics and comparisons. *Renewable and Sustainable Energy Reviews*, 12(5), pp.1221–1250. Retrieved from:http://linkinghub.elsevier.com/retrieve/pii/S1364032107000238.

[57]. Idan, M., Lior, D. & Shaviv, G., A robust controller for a novel variable speed wind turbine transmission. *Journal of solar energy engineering*, 120(4), pp.247–252. Retrieved from: http://cat.inist.fr/?aModele=afficheN&cpsidt=1620598 [Accessed October 15, 2012].

[58]. International Rectifier, 2004. *IRMCK203 Application Developer's Guide,* El Segundo.

[59]. James, L.P.E., 2012. *Compressed air energy storage*, Retrieved from: http://www.pdhengineer.com/courses/m/M-3051.pdf.

[60]. Jeffrey Logan & Stan Mark Kaplan, 2008. *Wind Power in the United States: Technology, Economic, and Policy Issues,* Retrieved from: http://www.fas.org/sgp/crs/misc/RL34546.pdf.

[61]. Jia, Y., Wang, Z. & Yang, Z., 2007. Experimental Study of Control Strategy for Wind Generation System. *Power Electronics Specialists Conference, 2007. PESC 2007. IEEE*, pp.1202–1207.

[62]. Jin, X., 2007. *The Research on System Modeling Theory and Simulation in Wind Turbine*. Chongqing University.

[63]. Jin, Z., Sheng, N. & Chen, Q., Neutral network model identification on wind turbine system. *ACTA Energiae Solaris Sinica*, pp.206–211.

[64]. Jin，X., *The Research on System Modeling Theory and Simulation in Wind Turbine* . Chongqing University.

[65]. John P., 2006. *Shaft Alignment Handbook.* Third edition. CRC Press.

[66]. Juliette, J., 2012. Windfarms axed as UK loses its taste for turbines. *The Guardian on 2nd March 2012*.

[67]. Kaldellis, J. & Zafirakis, D., 2007. Optimum energy storage techniques for the improvement of renewable energy sources-based electricity generation economic efficiency. *Energy*, 32(12), pp.2295–2305. Retrieved from: http://linkinghub.elsevier.com/retrieve/pii/S0360544207001302.

[68]. Ke, X. et al., 2007. Wind turbine simulator using PMSM. *Universities Power Engineering Conference, 2007. UPEC 2007. 42nd International*, pp.732–737.

[69]. Kluiters, E.C. et al., 1999. Testing of a sodium/nickel chloride (ZEBRA) battery for electric propulsion of ships and vehicles. *Journal of Power Sources*, 80(1–2), pp.261–264. Retrieved from: http://www.sciencedirect.com/science/article/pii/S0378775399000750.

[70]. Knospe, C., 2006. PID control. *IEEE Control Systems Magazine*, 26(1), pp.30–31.

[71]. Kojabadi, H.M., Chang, L. & Boutot, T., 2004. Development of a novel wind turbine simulator for wind energy conversion systems using an inverter-controlled induction motor. *Energy Conversion, IEEE Transactions on*, 19(3), pp.547–552.

[72]. Kondoh, J. et al., 2000. Electrical energy storage systems for energy networks. *Energy Conversion and Management*, 41(17), pp.1863–1874. Retrieved from: http://www.sciencedirect.com/science/article/pii/S0196890400000285.

[73]. Kumar, K.V. et al., 2010. Simulation and comparison of SPWM and SVPWM control for three phase inverter. *ARPN Journal of Engineering and Applied Sciences*, 5(7), pp.61–74.

[74]. Lackner, M.A., 2009. *Wind Turbine Control Systems: Current Status and Future Developments*, Retrieved from: http://web.mit.edu/windenergy/windweek/Presentations/P9 - Lackner.pdf.

[75]. Lang，Y., Zargari, N. & Kouro，S., 2011. *Power Conversion and Control of Wind Energy Systems* 1st ed., John Wiley & Sons.

[76]. Lawrence Berkeley National Laboratory, 2003. *Improving Compressed Air System Performance*, Washington, D.C.: U.S. Department of Energy.

[77]. Lei, Y. et al., 2006. Modeling of the Wind Turbine With a Doubly Fed Induction Generator for Grid Integration Studies. *IEEE Transactions on Energy Conversion*, 21(1), pp.257–264. Retrieved from: http://ieeexplore.ieee.org/lpdocs/epic03/wrapper.htm?arnumber=1597345.

[78]. Li, S. & Haskew, T.A., 2008. Characteristic study of vector-controlled direct driven permanent magnet synchronous generator in wind power generation. *Power and Energy Society General Meeting - Conversion and Delivery of Electrical Energy in the 21st Century, 2008 IEEE*, pp.1–9.

[79]. Lin, C. C. et al., 2003. Control system development for an advanced-technology medium-duty hybrid electric truck. *SAE paper*, 20.

[80]. Linden, S., 2007. Review of CAES systems development and current innovations that could bring commercialization to fruition. In *Electrical Energy Storage Applications & Technology Conference*. San Francisco.

[81]. Liu, J. & Peng, H., 2008. Modeling and Control of a Power-Split Hybrid Vehicle. *IEEE Transactions on Control Systems Technology*, 16(6), pp.1242–1251. Retrieved from: http://ieeexplore.ieee.org/xpls/abs_all.jsp?arnumber=4475524 [Accessed September 2, 2012].

[82]. Liu, W. et al., 2006. Wind energy and wind power generation technology. *Chemistry Industry Press*.

[83]. Lubosny, Z., 2003. *Wind Turbine Operation in Electric Power Systems*. First edition. Springer.

[84]. Luo, D.L.D. et al., 2008. *Control of direct-drive permanent-magnet wind power system connected to grid*,

[85]. Luo, X. et al., 2008. Development of a Mathematical Model for Vane-type Air Motors with Arbitrary N Vanes. In *Proceedings of the World Congress on Engineering 2008*. London.

[86]. Luo, X. et al., 2012. Feasibility study on recovering exhaust energy from a vehicle engine system by a scroll expander. *Advanced Intelligent Mechatronics (AIM), 2012 IEEE/ASME International Conference on*, pp.689–694.

[87]. Luo, X., *Mathematical modelling and energy conversion efficiency analysis of scroll air motors and its application to a pneumatic-electrical system*. University of Birmingham.

[88]. Luo, X. et al., 2012. Study of a New Strategy for Pneumatic Actuator System Energy Efficiency Improvement via the Scroll Expander Technology. *Mechatronics, IEEE/ASME Transactions on*, PP(99), pp.1–11.

[89]. Luo, X., Sun, H. & Wang, J., 2009. Air leakage study for energy efficiency improvement of a pneumatic-electricity conversion system. In *The Proceedings of the 15th International Conference on Automation and Computing*, Luton.

[90]. Luo, X., Sun, H. & Wang, J., 2011. An energy efficient pneumatic-electrical system and control strategy development. *American Control Conference (ACC), 2011*, pp.4743–4748.

[91]. Mack, D.R., 1993. Something new in power technology. *IEEE Potentials*, 12(2), pp.40–42. Retrieved from: http://ieeexplore.ieee.org/articleDetails.jsp?arnumber=283812&contentType=Journals+&+Magazines [Accessed August 17, 2012].

[92]. Majumdar, S.R., 1996. *Pneumatic systems: principles and maintenance*, Tata McGraw-Hill Education.

[93]. Makansi, J., 2007. *E n e r g y S t o r a g e-The Sixth Dimension of the Electricity Production and Delivery Value Chain*, Retrieved from: http://www.energystoragecouncil.org/1 - Jason Makansi-ESC.pdf.

[94]. Mandle, K.T., 1988. Dinorwig pumped-storage scheme. *Power Engineering Journal*, 2(5), pp.259–262.

[95]. Manwell, J.F., McgOWAN, J.G. & Rogers, A.L., 2009. *Wind Energy Explained Theory, Design and Application*. Second edition. Wiley.

[96]. Martínez, M., Molina, M.G. & Mercado, P.E., 2010. *Dynamic performance of compressed air energy storage (CAES) plant for applications in power systems*, IEEE.

[97]. Mashadi, B. & Emadi, S.A.M., 2010. *Dual-Mode Power-Split Transmission for Hybrid Electric Vehicles*,

[98]. Mathworks, 2012. Matlab R2012a Documentation-SimPowerSystems. Retrieved from: http://www.mathworks.co.uk/help/toolbox/physmod/powersys/ref/permanentmagnetsynchronousmachine.html.

[99]. McDowall, J., 2004. *High power batteries for utilities - the world's most powerful battery and other developments*, *IEEE*. Retrieved from: http://ieeexplore.ieee.org/lpdocs/epic03/wrapper.htm?arnumber=1373234.

[100]. McDowall, J.A., 2007. Status and Outlook of the Energy Storage Market. In *2007 IEEE Power Engineering Society General Meeting*. IEEE, pp. 1–3. Retrieved from:http://ieeexplore.ieee.org/articleDetails.jsp?arnumber=4275200&contentType=Conference+Publications [Accessed August 17, 2012].

[101]. Molina, M.G., 2010. Dynamic Modelling and Control Design of Advanced Energy Storage for Power System Applications. In *Dynamic Modelling*.

[102]. Muljadi, E. & Butterfield, C.P., 2001. Pitch-controlled variable-speed wind turbine generation. *Industry Applications, IEEE Transactions on*, 37(1), pp.240–246.

[103]. Muller, S., Deicke, M. & De Doncker, R.W., 2002. Doubly fed induction generator systems for wind turbines. *Industry Applications Magazine, IEEE*, 8(3), pp.26–33.

[104]. Nakhamkin, M., 2008. CAES Bottom Cycle Concept. Retrieved from:http://www.espcinc.com/ [Accessed October 6, 2012].

[105]. Neumiller, J.L., 2006. *Reservoir simulation of combined wind energy and compressed air energy storage in different Geologic settings.* Colorado School of Mines.

[106]. Nichita, C. et al., 2002. Large band simulation of the wind speed for real time wind turbine simulators. *Ieee Transactions on Energy Conversion*, 17(4), pp.523–529. Retrieved from: <Go to ISI>://000180231100013.

[107]. Nordex, 2008. Nordex N54 1000kw wind turbine. Retrieved from: http://www.nordex-online.com/en/.

[108]. United States Nuclear Regulatory Commission, 2012. Comanche Peak Nuclear Power Plant, Units 3 and 4 Application. *United States Nuclear Regulatory Commission*. Retrieved from: http://pbadupws.nrc.gov/docs/ML1118/ML11186A372.pdf [Accessed December 13, 2012].

[109]. Ochs, D.S., 2010. Design of detailed models for use in fast aeroelastic simulations of permanent-magnet direct-drive wind turbines. Kansas State University.

[110]. Ovando, R.I., Aguayo, J. & Cotorogea, M., 2007. Emulation of a Low Power Wind Turbine with a DC motor in Matlab/Simulink. *Power Electronics Specialists Conference, 2007. PESC 2007. IEEE*, pp.859–864.

[111]. Pandian, S.R. et al., 1999. Control performance of an air motor-can air motors replace electric motors? *Robotics and Automation, 1999. Proceedings. 1999 IEEE International Conference on*, 1, pp.518–524 vol.1.

[112]. Park, H.-G. et al., 2007. Low-cost converters for micro wind turbine systems using PMSG. In *2007 7th Internatonal Conference on Power Electronics*. IEEE, pp. 483–487. Retrieved from:http://ieeexplore.ieee.org/xpls/abs_all.jsp?arnumber=4692434 [Accessed September 5, 2012].

[113]. Du Pasquier, A. et al., 2003. A comparative study of Li-ion battery, supercapacitor and nonaqueous asymmetric hybrid devices for automotive applications. *Journal*

of Power Sources, 115(1), pp.171–178. Retrieved from: http://linkinghub.elsevier.com/retrieve/pii/S0378775302007188.

[114]. Pena, R., Clare, J.C. & Asher, G.M., 1996. Doubly fed induction generator using back-to-back PWM converters and its application to variable-speed wind-energy generation. *Electric Power Applications, IEE Proceedings* -, 143(3), pp.231–241.

[115]. Pillay, P. & Krishnan, R., 1988. *Modeling of permanent magnet motor drives*, IEEE. Retrieved from: http://ieeexplore.ieee.org/lpdocs/epic03/wrapper.htm?arnumber=9176.

[116]. Pillay, P. & Krishnan, R., 1989. *Modeling, simulation, and analysis of permanent-magnet motor drives. I. The permanent-magnet synchronous motor drive*, Retrieved from:http://ieeexplore.ieee.org/lpdocs/epic03/wrapper.htm?arnumber=25542.

[117]. Pollak, R., 1994. *History of First U.S. Compressed-Air Energy Storage (CAES) Plant (110 MW 26h): Volume 2: Construction*,

[118]. Porkhial, S., Khastoo, B. & Modarres Razavi, M.R., 2002. Transient characteristic of reciprocating compressors in household refrigerators. *Applied Thermal Engineering*, 22(12), pp.1391–1402. Retrieved from:http://www.sciencedirect.com/science/article/pii/S1359431102000467.

[119]. Prats, M.A.M. et al., 2000. Improving transition between power optimization and power limitation of variable speed, variable pitch wind turbines using fuzzy control techniques. *Industrial Electronics Society, 2000. IECON 2000. 26th Annual Confjerence of the IEEE*, 3, pp.1497–1502 vol.3.

[120]. Pu, J., Moore, P.R. & Weston, R.H., 1991. Digital servo motion control of air motors. *International Journal of Production Research*, 29(3), pp.599–618. Retrieved from: http://dx.doi.org/10.1080/00207549108930091.

[121]. Rahman, M.A. et al., 1996. Modelling and controller design of an isolated diesel engine permanent magnet synchronous generator. *IEEE Transactions on Energy Conversion*, 11(2), pp.324–330. Retrieved from: http://ieeexplore.ieee.org/lpdocs/epic03/wrapper.htm?arnumber=507185.

[122]. Rahman, S.A. & Varma, R.K., 2011. PSCAD/EMTDC model of a 3-phase grid connected photovoltaic solar system. *North American Power Symposium (NAPS), 2011*, pp.1–7.

[123]. RenewableUK, 2010. Press release on 23rd September, 2010. Retrieved from: http://www.bwea.com/media/news/articles/pr20100923-2.html.

[124]. RenewableUK, 2012. Wind power generation statistics. Retrieved from: http://www.bwea.com/statistics/.

[125]. Ribeiro, P.F. et al., 2001. Energy storage systems for advanced power applications. *Proceedings of the IEEE*, 89(12), pp.1744–1756.

[126]. Ridge Energy Storage & Grid Services L.P, 2005. *The Economic Impact of CAES on Wind in TX, OK, and NM*, Retrieved from: http://www.seco.cpa.state.tx.us/zzz_re/re_wind_projects-compressed2005.pdf.

[127]. Rolan, A. et al., 2009. Modeling of a variable speed wind turbine with a Permanent Magnet Synchronous Generator. In *2009 IEEE International Symposium on Industrial Electronics*. IEEE, pp. 734–739. Retrieved from:http://ieeexplore.ieee.org/articleDetails.jsp?arnumber=5218120&contentType=Conference+Publications [Accessed September 7, 2012].

[128]. Salgi, G. & Lund, H., 2008. System behaviour of compressed-air energy-storage in Denmark with a high penetration of renewable energy sources. *Applied Energy*, 85(4), pp.182–189. Retrieved from: http://linkinghub.elsevier.com/retrieve/pii/S0306261907001134.

[129]. Sannomiya, T. et al., 2001. *Test results of compensation for load fluctuation under a fuzzy control by a 1 kWh/1 MW SMES* H. Hayashi, ed.,

[130]. Sasaki, S., Toyota's newly developed hybrid powertrain. In *Proceedings of the 10th International Symposium on Power Semiconductor Devices and ICs. ISPSD'98 (IEEE Cat. No.98CH36212)*. Inst. Electr. Eng. Japan, pp. 17–22. Retrieved from: http://ieeexplore.ieee.org/xpls/abs_all.jsp?arnumber=702540 [Accessed September 2, 2012].

[131]. Schmid, C., 2005. *Course on Dynamics of multidisplicinary and controlled Systems*, Ruhr-Universität Bochum.

[132]. Schulte，R., 2011. Iowa Stored Energy Park(ISEP) Update, Retrieved from: http://www.carebs.org/ISEP.pdf.

[133]. Slootweg, J.G. et al., 2003. General model for representing variable speed wind turbines in power system dynamics simulations. *Power Systems, IEEE Transactions on*, 18(1), pp.144–151.

[134]. Slootweg, J.G., Polinder, H. & Kling, W.L., 2001. *Dynamic modelling of a wind turbine with doubly fed induction generator*, IEEE. Retrieved from:http://ieeexplore.ieee.org/lpdocs/epic03/wrapper.htm?arnumber=970114.

[135]. Sopanen, J. et al., 2011. *Dynamic Torque Analysis of a Wind Turbine Drive Train Including a Direct-Driven Permanent-Magnet Generator*, IEEE. Retrieved from:http://ieeexplore.ieee.org/xpls/abs_all.jsp?arnumber=5601770.

[136]. Sørensen, P. et al., 2001. *Simulation of Interaction between Wind Farm and Power System*, Roskilde.

[137]. Stoecker, W.F., 1998. *Industrial refrigeration handbook, Chapter 4 reciprocating compressors*, McGraw-Hill.

[138]. Strachan, N.P.W. & Jovcic, D., 2007. Dynamic Modelling, Simulation and Analysis of an Offshore Variable-Speed Directly-Driven Permanent-Magnet Wind Energy Conversion and Storage System (WECSS). In *OCEANS 2007 Europe*. IEEE, pp. 1–6. Retrieved from:http://ieeexplore.ieee.org.proxy.tritonia.fi/ielx5/4302188/4302189/04302438.pdf?tp=&arnumber=4302438&isnumber=4302189.

[139]. Strbac, G. et al., 2012. *Strategic Assessment of the Role and Value of Energy Storage Systems in the UK Low Carbon Energy Future*, London.

[140]. Succar, S., *Large Energy Storage Systems Handbook* J. G. Levine, ed., CRC Press.

[141]. Succar, S. & Williams, R.H., 2008. *Compressed Air Energy Storage: Theory, Resources,And Applications For Wind Power*, Retrieved from: http://www.princeton.edu/pei/energy/publications/texts/SuccarWilliams_PEI_CAES_2008April8.pdf.

[142]. Sun, H., Wang, J., et al., 2011. Study on a Wind Turbine in Hybrid Connection with an Energy Storage System. In *Electrical Engineering and Applied Computing*. Springer Netherlands, pp. 39–52.

[143]. Sun, H., Luo, X. & Wang, J., 2011. Management and control strategy study for a new hybrid wind turbine system. In *IEEE Conference on Decision and Control and European Control Conference*. IEEE, pp. 3671–3676.

[144]. Sun, H., Luo, X. & Wang, J., 2013. Simulation study of energy efficiency for a hybrid wind turbine system. *Industrial Technology (ICIT), 2013 IEEE International Conference on*, pp.781–786.

[145]. Tan, K. & Islam, S., 2004. Optimum control strategies in energy conversion of PMSG wind turbine system without mechanical sensors. *Energy Conversion, IEEE Transactions on*, 19(2), pp.392–399.

[146]. Taylor, J. & Halnes, A., 2010. Analysis Of compressed air energy storage. In *PCIC Europe 2010 Conference*. Oslo. Retrieved from:http://ieeexplore.ieee.org/xpl/articleDetails.jsp?arnumber=5525746 [Accessed August 17, 2012].

[147]. Ter-Gazarian，A., 1994. *Energy Storage for Power Systems*, IET.

[148]. Thongam, J.S. et al., 2009. *Wind speed sensorless maximum power point tracking control of variable speed wind energy conversion systems*, IEEE. Retrieved from: http://ieeexplore.ieee.org/lpdocs/epic03/wrapper.htm?arnumber=5075452.

[149]. U.S. Department of Energy, 2006. Energy Storage. Retrieved from:http://energy.gov/oe/technology-development/energy-storage.

[150]. U.S. Department of Energy, 2001. *Hydrogen properties*, Retrieved from: http://www1.eere.energy.gov/hydrogenandfuelcells/tech_validation/pdfs/fcm01r0.pdf.

[151]. Ueno, K., Bye, R.E. & Hunter, K.S., 2003. *Compressor Efficiency Denitions*,

[152]. United Nations Environment Programme, 2006. *Compressors and Compressed Air Systems*,

[153]. University of California, 2012. *2020 strategic analysis of energy storage in California*, Retrieved from:

http://www.energy.ca.gov/2011publications/CEC-500-2011-047/CEC-500-2011-047.pdf.

[154]. Vadim I. U. & Hao-Chi C., 2002. Sliding mode control on electro-mechanical systems. *Mathematical Problems in Engineering*, 8(4-5), pp.451–473.

[155]. Visioli, A., 2006. *Practical PID control*, Springer.

[156]. Wang, J., Yang, L., et al., 2011. Mathematical Modeling Study of Scroll Air Motors and Energy Efficiency Analysis-Part I. *Mechatronics, IEEE/ASME Transactions on*, 16(1), pp.112–121.

[157]. Wang, J., Luo, X., et al., 2011a. Mathematical Modeling Study of Scroll Air Motors and Energy Efficiency Analysis-Part II. *Mechatronics, IEEE/ASME Transactions on*, 16(1), pp.122–132.

[158]. Wang, J., Luo, X., et al., 2011b. Mathematical Modeling Study of Scroll Air Motors and Energy Efficiency Analysis-Part II. *Mechatronics, IEEE/ASME Transactions on*, 16(1), pp.122–132.

[159]. Wang, J. et al., 1998. Modelling study and servo-control of air motor systems. *International Journal of Control*, 71(3), pp.459–476. Retrieved from: http://dx.doi.org/10.1080/002071798221777.

[160]. Wei, J. L., Wang, J. & Wu, Q.H., 2007. Development of a Multisegment Coal Mill Model Using an Evolutionary Computation Technique. *Energy Conversion, IEEE Transactions on*, 22(3), pp.718–727.

[161]. Welfonder, E., Neifer, R. & Spanner, M., 1997. Development and experimental identification of dynamic models for wind turbines. *Control Engineering Practice*, 5(1), pp.63–73. Retrieved from: http://www.sciencedirect.com/science/article/pii/S0967066196002080.

[162]. Westlake, A.J.G., Bumby, J.R. & Spooner, E., 1996. Damping the power-angle oscillations of a permanent-magnet synchronous generator with particular reference to wind turbine applications. *Electric Power Applications, IEE Proceedings* -, 143(3), pp.269–280.

[163]. Wikipedia-Compressed air energy storage, 2012a. No Title. Retrieved from: http://en.wikipedia.org/wiki/Compressed_air_energy_storage [Accessed October 1, 2012].

[164]. Wikipedia-Compressed air energy storage, 2012b. No Title. Retrieved from: http://en.wikipedia.org/wiki/Compressed_air_energy_storage [Accessed October 1, 2012].

[165]. Wolf, D. et al., 2011. Adiabatic Compressed Air Energy Storage co-located with wind energy—multifunctional storage commitment optimization for the German market using GOMES. *Energy Systems*, 3(2), pp.181–208. Retrieved from:http://www.springerlink.com/content/8h2168p276617855/.

[166]. World Wind Energy Association, 2012. *World Wind Energy Report 2011*, Bonn. Retrieved from:http://www.wwindea.org/webimages/WorldWindEnergyReport2011.pdf.

[167]. Wu, J. et al., 2009. Energy Saving Analysis Using Pulse Width Modulation Techniques Controlling Electromagnetic Clutch in EPS System. *Information Processing, 2009. APCIP 2009. Asia-Pacific Conference on*, 1, pp.394–397.

[168]. Wu, X. et al., 2008. Control of electromagnetic clutch during vehicles start. *Vehicle Power and Propulsion Conference, 2008. VPPC '08. IEEE*, pp.1–5.

[169]. Yang, X. et al., 2009. *Low Voltage Ride-Through of Directly Driven Wind Turbine with Permanent Magnet Synchronous Generator*, Ieee. Retrieved from:http://ieeexplore.ieee.org/lpdocs/epic03/wrapper.htm?arnumber=4918470.

[170]. Yang, L. et al., 2007. Energy Efficiency Analysis of a Scroll-type Air Motor Based on a Simplified Mathematical Model. In *Proceedings of the World Congress on Engineering 2007*. London.

[171]. Yang, Y. & Emadi, A., 2011. *Integrated electro-mechanical transmission systems in hybrid electric vehicles*, IEEE.

[172]. Yang, Y. et al., 2009. Grid-connected inverter for wind power generation system. *Journal of Shanghai University*, 13(1), pp.51–56 LA – English. English Edition. Retrieved from:http://dx.doi.org/10.1007/s11741-009-0110-3.

[173]. Yeung, Y.P.B. et al., 2009. Automobile hybrid air conditioning technology. *Power Electronics Systems and Applications, 2009. PESA 2009. 3rd International Conference on*, pp.1–5.

[174]. Yin, M. et al., 2007. Modeling of the Wind Turbine with a Permanent Magnet Synchronous Generator for Integration. *Power*, 11(1), pp.1–6. Retrieved from:http://ieeexplore.ieee.org/lpdocs/epic03/wrapper.htm?arnumber=4275748.

[175]. Zhang, J. et al., 2008. Pitch angle control for variable speed wind turbines. *Electric Utility Deregulation and Restructuring and Power Technologies, 2008. DRPT 2008. Third International Conference on*, pp.2691–2696.

[176]. Zhang, P., 2012. *Small Wind World Report Summary 2012*, Retrieved from:http://www.wwindea.org/webimages/WWEA Small Wind World Report Summary 2012.pdf.

[177]. Zimmels, Y. et al., 2002. Design Criteria for Compressed Air Storage in Hard Rock. *Energy Environment*, 13(6), pp.851–872. Retrieved from:http://dx.doi.org/10.1260/095830502762231313.

[178]. Zinger, D.S. & Muljadi, E., 1997. Annualized wind energy improvement using variable speeds. *Industry Applications, IEEE Transactions on*, 33(6), pp.1444–1447.

Appendix

This appendix shows drawings of the various parts used in the mechanical setups. All drawings were made with AutoCAD 2004.

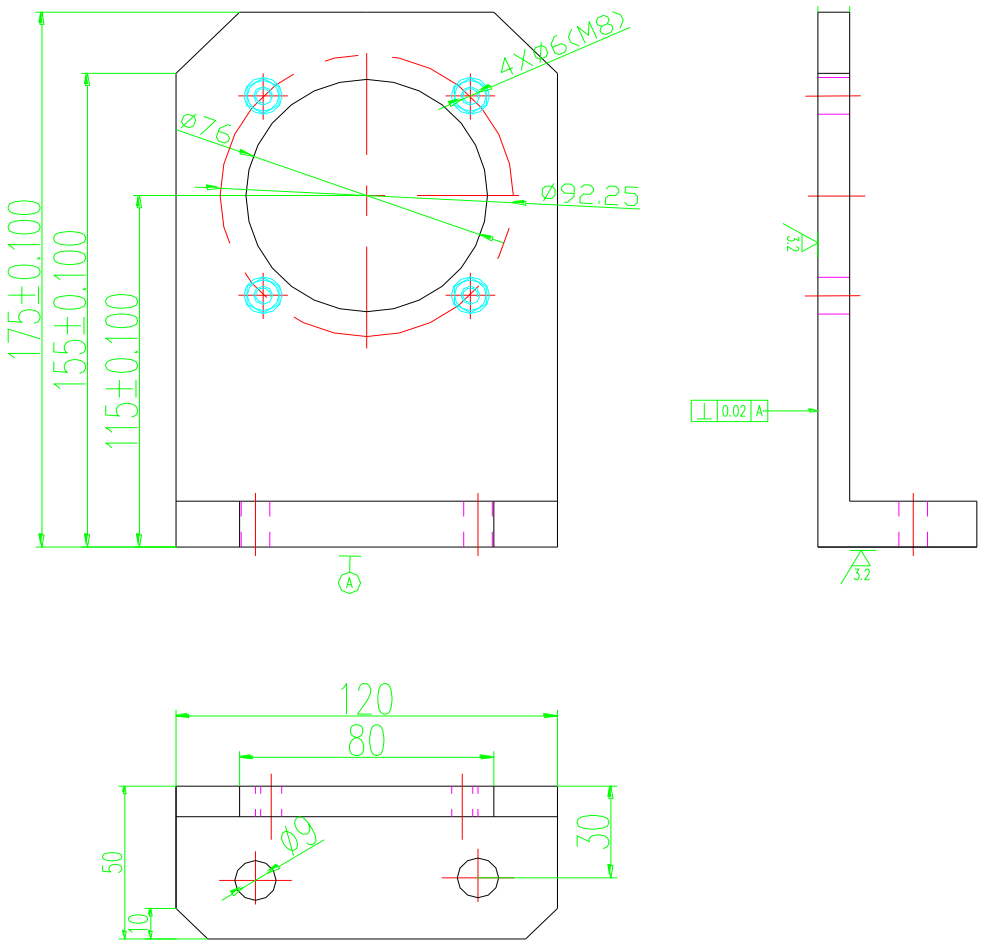

Figure A.1 DC motor flanges

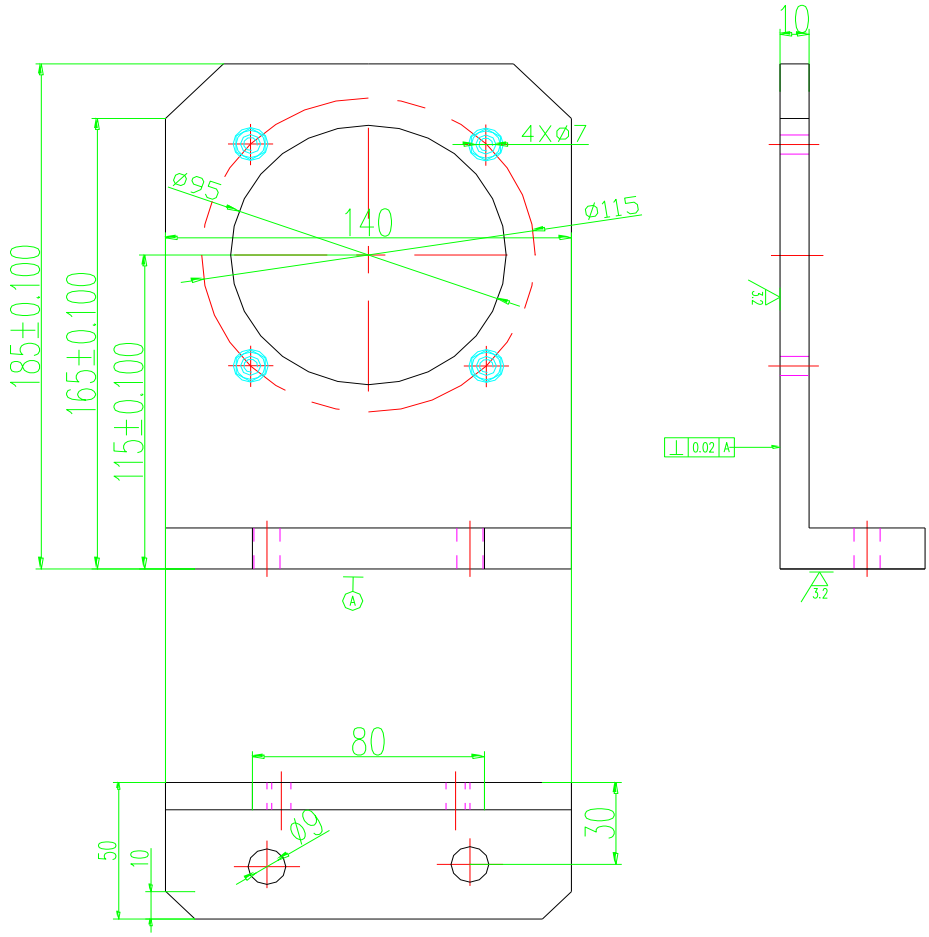

Figure A.2 PMSG flange

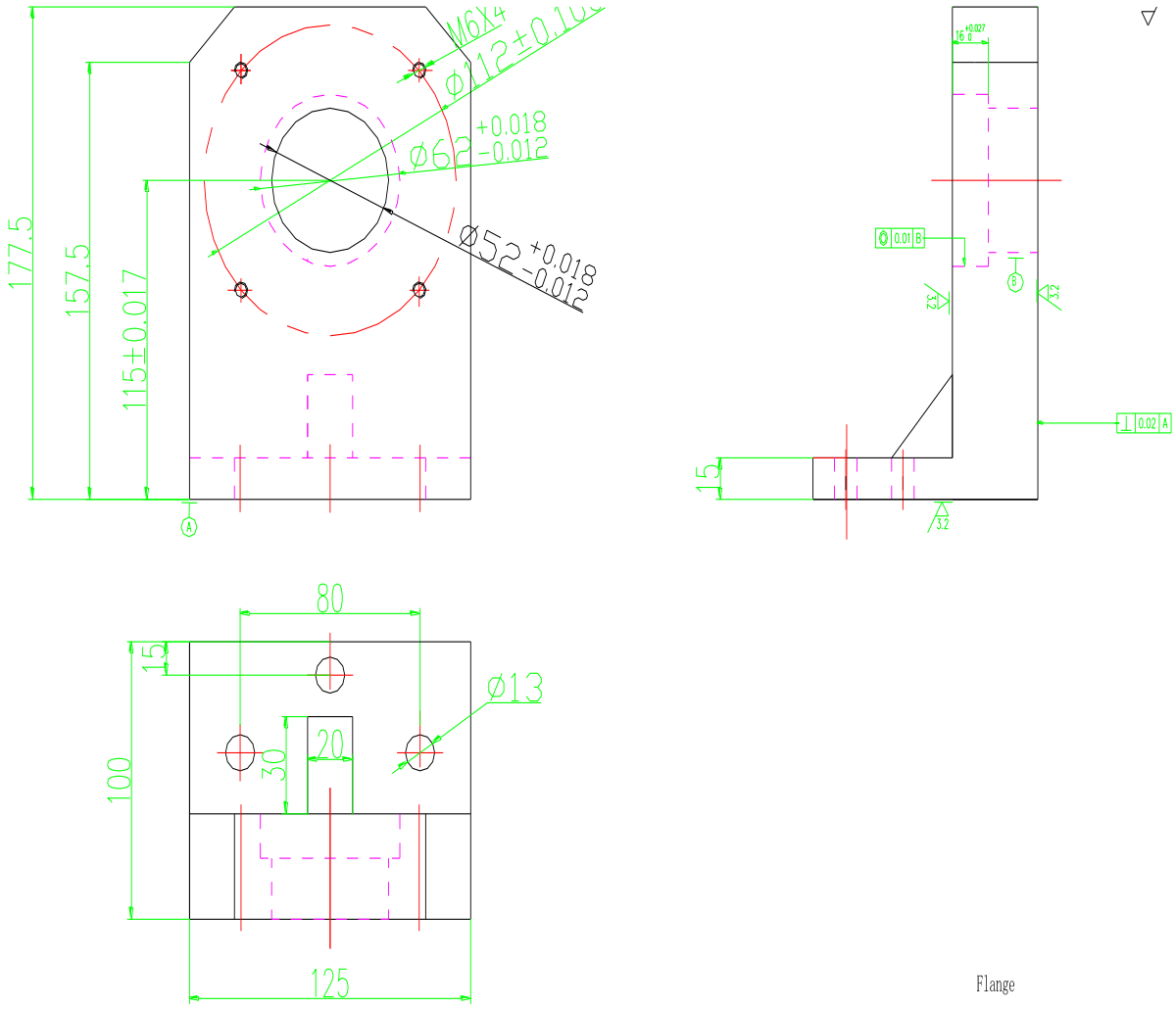

Figure A.3 Clutch 2 flange

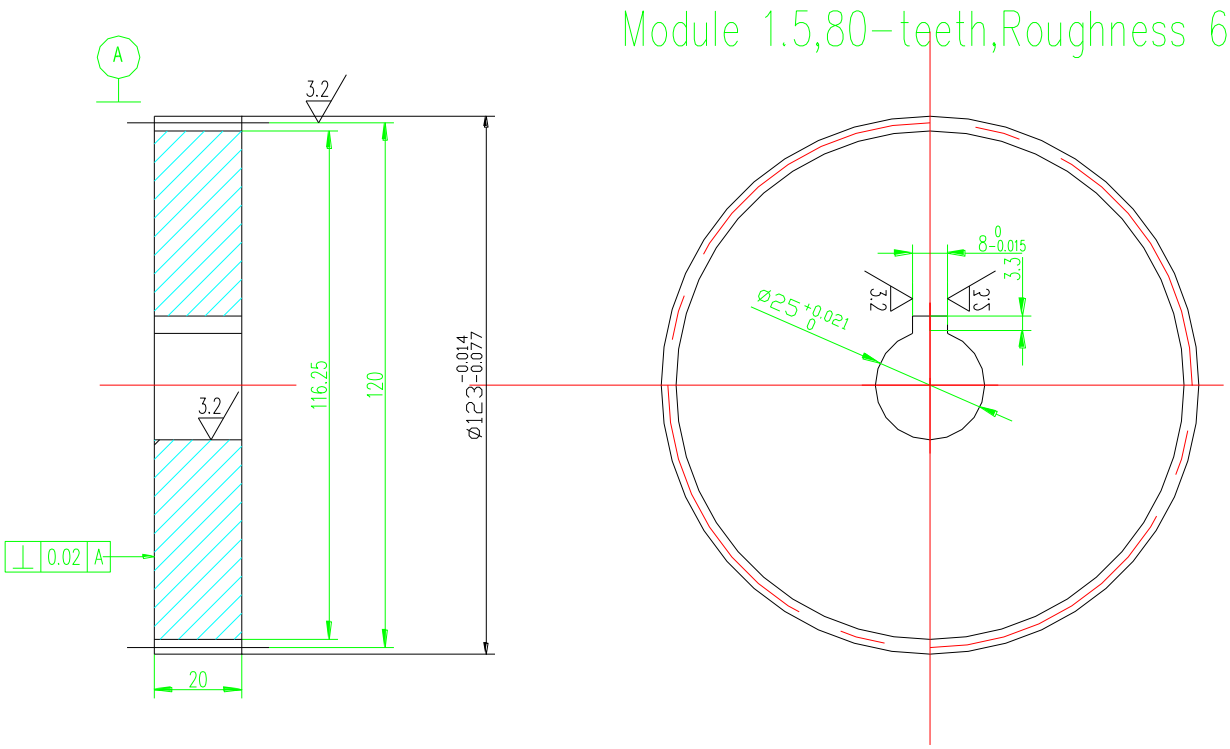

Figure A.4 No. 20 and 23 spur cylindrical gears

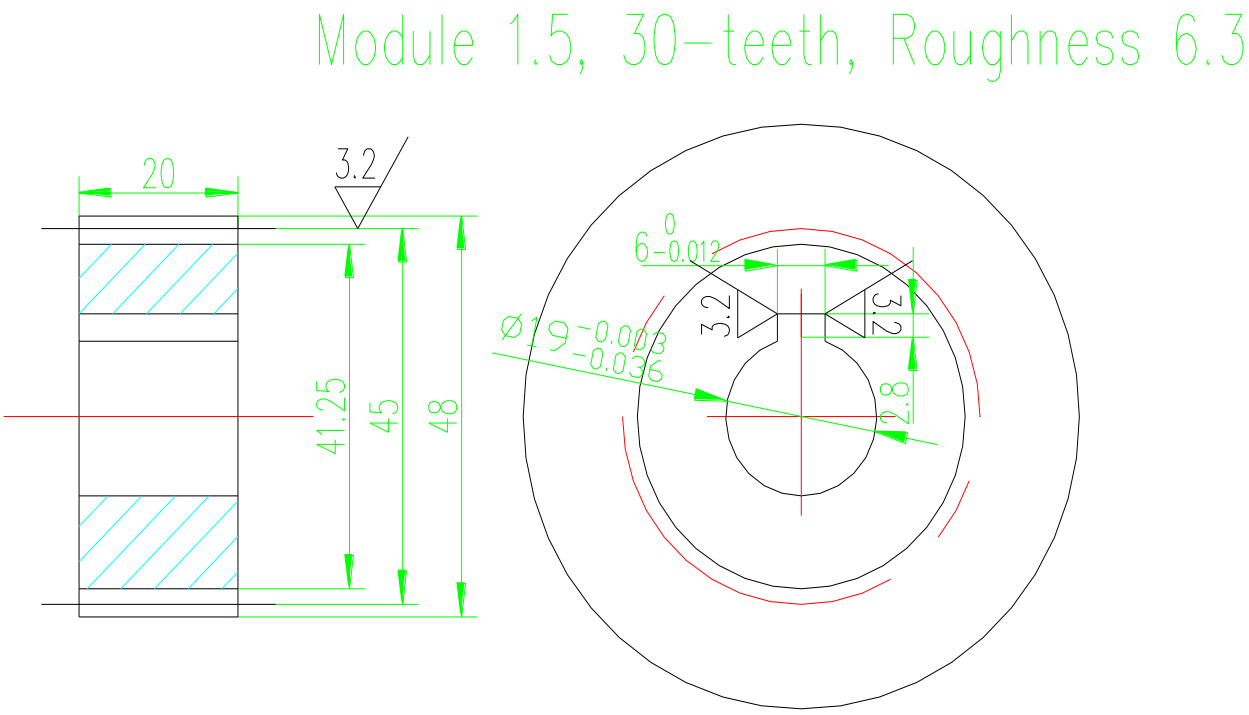

Figure A.5 No. 19 and 21 spur cylindrical gears

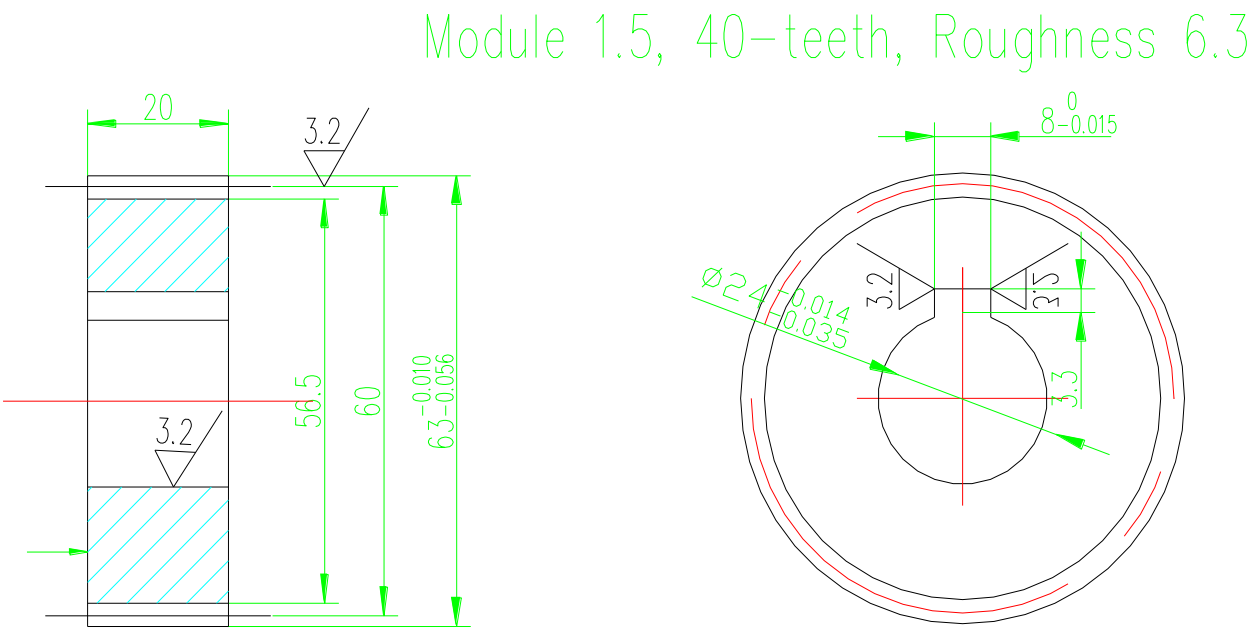

Figure A.6 No. 24 spur cylindrical gears

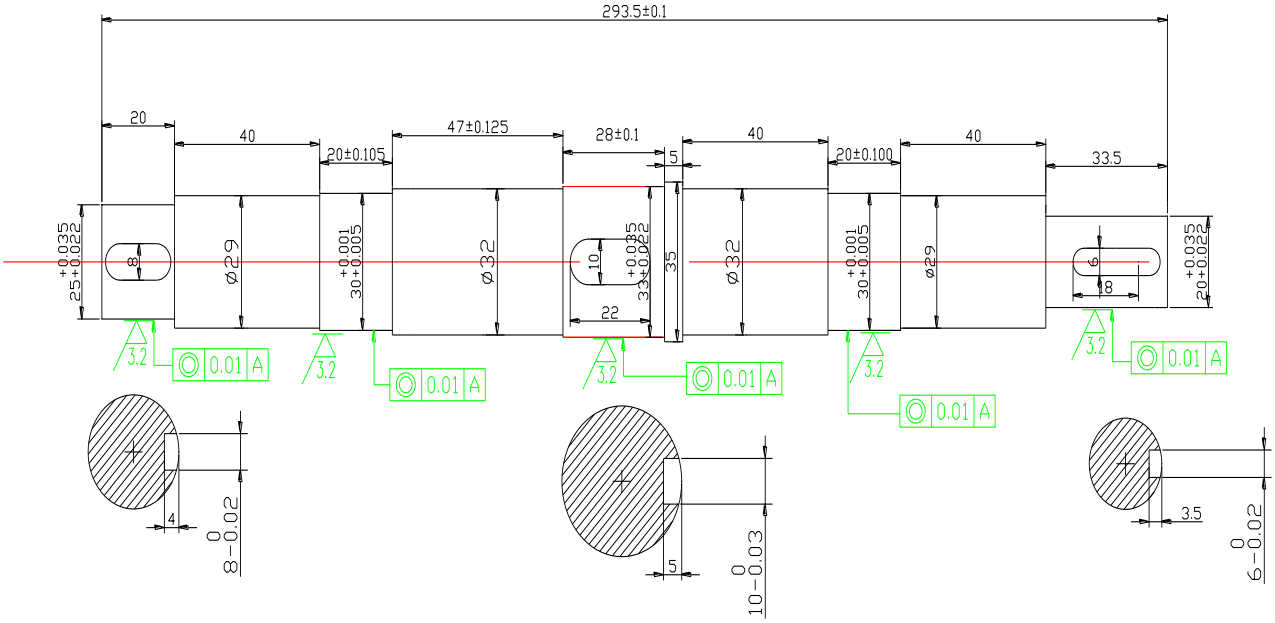

Figure A.7 Shaft 1

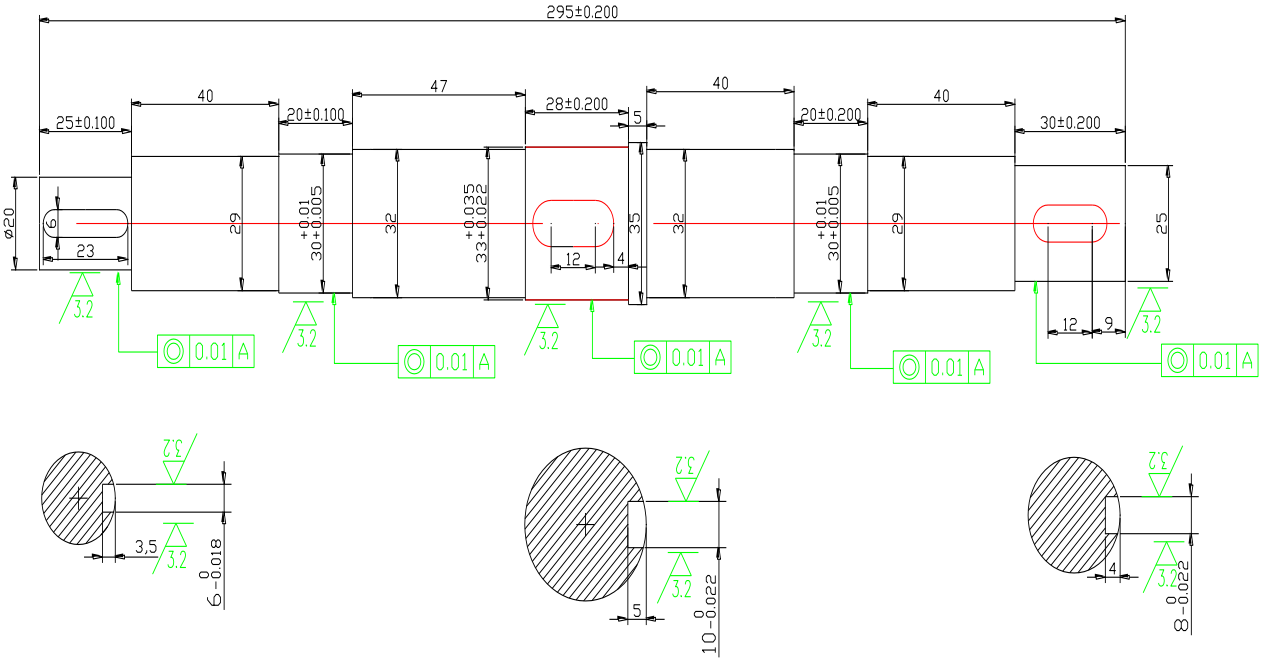

Figure A.8 Shaft 2

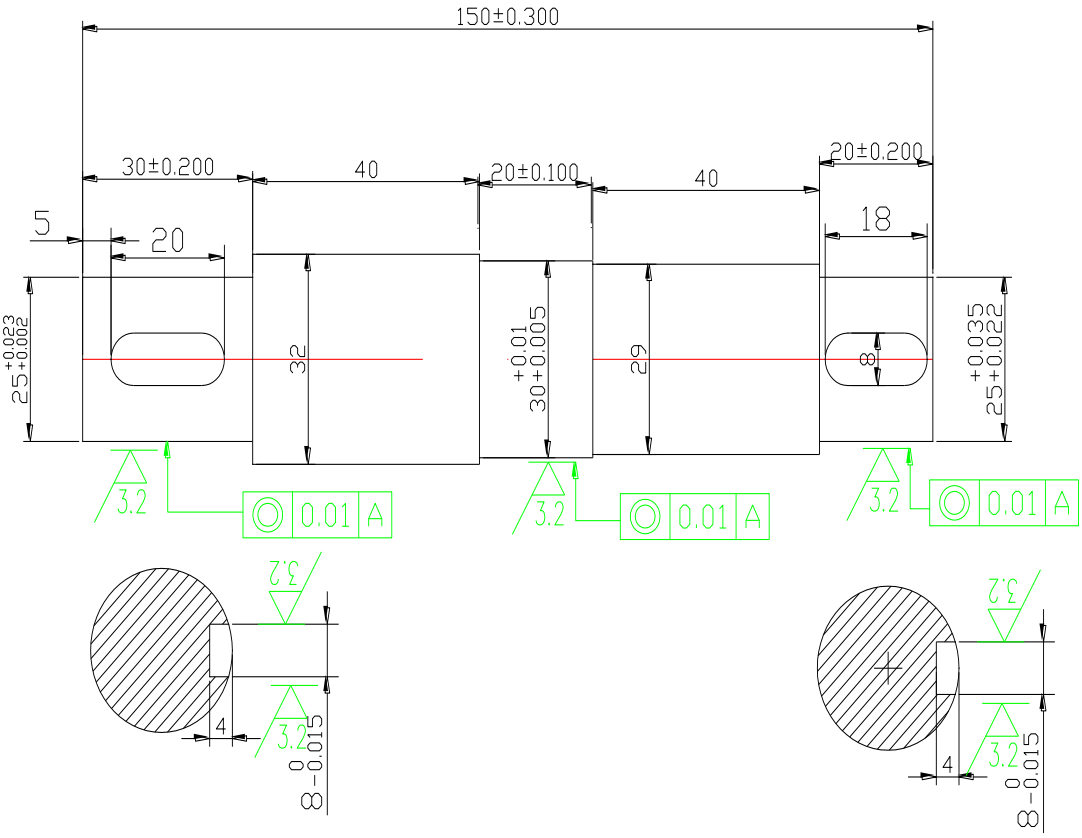

Figure A.9 Shaft 3

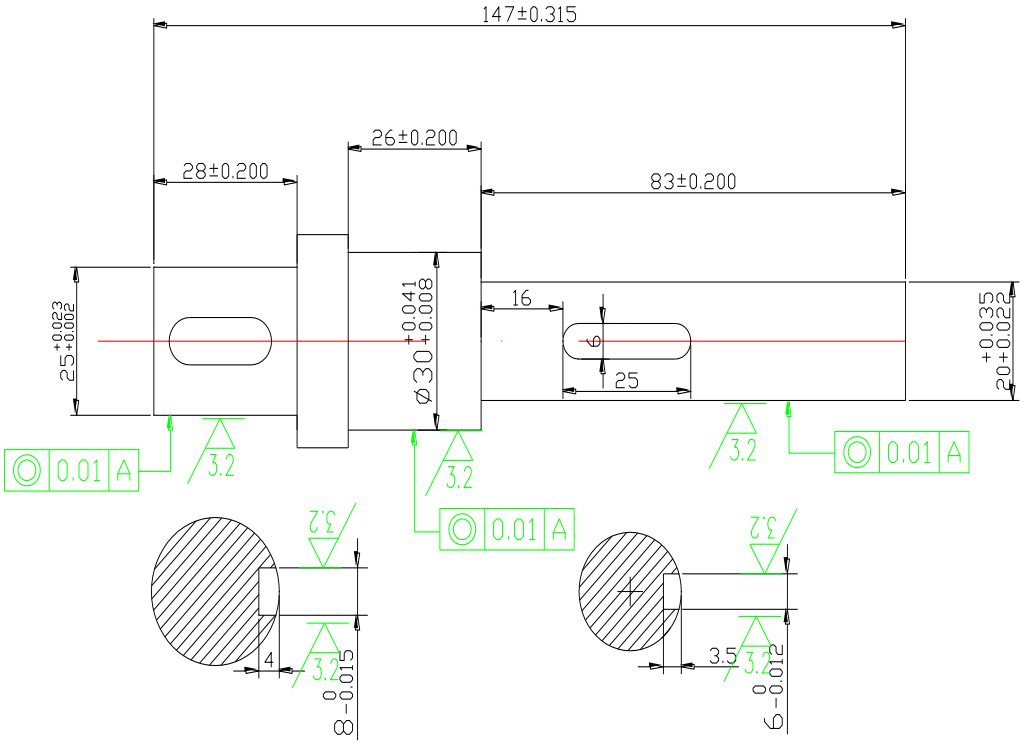

Figure A.10 Shaft 4

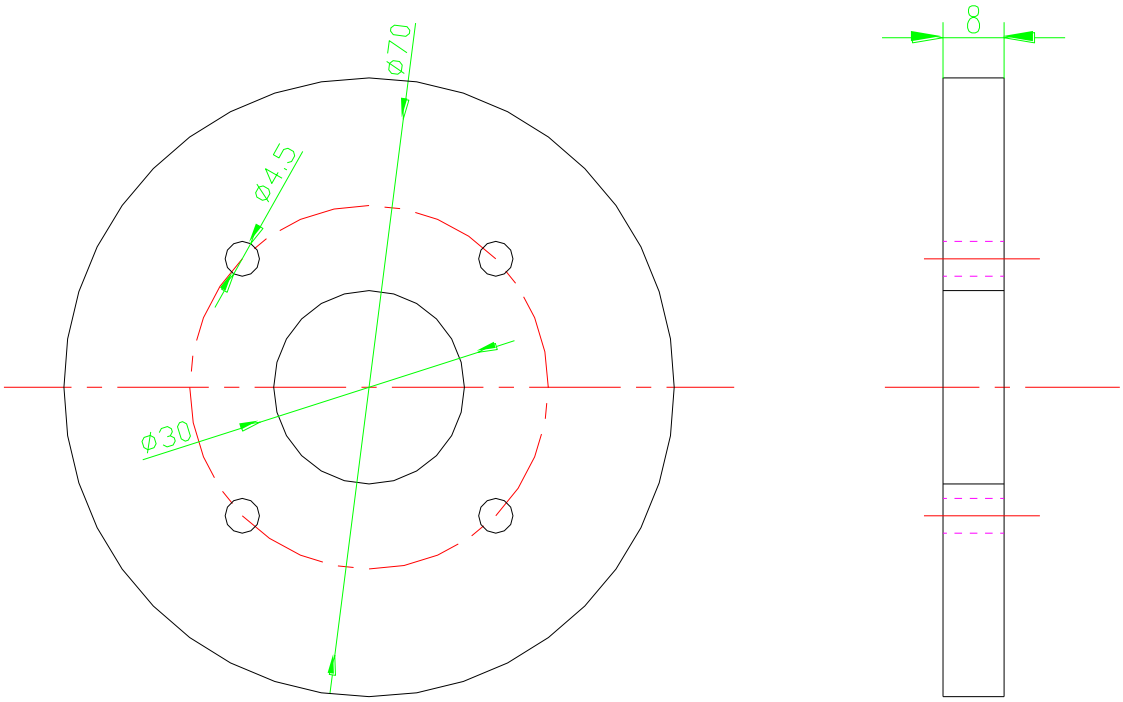

Figure A.11 Belt plate washer

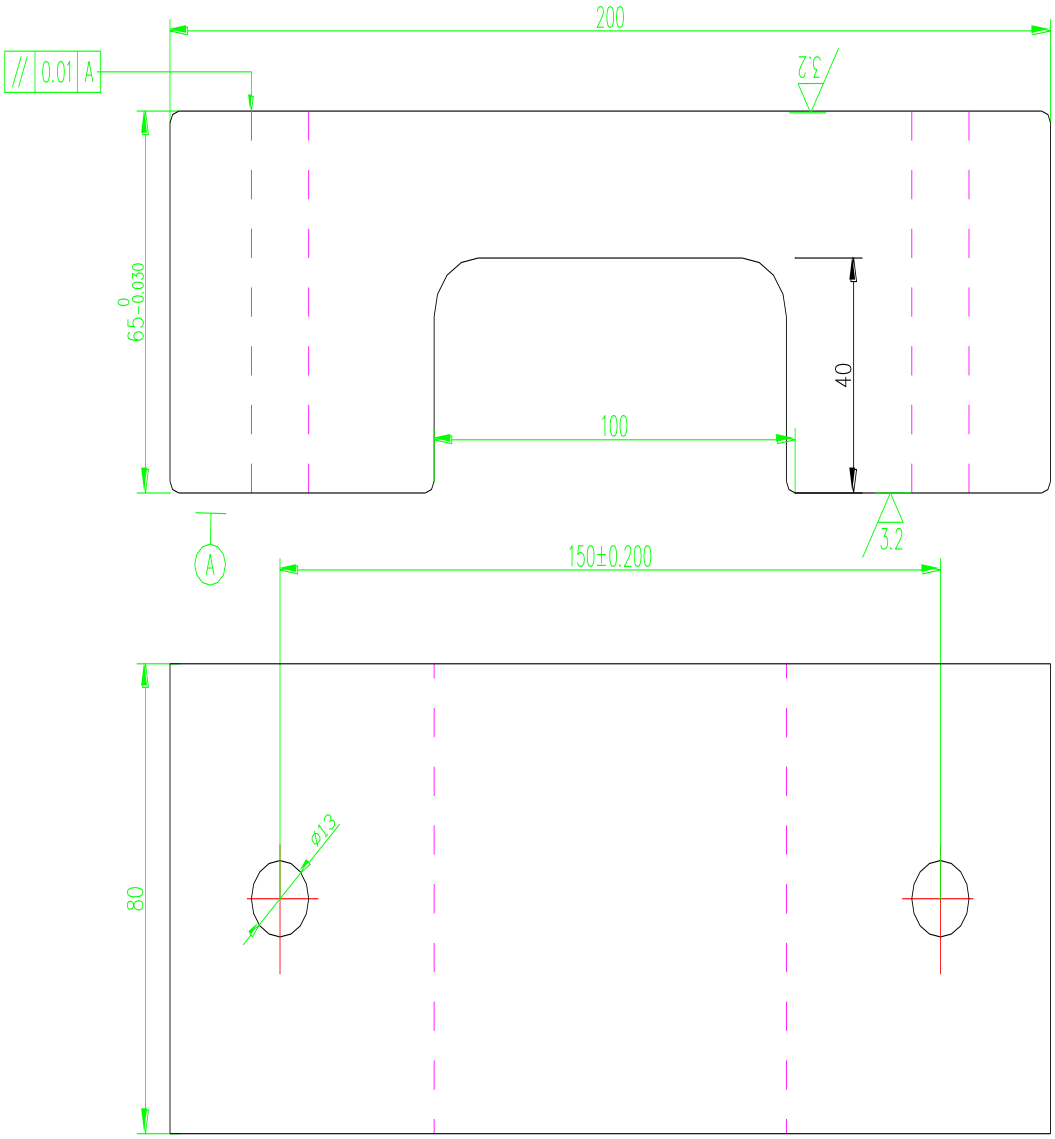

Figure A.12 Block